November 1990 UILU-ENG-90-2252

ASYMPTOTIC AND ABSORBING BOUNDARY CONDITIONS FOR FINITE ELEMENT ANALYSIS OF DIGITAL CIRCUIT AND SCATTERING PROBLEMS

Ahmed Khebir
Raj Mittra

Coordinated Science Laboratory
College of Engineering
UNIVERSITY OF ILLINOIS AT URBANA-CHAMPAIGN

REPORT DOCUMENTATION PAGE

Form Approved
OMB No. 0704-0188

1a. REPORT SECURITY CLASSIFICATION Unclassified	1b. RESTRICTIVE MARKINGS None
2a. SECURITY CLASSIFICATION AUTHORITY	3. DISTRIBUTION/AVAILABILITY OF REPORT Approved for public release; distribution unlimited
2b. DECLASSIFICATION/DOWNGRADING SCHEDULE	
4. PERFORMING ORGANIZATION REPORT NUMBER(S) UILU-ENG-90-2252	5. MONITORING ORGANIZATION REPORT NUMBER(S)
6a. NAME OF PERFORMING ORGANIZATION Coordinated Science Lab University of Illinois 6b. OFFICE SYMBOL (If applicable) N/A	7a. NAME OF MONITORING ORGANIZATION Office of Naval Research
6c. ADDRESS (City, State, and ZIP Code) 1101 W. Springfield Ave. Urbana, IL 61801	7b. ADDRESS (City, State, and ZIP Code) Arlington, VA 22217
8a. NAME OF FUNDING/SPONSORING ORGANIZATION Joint Services Electronics Program 8b. OFFICE SYMBOL (If applicable)	9. PROCUREMENT INSTRUMENT IDENTIFICATION NUMBER N00014-90-J-1270
8c. ADDRESS (City, State, and ZIP Code) Arlington, VA 22217	10. SOURCE OF FUNDING NUMBERS PROGRAM ELEMENT NO. / PROJECT NO. / TASK NO / WORK UNIT ACCESSION NO.

11. TITLE (Include Security Classification)
Asymptotic and Absorbing Boundary Conditions for Finite Element Analysis of Digital Circuit and Scattering Problems.

12. PERSONAL AUTHOR(S)
Ahmed Khebir and Raj Mittra

13a. TYPE OF REPORT	13b. TIME COVERED	14. DATE OF REPORT (Year, Month, Day)	15. PAGE COUNT
Technical	FROM _____ TO _____	November 8, 1990	123

16. SUPPLEMENTARY NOTATION

17. COSATI CODES			18. SUBJECT TERMS (Continue on reverse if necessary and identify by block number)
FIELD	GROUP	SUB-GROUP	

19. ABSTRACT (Continue on reverse if necessary and identify by block number)

The finite element method (FEM) is very appealing for solving open region digital circuit and scattering problems due to its simplicity in modeling complex-shaped structures and inhomogeneous dielectric scatterers. However, it must deal with the practical problems of mesh truncation and the introduction of an artificial outer boundary in order to limit the number of node points to a manageable size. Therefore, the major difficulty encountered when using FEM is how to find a boundary condition operator which when applied on the artificial outer boundary mimics the asymptotic behavior of the field at infinity and yields reasonably accurate results in the interior region without the need of an exorbitantly large number of mesh points.

This report is an effort to provide some techniques to deal with the FEM mesh truncation, in an efficient manner, through the introduction of three new boundary condition concepts, viz., the boundary conditions for arbitrary outer boundaries, the asymptotic boundary condition for digital circuit applications, and the higher-order asymptotic and absorbing —

20. DISTRIBUTION/AVAILABILITY OF ABSTRACT ☒ UNCLASSIFIED/UNLIMITED ☐ SAME AS RPT. ☐ DTIC USERS	21. ABSTRACT SECURITY CLASSIFICATION Unclassified
22a. NAME OF RESPONSIBLE INDIVIDUAL	22b. TELEPHONE (Include Area Code) / 22c. OFFICE SYMBOL

19. ABSTRACT (cont'd)

boundary conditions. The use of generalized boundary conditions or the boundary conditions for arbitrary outer boundaries enables one to reduce the number of node points significantly and to solve larger sized problems than had been possible in the past. The asymptotic boundary condition for digital circuit applications does not suffer from the complications associated with the infinite elements, and yet enables one to bring the outer boundary much closer to the structure than would be possible with a p.e.c. artifical outer boundary. The higher-order asymptotic and absorbing boundary conditions, unlike the available ABCs, e.g., the Bayliss, Gunzburger, and Turkel (BGT), which assume that in the far region the solution can adequately be represented by the first few terms of the series, require that the asymptotic representation be a combination of the lower- and higher-order terms. The higher-order boundary conditions help reduce the error in the finite element solution caused by the neglecting of the higher-order terms in other available ABC assumptions.

Various investigations of scattering as well as two- and three-dimensional digital circuit problems are presented. Numerical examples are shown for a variety of scatterers and transmission line configurations. Results show that the boundary condition concepts introduced in this work yield good agreement with work published elsewhere and significant improvements in computation time and storage compared to other available methods.

TABLE OF CONTENTS

CHAPTER 1

INTRODUCTION

With the continuous advances in solid state device technology in terms of both speed and size, a number of challenges are presented to the packaging engineer who has to accommodate a multitude of these devices on the limited real estate available on the circuit board. In the absence of reliable design tools, digital circuit packaging is carried out through a costly and lengthy trial and error process. Thus, a critical need exists for computer-aided design tools that are capable of predicting the electrical performance of a given package, e.g., crosstalk and signal distortion, in a reliable fashion. Understanding how printed circuit layouts can affect these quantities is essential for improved package designs.

Similarly, in the area of aircraft design the interaction of the aircraft with electromagnetic waves is of crucial importance. In recent years, the reduction of the amount of radar power reflected by a complex object like an aircraft, known as the radar cross section (RCS), has become a major objective of aircraft designers. Therefore, there is a critical need for efficient electromagnetic computer-aided design tools in the area of circuit design, where the major concern is the reduction of crosstalk and signal distortion for a printed circuit board, as well as in the area of aircraft design, where the major concern is the reduction of radar cross section of an aircraft.

A plethora of techniques is available in the literature for dealing with different transmission line and electromagnetic scattering problems, e.g., the method of moments, Fourier transform method, variational method, and conformal mapping method. However, all of these approaches are limited in their application to homogeneous media and simple geometries. Furthermore, for large problems, these methods become numerically

inefficient because they give rise to full matrices which require large computer memory and solution times, especially for open region problems. In contrast, the finite element method (FEM) can handle complex-shaped structures and highly inhomogeneous dielectrics. In the FEM, the region of interest is bounded by an artificial boundary to limit the number of unknowns. Over the bounded region, the Helmholtz or Laplace equation is solved at a finite number of grid points. These equations are discretized through the use of a weak variational formulation. Although the resulting matrix equation is substantially larger than that obtained in other methods, especially the method of moments, it is, nevertheless, highly sparse and can be inverted rather efficiently using special algorithms that store only the nonzero entries of the matrix. The major advantage in using FEM is the simplicity with which complex-shaped structures can be modeled. Another advantage is the great improvement in storage and even in the computational time, over the method of moments, especially in the case of inhomogeneous dielectric scatterers where a volume formulation of the integral equation is required These features of the FEM formulation make it a good candidate for CAD packages. However, one drawback of FEM is that, in dealing with open region problems, they require the introduction of an artificial outer boundary in order to limit the number of node points to a manageable size. The major difficulty encountered when using FEM is how to find the proper boundary condition that can be applied on the artificial outer boundary to make it as transparent as possible in other words, how to impose the corresponding behavior at infinity on the finite distance boundary and obtain an accurate solution in the interior region. The answer to this important question is of a crucial importance for the development of efficient electromagnetic computer-aided design tools. There have been different approaches to model the outer boundary both for electromagnetic scattering and digital circuit problems.

For the quasi-static analysis of digital circuit problems, it is customary to use either the natural boundary condition or the infinite elements for mesh truncation. The first

approach consists of introducing a fictitious conducting enclosure at the outer boundary [1]-[4]. This approach gives satisfactory results only if the actual field has decayed sufficiently well as it reaches the outer boundary. In most cases, this approach, which assumes that the field decays significantly before reaching the outer boundary, results in an undesirably large mesh, especially for three-dimensional problems. The second approach uses the infinite elements which extend to infinity [5]-[7]. Although this approach is superior to the artificial p.e.c. boundary method, it also has its own drawbacks. First, the infinite elements require special care during the matrix filling. Second, one needs to assume a certain field behavior within the infinite elements, and this behavior may not be known.

For electromagnetic scattering problems, the Helmholtz type of equation is solved. In order to model the field behavior at the outer boundary, the so-called local and local boundary conditions have been used. In the first type, the surface integral equation involving the free-space Green's function is used as the boundary constraint [8]-[11] and [13]-[15]. Mei [12] has used a similar approach where an eigenfunction expansion of the field and its derivative are used as constraints on the outer boundary. Both of these methods are sometimes classified in the literature under the umbrella of global or local boundary conditions. The reason for this classification is that all of the field values at the boundary are related through the surface integral constraint. An important drawback in using a nonlocal type of boundary condition is that it spoils the sparsity of the system matrix and, consequently, becomes time-consuming for large problems.

In the local boundary condition approach, an asymptotic differential boundary operator, referred to in the literature as an Absorbing Boundary Condition (ABC) [16]-[28], is used as a constraint on the normal derivative of the field at the outer boundary. This boundary operator attempts to impose an outward propagating character on the scattered field, i.e., tries to eliminate the nonphysical reflections at the boundary that

generate incoming waves. The ABC operator is only asymptotic in nature, and does not satisfy the near-field radiation condition in the exact sense. Thus, it introduces an error in the FEM solution because it is not totally free of incoming waves generated by the artificial outer boundary; however, this error is often quite small, and hence acceptable for many practical applications. Furthermore, in contrast to the local boundary conditions, the ABC does preserve the sparsity of the discretized FEM matrix and is, therefore, an attractive candidate for numerical applications. Nevertheless, there have been two major limitations associated with this type of boundary conditions. First, most attempts to solve the open region scattering problem using the local-type boundary operators have been limited to separable types of geometry for the outer boundary. This may be attributable to the form in which these operators were cast in their original versions. However, for a class of scatterers that are long, such as a perfectly conducting strip or an air foil, truncating the open region with a circular outer boundary requires solving for the field over a very large mesh region surrounding the scatterer, which, in turn, requires the solution of a large matrix. In such situations, the FEM becomes less efficient than the method of moments. Second, most forms of the absorbing boundary condition operators have been based on the use of only the first few terms of the asymptotic representation of the solution to the differential equation. In [24] and [27]-[28], it was demonstrated that while the absorbing boundary condition, which is based on the first terms of the series, works quite well for the lower-order harmonics, it exhibits a significant error for the higher-order harmonics, especially if the outer boundary is placed very close to the surface of the object.

The goal of this study is the circumvent some of the above-mentioned problems that are encountered in FEM mesh truncation. First, the Bayliss, Gunzburger, and Turkel (BGT) [9] boundary condition is generalized so as to make it applicable to an arbitrary, rather than circular, outer boundary. The use of the generalized version of the BGT enables one to reduce the number of node points significantly and solve larger sized

problems than had been possible in the past. Second, an asymptotic differential operator for the quasi-static analysis of two-dimensional transmission line structures is obtained. This operator, which is also valid for an arbitrary outer boundary, not only allows one to bring the outer boundary much closer than is possible with a p.e.c. artificial boundary, but does not suffer from the complications associated with the infinite elements. Third, a set of asymptotic boundary condition operators for finite element quasi-TEM analysis of three-dimensional transmission line discontinuities is derived from the general solution to the three-dimensional Laplace equation in spherical coordinates. The second-order three-dimensional asymptotic boundary condition is then applied on a box-shaped outer boundary for the purpose of truncating the mesh in an efficient manner. With this boundary condition, it becomes possible to consider general three-dimensional discontinuities and consider more practical problems. Fourth, the general form of the solution to the two-dimensional Laplace equation is used to derive a higher-order asymptotic boundary condition for transmission line circuits. This boundary condition, unlike the one discussed earlier which assumes that in the far region the solution can adequately be represented by the first two terms of the series, requires that the asymptotic representation be a combination of lower- and higher-order terms. Therefore, it corrects, to a good degree, the error caused by the neglecting of the higher-order terms by the simple asymptotic boundary condition, which, in turn, yields a significant improvement in the finite element solution. Last, a higher-order absorbing boundary condition for scattering problems is derived from the asymptotic solution of the Helmholtz equation. This higher-order boundary condition, which takes into account both the lower- and higher-order harmonics, considerably reduces the error caused by the neglecting of the higher-order harmonics by most of the available absorbing boundary conditions.

Chapter 2 gives some background on the finite element method and the absorbing and asymptotic boundary conditions. Chapter 3 deals with the open region scattering

problem and the generalization of the original BGT boundary condition so as to make it applicable to an arbitrary outer boundary. The asymptotic boundary condition for finite element quasi-TEM analysis of two-dimensional transmission line structures is discussed in Chapter 4. The corresponding analysis for three-dimensional transmission line discontinuities is addressed in Chapter 5. Chapter 6 deals with the higher-order boundary condition for both the scattering as well as the transmission line circuit problems and the improvement on the simple boundary conditions. In Chapter 7 the conclusions drawn from this study are discussed.

CHAPTER 2

THE FINITE ELEMENT METHOD, THE ASYMPTOTIC, AND THE ABSORBING BOUNDARY CONDITIONS

2.1 Introduction

The finite element method (FEM) has become an important numerical technique to solve open region problems because of its flexibility in handling arbitrary structures and highly inhomogeneous materials. However, it must deal with the practical problem of mesh truncation and the large number of mesh nodes. By imposing an asymptotic or an absorbing boundary condition (ABC) on the field at the outer boundary, it becomes possible to reduce the number of unknowns to a manageable size while modeling the physical problem as correctly as possible.

In this chapter, a general background on the finite element method will be presented and the derivations of the Bayliss, Gunzburger, and Turkel (BGT) [17] boundary operators for both the Helmholtz and Laplace equations will be reviewed.

2.2 The Finite Element Method

In the finite element method the Helmholtz or Laplace equation is solved at a finite number of grid points. These equations are discretized through the use of a weak variational formulation. In this section only Laplace's equation will be treated; the extension to the Helmholtz equation should be straightforward.

Consider the N-conductor configuration shown in Figure 2.1. The potential, u, satisfies the Laplace equation [1]

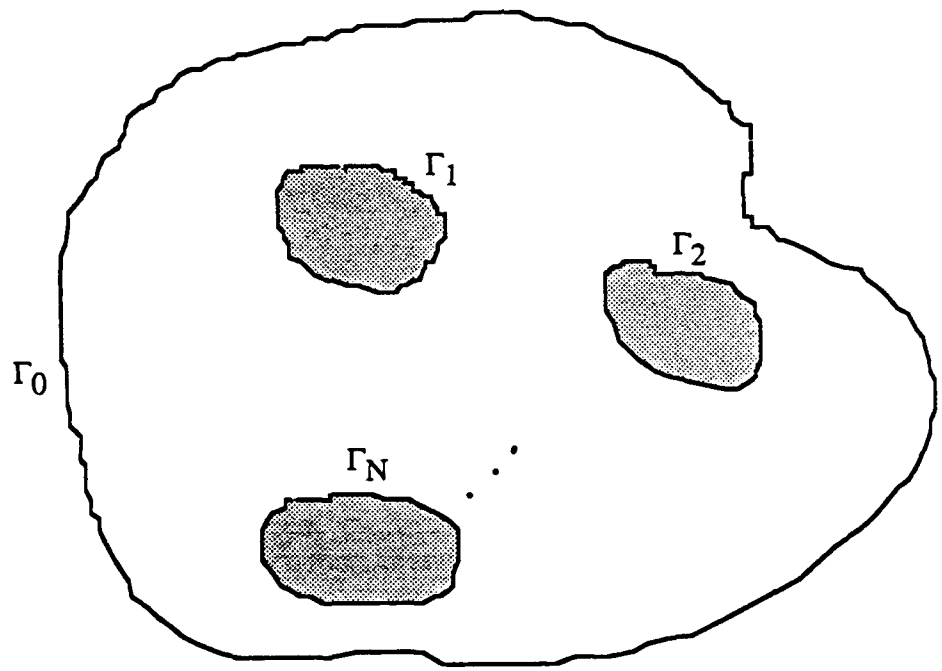

Figure 2.1. Cross section of a multiconductor transmission line configuration.

$$\nabla\cdot(\varepsilon\nabla u) = 0 \tag{2.1}$$

where $\varepsilon = \varepsilon(x,y)$ is the permittivity of the dielectric. The following boundary conditions should be satisfied

$$\begin{aligned} &u = \phi_1 \text{ on } \Gamma_1 \\ &u = \phi_2 \text{ on } \Gamma_2 \\ &\quad . \\ &\quad . \\ &\quad . \\ &u = \phi_n \text{ on } \Gamma_n \end{aligned} \tag{2.2}$$

Multiplying (2.1) by a testing function v and integrating over the domain of the problem Ω, we obtain

$$\int_\Omega v\nabla\cdot(\varepsilon\nabla u)\, ds = 0 \tag{2.3}$$

From Green's identity we have

$$\int_\Omega v\nabla\cdot(\varepsilon\nabla u)\, ds = -\int_\Omega \varepsilon\nabla u\cdot\nabla v\, ds + \int_{\Gamma_0} v\varepsilon \frac{\partial u}{\partial n}\, dt \tag{2.4}$$

Inserting the above in (2.3), we obtain

$$\int_\Omega \varepsilon\nabla u\cdot\nabla v\, ds - \int_{\Gamma_0} v\varepsilon \frac{\partial u}{\partial n}\, dt = 0 \tag{2.5}$$

Only the first term of Equation (2.5) is treated in this section. The second term will be examined when the absorbing boundary condition is discussed.

To construct an approximate solution, the domain Ω is broken into a number of triangles. Over each triangle the unknown potential is expressed in terms of a set of approximating basis functions

$$u(\xi_1 , \xi_2 , \xi_3) = \sum_{ijk} u_{ijk}\, \alpha_{ijk}(\xi_1 , \xi_2 , \xi_3) \tag{2.6}$$

The arguments ξ_1, ξ_2, and ξ_3 are called simplex or area coordinates and can be related to the Cartesian coordinates by

$$x = \xi_1 x_1 + \xi_2 x_2 + \xi_3 x_3 \tag{2.7}$$

$$y = \xi_1 y_1 + \xi_2 y_2 + \xi_3 y_3 \tag{2.8}$$

where x_k and y_k are the coordinates of the k^{th} vertex shown in Figure 2.2.

Note that each approximating function is equal to one at its corresponding node and zero at all other nodes. It suffices to impose continuity of the functions at triangle vertices to guarantee the continuity of the potential across all of the triangle edges. It should also be noted that the simplex coordinates are purely local in nature which makes the analysis independent of the position of the triangular elements in the Cartesian coordinate system.

In order to determine the basis function α_{ijk}, we need to first define a family of auxiliary polynomials R of degree n. Keeping in mind that α_{ijk} must take the value of

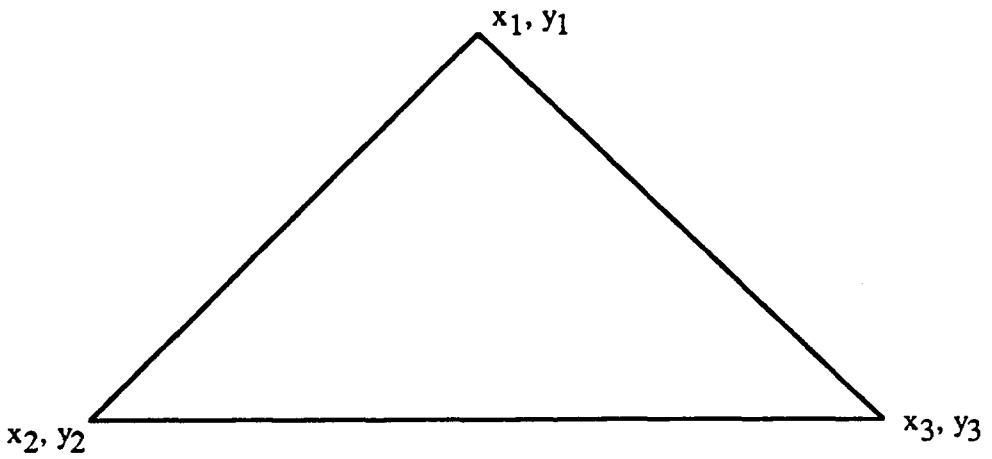

Figure 2.2. Triangular element.

unity at node ijk, and zero at all other nodes, a proper choice of the auxiliary polynomials will be

$$R_m(n,\xi) = \prod_{k=0}^{m-1} \frac{\xi - k/n}{m/n - k/n} = \frac{1}{m!} \prod_{k=0}^{m-1} (n\xi - k), \quad m>0$$

$$R_0(n,\xi) = 1 \tag{2.9}$$

The polynomial has exactly m equispaced zeros at ξ = 0, 1/n, ..., (m-1)/n, all of which lie to the left of ξ = m/n, and takes on the value of unity at ξ= m/n. A family of interpolation functions that are suitable for two-dimensional problems is defined by

$$\alpha_{ijk} = R_i(n,\xi_1)R_j(n,\xi_2)R_k(n,\xi_3) \qquad i + j + k = n \tag{2.10}$$

Clearly, the constructed interpolation functions are independent of the global coordinate system because they are defined in terms of simplex coordinates. Therefore, the creation of the finite element matrices can be done using the simplex coordinates. The filling of the finite element matrices can then be placed in subroutines that can be called for each triangular element regardless of its position in the global coordinate system.

Expressing the unknown potential u as in Equation (2.6), the first term of equation (2.5) will take the form

$$\bar{\bar{S}} = \varepsilon \sum_i u_i S_{ij} \tag{2.11}$$

where

$$S_{ij} = \int \nabla\alpha_i \cdot \nabla\alpha_j \, ds \tag{2.12}$$

The element matrix S may be written in detail as

$$S_{ij} = \int \left(\frac{\partial\alpha_i}{\partial x}\frac{\partial\alpha_j}{\partial x} + \frac{\partial\alpha_i}{\partial y}\frac{\partial\alpha_j}{\partial y} \right) ds \tag{2.13}$$

which may be expressed in terms of only simplex coordinates and Cartesian coordinates of the vertices of each triangle

$$S_{ij} = \frac{1}{4A^2} \sum_n \sum_m (b_n b_m + c_n c_m) \int \frac{\partial\alpha_i}{\partial\xi_n}\frac{\partial\alpha_j}{\partial\xi_m} \, ds$$

$$= \sum_{k=1}^{3} \cot\theta_k \int \left(\frac{\partial\alpha_i}{\partial\xi_{k+1}} - \frac{\partial\alpha_i}{\partial\xi_{k-1}} \right) \left(\frac{\partial\alpha_j}{\partial\xi_{k+1}} - \frac{\partial\alpha_j}{\partial\xi_{k-1}} \right) \frac{ds}{2A} \tag{2.14}$$

where the subscripts n and m progress modulo 3, A is the area of the triangle, and

$$b_n = y_{n+1} - y_{n-1} \tag{2.15}$$

$$c_n = x_{n-1} - x_{n+1} \tag{2.16}$$

θ_k denotes the included angle at vertex k and it is given by

$$\cot\theta_k = -\frac{1}{2A}(b_n b_m + c_n c_m) \quad n \neq m \tag{2.17}$$

The right-hand side of Equation (2.14) is dimensionless and depends only on the simplex

coordinates. The matrix S_{ij} can be evaluated for a triangle of any size or shape which can then be stored for permanent reference. All integrations and differentiations can be carried out in a universal manner valid for any triangle due to the use of simplex coordinates [1].

Each element matrix is then calculated and added to the global system of equations on an element by element basis using the connectivity matrix which has information on the global and the local node numberings. If two nodes numbered 1 and i are not in adjacent elements, the entry (1, i) in the global matrix would be zero. This elegant feature of the finite element method leads to a very sparse system of equations that can be easily handled using special techniques. Typically, a finite element problem would have a large number of unknowns but since the resulting system of equations is very sparse it can be solved efficiently. The truncation from an infinite region to a finite region may cause a significant error in the solution. The best known method of dealing with this problem is to use an absorbing boundary condition at the outer boundary. In the following section a review of the absorbing boundary conditions will be given.

2.3 The Absorbing and Asymptotic Boundary Conditions

When using FEM to solve open region problems, one needs to introduce an artificial outer boundary in order to limit the number of unknowns. Since the outside region is unbounded, one needs to impose the corresponding behavior at infinity on the finite distance boundary and obtain an accurate solution in the interior region [29]. Such boundary conditions that dictate the behavior at infinity are commonly referred to as asymptotic or absorbing boundary conditions (ABC). In what follows, the derivations of the Bayliss, Gunzburger, and Turkel (BGT) [17] boundary operators for both the Helmholtz and Laplace equations are reviewed.

2.3.1 The BGT operator for the Helmholtz equation

Consider the region Ω, bounded with the contour Γ_1, shown in Figure 2.3. Let the exterior region to Ω be Ω_T [29]. This problem is equivalent to

$$\nabla^2 u + k^2 u = 0 \text{ in } \Omega_T \tag{2.18}$$

$$\frac{\partial u}{\partial n} = g \text{ on } \Gamma_1 \tag{2.19}$$

u satisfies a radiation condition (2.20)

where u is the scattered field and g is the contribution from the incident field. In the far region the solution of (2.18) takes an asymptotic form

$$u \equiv \frac{e^{-jk\rho}}{\sqrt{\rho}}\left(a_0(\phi)+\frac{a_1(\phi)}{\rho}+\frac{a_2(\phi)}{\rho^2}+\ \ldots\right)+\frac{e^{jk\rho}}{\sqrt{\rho}}\left(b_0(\phi)+\frac{b_1(\phi)}{\rho}+\frac{b_2(\phi)}{\rho^2}+\ \ldots\right) \tag{2.21}$$

The first term of Equation (2.21) designates the outgoing waves and the second part designates the incoming waves. In the far region there are only outgoing waves; therefore, the second term of Equation (2.21) is not physically meaningful and only the first term should be kept. In other words, the scattered field in the far region should behave as

$$u \equiv \frac{e^{-jk\rho}}{\sqrt{\rho}}\left(a_0(\phi)+\frac{a_1(\phi)}{\rho}+\frac{a_2(\phi)}{\rho^2}+\ \ldots\right) \tag{2.22}$$

If u_ρ designates the radial derivative of u, we have from the above equation,

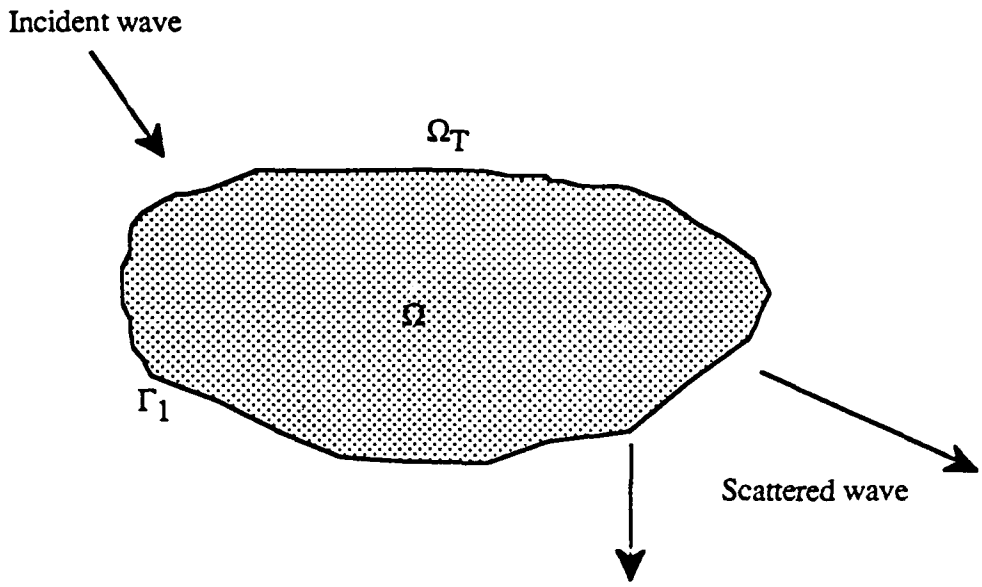

Figure 2.3. Two-dimensional scattering problem.

$$u_\rho + jku = -\frac{e^{-jk\rho}}{2\rho^{3/2}}\left(a_0(\phi) + \frac{a_1(\phi)}{\rho} + \frac{a_2(\phi)}{\rho^2} + \ldots\right) - \frac{e^{-jk\rho}}{\sqrt{\rho}}\left(\frac{a_1(\phi)}{\rho^2} + \frac{2a_2(\phi)}{\rho^3} + \ldots\right) \tag{2.23}$$

Clearly, Equation (2.23) is equivalent to

$$u_\rho + jku = O\left(\frac{1}{\rho^{3/2}}\right) \tag{2.24}$$

As ρ goes to infinity, the right-hand side of Equation (2.24) goes to zero, which is equivalent to imposing the Sommerfeld radiation condition on the field u. Examining the first term of Equation (2.23), we note that it is equal to $-u/2\rho$. Consequently, we can obtain a higher-order boundary condition by writing

$$u_\rho + jku + \frac{u}{2\rho} = O\left(\frac{1}{\rho^{5/2}}\right) \tag{2.25}$$

This type of analysis was first carried out by Bayliss and Turkel [21] as well as Engquist and Majda [16] in connection with time-dependent problems. For time harmonic problems, their results reduce to Equation (2.25). Bayliss, Gunzburger, and Turkel [17] have generalized these results by writing

$$B_1 \equiv \frac{\partial}{\partial\rho} + jk + \frac{1}{2\rho} \tag{2.26}$$

or, equivalently,

$$B_1 u = -\frac{e^{-jk\rho}}{\sqrt{\rho}}\left(\frac{a_1(\phi)}{\rho^2} + \frac{2a_2(\phi)}{\rho^3} + \ldots\right) \tag{2.27}$$

They were able to obtain a higher-order operator by letting $v = B_1 u$ and observing that

$$\frac{\partial v}{\partial \rho} + jkv - \frac{5}{2\rho} v = O\left(\frac{1}{\rho^{9/2}}\right)$$

or

$$B_2 u = \left(\frac{\partial}{\partial \rho} + jk + \frac{5}{2\rho}\right)\left(\frac{\partial}{\partial \rho} + jk + \frac{1}{2\rho}\right) u = O\left(\frac{1}{\rho^{9/2}}\right) \tag{2.28}$$

Furthermore, they were able to generalize the procedure by deriving an m^{th} operator , B_m, such that

$$B_m u = O\left(\frac{1}{\rho^{2m+1/2}}\right) \tag{2.29}$$

and

$$B_m = \prod_{l=1}^{m}\left(\frac{\partial}{\partial \rho} + \frac{\left(2l - \frac{3}{2}\right)}{\rho} + jk\right) \tag{2.30}$$

The original problem has now been slightly modified. That is, the infinite exterior region, Ω_T, is now truncated and bounded by a circular contour Γ_2 where the m^{th} operator can be applied. Obviously, one can now use a PDE technique to solve the approximate problem provided the region bounded by Γ_2 is not so large as to require an unmanageable number of unknowns. The approximate problem, shown in Figure 2.4, is equivalent to

$$\nabla^2 u + k^2 u = 0 \text{ in } \Omega_T \tag{2.31}$$

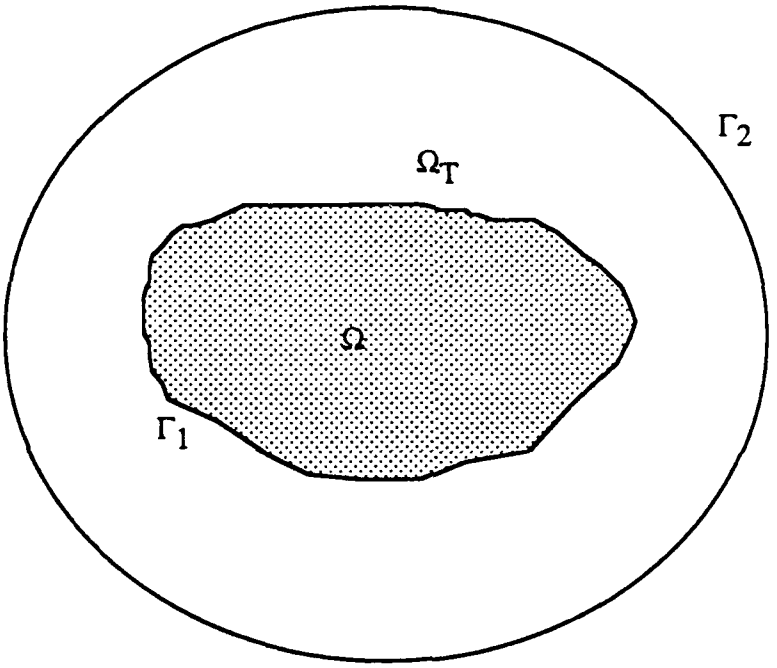

Figure 2.4. Computational domain.

$$\frac{\partial u}{\partial \rho} = g \text{ on } \Gamma_1 \tag{2.32}$$

$$B_m u = 0 \text{ on } \Gamma_2 \tag{2.33}$$

Note that the m^{th} order operator has an m^{th} order radial derivative. By invoking the Helmholtz equation we can trade the m^{th} order radial derivatives for the first-order radial derivatives plus derivatives in the tangential directions. Note also that there is an error introduced by the approximate problem of the order $O(1/R^{2m+1/2})$, where R is the distance from the outer boundary to the origin. In two dimensions, it is impossible to know the corresponding error in $\|u-u_{apro}\|$, where u_{apro} is the solution of the approximate problem. In three dimensions, however, Bayliss, Gunzburger, and Turkel were able to prove, for m=1 and m=2, the following theorem

$$\| u_{dif} \| = \frac{C}{r^{m+1}} \tag{2.34}$$

where $u_{dif} = u-u_{apro}$, C depends on k and the outer boundary, and the surface norm is defined as

$$\| u_{apro} \|^2 = \int_\Gamma | u_{apro} |^2 \, ds \tag{2.35}$$

Hence, the error in the solution caused by the truncation of the infinite domain is the same on the artificial boundary as on the interior boundary and is inversely proportional to $1/r^{m+1}$.

2.3.2 The BGT operator for the Laplace equation

Again consider the problem described in Figure 2.3. This time we would like to consider Laplace's equation which means that there is neither an incident nor a scattered wave. The problem at hand is equivalent to

$$\nabla^2 u = 0 \text{ in } \Omega_T \tag{2.36}$$

$$u = g \text{ on } \Gamma_1 \tag{2.37}$$

$$u \equiv \log\rho \text{ as } \rho \to \infty \tag{2.38}$$

where u is the electrostatic potential.

The general solution of this problem can written as

$$u(\rho,\phi) = \log\rho + \sum_{n=0}^{\infty} \frac{a_n}{\rho^n} \cos n\phi \tag{2.39}$$

or more explicitly as

$$u(\rho,\phi) = \log\rho + a_0 + \frac{a_1}{\rho}\cos\phi + \frac{a_2}{\rho^2}\cos 2\phi + \frac{a_3}{\rho^3}\cos 3\phi + \ldots \tag{2.40}$$

We will now derive a set of boundary condition operators that can be applied on the artificial outer boundary. If we let $v = u - \log\rho - a_0$, we can see that

$$\frac{\partial v}{\partial \rho} = -\frac{a_1}{\rho^2}\cos\phi - \frac{2a_2}{\rho^3}\cos 2\phi - \frac{3a_3}{\rho^4}\cos 3\phi - \ldots \tag{2.41}$$

It can be seen that

$$\frac{\partial v}{\partial \rho} + \frac{v}{\rho} = -\frac{1}{\rho^3}\left(a_2\cos 2\phi + \frac{2a_3}{\rho}\cos 3\phi + \ldots\right) \tag{2.42}$$

Thus,

$$\frac{\partial v}{\partial \rho} + \frac{v}{\rho} = O\left(\frac{1}{\rho^3}\right) \tag{2.43}$$

We then define the first-order operator to be

$$B_1 \equiv \frac{\partial}{\partial \rho} + \frac{1}{\rho} \tag{2.44}$$

The second-order operator can be obtained by letting $w = B_1 v$ and observing that

$$\frac{\partial w}{\partial \rho} + \frac{3w}{\rho} = \frac{2a_3}{\rho^5}\cos 3\phi + \ldots \tag{2.45}$$

It can readily be verified that

$$B_2 \equiv \left(\frac{\partial}{\partial \rho} + \frac{3}{\rho}\right)\left(\frac{\partial}{\partial \rho} + \frac{1}{\rho}\right) = O\left(\frac{1}{\rho^5}\right) \tag{2.46}$$

The process can be repeated to obtain the m^{th} order operator which can be written as

$$B_m \equiv \prod_{l=1}^{m}\left(\frac{\partial}{\partial\rho} + \frac{2l-1}{\rho}\right) = O\left(\frac{1}{\rho^{2m+1}}\right) \tag{2.47}$$

The infinite exterior region Ω_T is now truncated and bounded by a circular contour Γ_2 where the m^{th} operator can be applied. The approximate problem described in the truncated region, shown in Figure 2.4, is equivalent to

$$\nabla^2 u = 0 \text{ in } \Omega_T \tag{2.48}$$

$$u = g \text{ on } \Gamma_1 \tag{2.49}$$

$$B_m u = 0 \text{ on } \Gamma_2 \tag{2.50}$$

In the region Ω_T one can now use a PDE technique to solve the approximate problem, provided that the region bounded by Γ_2 is not so large as to require an unmanageable number of unknowns.

2.4 Conclusions

In this chapter, a brief overview of the finite element method and its implementation were presented. Starting from the asymptotic representation of the solution for the Helmholtz and Laplace equations, the Bayliss, Gunzburger, and Turkel (BGT) m^{th} order absorbing and asymptotic boundary condition operators were derived for both electromagnetic scattering and electrostatic problems. In Chapter 3, the BGT operator for the Helmholtz equation will be used to derive an absorbing boundary condition operator that can be applied on an arbitrary boundary. The resulting operator will then be used to

study the scattering from some long scatterers where the outer boundary will be arbitrary. In Chapter 4, a similar operator for electrostatic problems, based on the BGT operator associated with Laplace's equation, will be derived.

CHAPTER 3

AN ABSORBING BOUNDARY CONDITION FOR AN ARBITRARY OUTER BOUNDARY

3.1 Introduction

The finite element method is very appealing for solving open region scattering problems because of its simplicity in modeling complex-shaped structures and inhomogeneous dielectrics. The local or the absorbing boundary condition makes the FEM even more powerful because it preserves the sparsity of the matrix. However, in the past, there has been a major limitation associated with the ABC as applied to scattering problems [32]. That is, most of the attempts to solve the open region scattering problem using the local-type boundary operators have been limited to separable types of geometry for the outer boundary. This may be attributable to the form in which these operators were cast in their original versions. However, for a class of scatterers that are long and slender, e.g., a strip or an airfoil, truncating the open region with a circular outer boundary requires solving for the field over a very large mesh region surrounding the scatterer, which, in turn, requires the solution of a large matrix. In such situations, the FEM becomes less efficient than the method of moments. However, if the outer boundary is made to conform to the geometry of the scatterer, a significant improvement in computation time and storage can be achieved.

In this chapter, we show how we can use an outer boundary of an arbitrary shape that can be made to conform to the geometry of the scatterer in order to minimize the size of the solution region. As will be shown below, this requires transformation of the boundary operator into a form that uses a local coordinate system. Once this is done, the operator can

be applied on a per element basis in the FEM formulation. To illustrate the application of the newly transformed boundary operator, we present the results for several p.e.c. scatterers.

3.2 Derivation of the Boundary Condition

In the previous chapter, a brief discussion of the finite element method and the absorbing boundary condition was presented. A detailed explanation of the implementation of the absorbing boundary condition in the finite element formulation for a two-dimensional scatterer enclosed by a circular outer boundary was given in [24]. For a complete coverage of the finite element method and absorbing boundary condition, the reader is referred to the work of various authors that appeared in [8]-[32]. In this section, we develop a finite element scheme for solving the problem of scattering by objects of arbitrary shape.

3.2.1 Formulation

Consider an arbitrarily-shaped perfectly conducting scatterer whose exterior region, Ω, is bounded by the contour Γ_1, as shown in Figure 3.1. For a TM or TE polarized incident wave, the scattered field, u, satisfies the wave equation

$$(\nabla^2 + k^2)u = 0 \tag{3.1}$$

To obtain the variational expression for this equation, we multiply (3.1) by a testing function, v, and integrate over the domain of the problem, Ω, to obtain

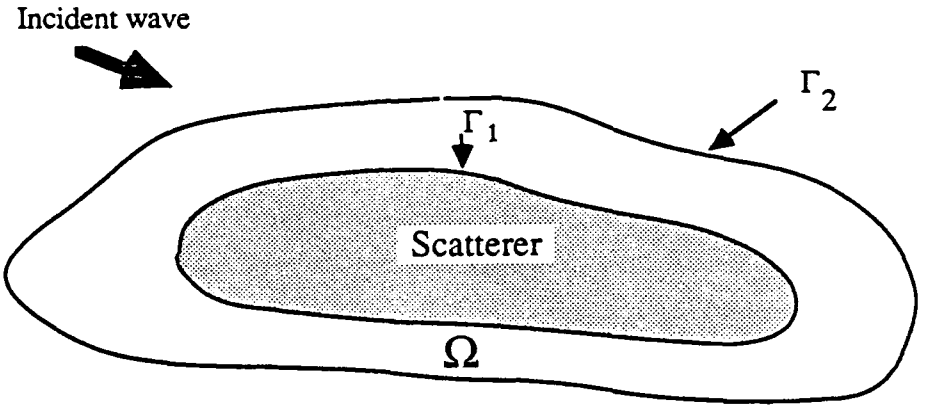

Figure 3.1. Geometry for the finite-mathematics approach to the scattering problem where the outer boundary is arbitrary.

$$\int_{\Omega} (v\nabla^2 u + k^2 vu)\, ds = 0 \tag{3.2}$$

Using the Green's identity to transfer the differentiation from the unknown function u to the testing function v, we obtain

$$\int_{\Omega} v\nabla^2 u\, ds = -\int_{\Omega} \nabla u \cdot \nabla v\, ds + \int_{\Gamma_1} v \frac{\partial u}{\partial n}\, dl + \int_{\Gamma_2} v \frac{\partial u}{\partial n}\, dl \tag{3.3}$$

In the case of TM polarization, where the total field at the p.e.c. scatterer's surface is zero, there will not be any contribution from the boundary integral on Γ_1, because the field values are specified on the surface of the scatterer.

Substituting (3.3) in (3.2) , we have

$$\int_{\Omega} (\nabla u \cdot \nabla v - k^2 vu)\, ds = \int_{\Gamma_1} v \frac{\partial u}{\partial n}\, dl + \int_{\Gamma_2} v \frac{\partial u}{\partial n}\, dl \tag{3.4}$$

The second term of the right-hand side of Equation (3.4) involves an integral over the outer boundary, Γ_2, and the normal derivative of u appears in this integrand. Obviously, the absorbing boundary condition has to be applied on the outer boundary Γ_2. Since the normal derivative of u appears in the boundary integral contribution , the absorbing boundary condition has to be imposed on that quantity. Hence, for our purposes, it is more desirable to find an asymptotic representation for the normal derivative of u rather than make direct use of the BGT operator B_2 as given in (2.28). For a circular outer boundary, the normal derivative is simply the radial one. Using the BGT operator B_2 as given in (2.28) in conjunction with (3.1), we obtain an asymptotic representation for the radial derivative that reads

$$u_\rho = \alpha(\rho)\, u + \beta(\rho)\, u_{\phi\phi} \tag{3.5}$$

where u is the scattered field, $u_{\phi\phi}$ is the second-order angular derivative, and $\alpha(\rho)$ and $\beta(\rho)$ are given by the following asymptotic series :

$$\alpha(\rho) = -jk - \frac{1}{2\rho} - \frac{j}{8k\rho^2} + \frac{1}{8k^2\rho^3} \tag{3.6}$$

$$\beta(\rho) = -\frac{j}{2k\rho^2} + \frac{1}{2k^2\rho^3} \tag{3.7}$$

In a previous work [24], Γ_2 was chosen to be a circle enclosing the scatterer. Thus, the normal derivative of u was simply its radial derivative u_ρ. Our next task is to transform the absorbing boundary operator, as given in (3.5), into a form suitable for arbitrary boundaries. In view of (3.4), it is natural to attempt to write the new operator in terms of the normal derivative of the field on the boundary. Since the region of solution will be discretized into finite elements, the transformed operator will be made local, i.e., the normal derivative on the outer boundary will depend locally on the coordinates of each element. This will be demonstrated below when we derive the expression for the transformed operator.

Consider the triangle shown in Figure 3.2. The edge 1-2 resides on the outer contour Γ_2. Let n-t represent a new coordinate system with the origin at node 1 with coordinates (x_0, y_0). The relationship between the cartesian coordinate system and the new local coordinate system can be obtained via the following equations that pertain to a translation and rotation of the coordinate system:

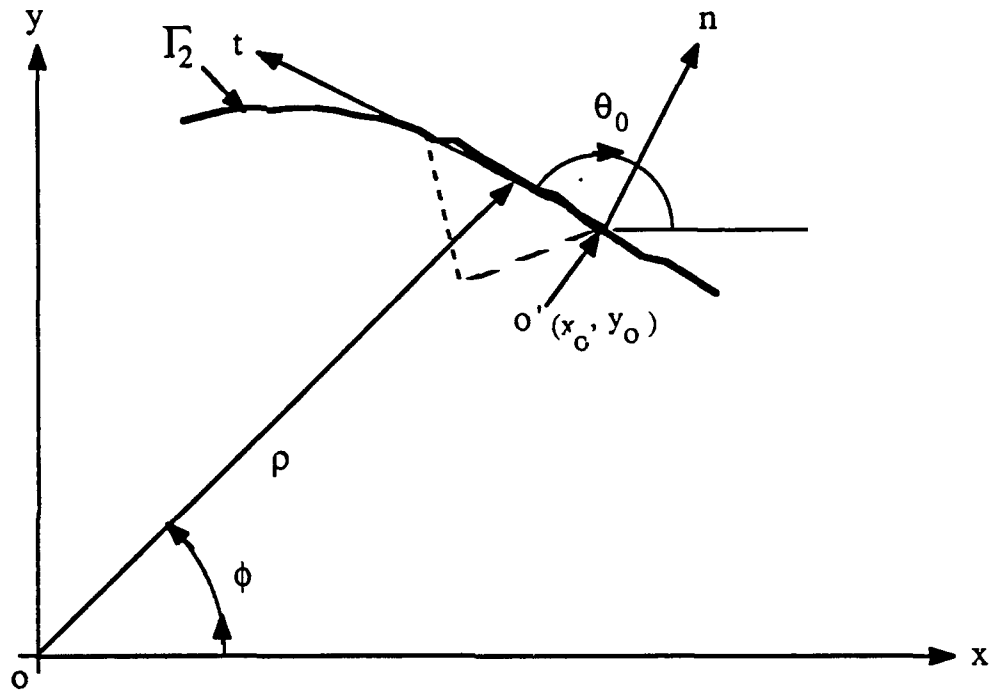

Figure 3.2. A triangular element residing on the arbitrary outer boundary and its local coordinates.

$$n = (x-x_0)\sin\theta_0 - (y-y_0)\cos\theta_0 \tag{3.8}$$

$$t = (x-x_0)\cos\theta_0 + (y-y_0)\sin\theta_0 \tag{3.9}$$

or

$$x = n\sin\theta_0 + t\cos\theta_0 + x_0 \tag{3.10}$$

$$y = -n\cos\theta_0 + t\sin\theta_0 + y_0 \tag{3.11}$$

where θ_0 is the angle the tangent vector makes with the positive x-axis.

Our aim is to obtain an expression for the normal derivative u_n on the t-axis in terms of tangential derivatives. Using the chain rule on u_n, we have

$$\frac{\partial u}{\partial n} = \frac{\partial u}{\partial \rho}\frac{\partial \rho}{\partial n} + \frac{\partial u}{\partial \phi}\frac{\partial \phi}{\partial n} \tag{3.12}$$

where ρ and ϕ are the cylindrical coordinates of a point on the outer boundary Γ_2.

To this end, the radial derivative u_ρ is given by (3.5). Expressions for the remaining partial derivatives are then obtained:

$$\frac{\partial \rho}{\partial n} = \frac{\partial \rho}{\partial x}\frac{\partial x}{\partial n} + \frac{\partial \rho}{\partial y}\frac{\partial y}{\partial n} \tag{3.13}$$

$$\frac{\partial \phi}{\partial n} = \frac{\partial \phi}{\partial x}\frac{\partial x}{\partial n} + \frac{\partial \phi}{\partial y}\frac{\partial y}{\partial n} \tag{3.14}$$

For the triangular element edge residing on the t-axis, the normal component in the n-t coordinate system is zero. Consequently, Equations (3.10) and (3.11) become

$$x = t\cos\theta_0 + x_0 \tag{3.15}$$

$$y = t\sin\theta_0 + y_0 \tag{3.16}$$

Thus, we obtain:

$$\frac{\partial \rho}{\partial x} = \frac{t\cos\theta_0 + x_0}{\sqrt{t^2 + x_0^2 + y_0^2 + 2t\,(x_0\cos\theta_0 + y_0\sin\theta_0)}} \tag{3.17}$$

$$\frac{\partial \rho}{\partial y} = \frac{t\sin\theta_0 + y_0}{\sqrt{t^2 + x_0^2 + y_0^2 + 2t\,(x_0\cos\theta_0 + y_0\sin\theta_0)}} \tag{3.18}$$

$$\frac{\partial \phi}{\partial x} = -\frac{t\sin\theta_0 + y_0}{t^2 + x_0^2 + y_0^2 + 2t\,(x_0\cos\theta_0 + y_0\sin\theta_0)} \tag{3.19}$$

$$\frac{\partial \phi}{\partial y} = \frac{t\cos\theta_0 + x_0}{t^2 + x_0^2 + y_0^2 + 2t\,(x_0\cos\theta_0 + y_0\sin\theta_0)} \tag{3.20}$$

In order to obtain an expression for the angular derivative u_ϕ, we use the following approximation:

$$\frac{\partial u}{\partial \phi} \approx \frac{\partial u}{\partial t}\,\frac{\partial t}{\partial \phi} \tag{3.21}$$

Using the chain rule, we obtain

$$\frac{\partial t}{\partial \phi} = x_0\sin\theta_0 - y_0\cos\theta_0 \tag{3.22}$$

Consequently, the first-order angular and tangential derivatives are related by

$$\frac{\partial u}{\partial \phi} \approx \frac{\partial u}{\partial t}\,(x_0 \sin\theta_0 - y_0 \cos\theta_0) \tag{3.23}$$

and the second-order angular and tangential derivatives by

$$\frac{\partial^2 u}{\partial^2 \phi} \approx \frac{\partial^2 u}{\partial^2 t}\,(x_0 \sin\theta_0 - y_0 \cos\theta_0)^2 \tag{3.24}$$

Using the expressions of the various partial derivatives obtained so far along with Equations (3.5)-(3.7), we arrive at the final form of the normal derivative u_n

$$\frac{\partial u}{\partial n} = \overline{\alpha}\, u + \overline{\gamma}\, u_t + \overline{\beta}\, u_{tt} \tag{3.25}$$

where

$$\overline{\alpha} = (x_0 \sin\theta_0 - y_0 \cos\theta_0)\left(-\frac{jk}{\rho} - \frac{1}{2\rho^2} - \frac{j}{8k\rho^3} + \frac{1}{8k^2\rho^4}\right) \tag{3.26}$$

$$\overline{\gamma} = \frac{-t\,(x_0 \sin\theta_0 - y_0 \cos\theta_0) + \frac{1}{2}\sin 2\theta_0\,(y_0^2 - x_0^2) + x_0 y_0 \cos 2\theta_0}{\rho^2} \tag{3.27}$$

$$\overline{\beta} = (x_0 \sin\theta_0 - y_0 \cos\theta_0)^3\left(-\frac{j}{2k\rho^3} + \frac{1}{2k^2\rho^4}\right) \tag{3.28}$$

where ρ is given by

$$\rho = \sqrt{t^2 + x_0^2 + y_0^2 + 2t\,(x_0 \cos\theta_0 + y_0 \sin\theta_0)} \tag{3.29}$$

Substituting the expression for the normal derivative u_n (3.25) back into the weak form of the Helmholtz Equation (3.4) and integrating by parts, we obtain

$$\int_{\Omega} (\nabla u \cdot \nabla v - k^2 vu)\, ds = \int_{\Gamma_1} v \frac{\partial u}{\partial n}\, dl + \int_{\Gamma_2} v(\overline{\alpha}\, u + \overline{\gamma}\, u_t + \overline{\beta}\, u_{tt})\, dl \qquad (3.30)$$

Integration by parts gives

$$\int_{\Omega} (\nabla u \cdot \nabla v - k^2 vu)\, ds = \int_{\Gamma_1} v \frac{\partial u}{\partial n} dl + \int_{\Gamma_2} (\overline{\alpha}\, vu + \overline{\gamma}\, vu_t - \overline{\beta}\, v_t u_t - \overline{\zeta}\, vu_t)\, dl \qquad (3.31)$$

where

$$\overline{\zeta} = (x_0 \sin\theta_0 - y_0 \cos\theta_0)^3 (t + x_0 \cos\theta_0 + y_0 \sin\theta_0) \left(\frac{3j}{2k\rho^5} - \frac{2}{k^2 \rho^6} \right) \qquad (3.32)$$

The form given in (31) is well-suited for numerical implementation for any arbitrary scatterer enclosed by any arbitrarily-shaped outer boundary Γ_2.

3.2.2 Radar cross-section calculation

The radar cross-section is an important quantity that needs to be computed for scattering problems. It is defined in [33] as the area for which the incident wave contains sufficient power to produce, by omnidirectional radiation, the same back-scattered power density.

3.2.2.1 TM case

For TM incidence, the two-dimensional radar cross-section is

$$\sigma_{TM}(\phi,\phi_{inc}) = Li\underset{\rho\to\infty}{m}\, 2\Pi\rho\, \frac{|E_z^s(\rho,\phi)|^2}{|E_z^i(0,0)|^2} \tag{3.33}$$

where (ρ,ϕ) are polar coordinates. For a plane wave incident of the form

$$E_z^i(x,y) = e^{-jk(x\cos\phi_{inc} + y\sin\phi_{inc})} \tag{3.34}$$

The scattered field is equal to

$$E_z^s(x,y) = -jk\eta A_z - \frac{\partial F_y}{\partial x} + \frac{\partial F_x}{\partial y} \tag{3.35}$$

where

$$A_z(x,y) = \int\int J_z(x',\, y')\, \frac{1}{4j}\, H_0^{(2)}(kR)\, dx'dy' \tag{3.36}$$

$$\bar{F}(x,y) = \int\int \bar{K}(x',\, y')\, \frac{1}{4j}\, H_0^{(2)}(kR)\, dx'dy' \tag{3.37}$$

and

$$R = \rho\sqrt{1 - \frac{2}{\rho}(x'\cos\phi + y'\sin\phi) + \frac{(x')^2 + (y')^2}{\rho^2}} \tag{3.38}$$

In the far region, the third term under the radical is negligible. Thus using the

approximation

$$\sqrt{1+\varepsilon} \approx 1 + \frac{\varepsilon}{2} \tag{3.39}$$

R takes the form

$$R \approx \rho - x'\cos\phi - y'\sin\phi \quad \text{as } \rho \to \infty \tag{3.40}$$

Using the asymptotic form of the Hankel function

$$H_0^{(2)}(\alpha) \approx \sqrt{\frac{2j}{\Pi\alpha}}\, e^{-j\alpha} \text{ as } \alpha \to \infty \tag{3.41}$$

in Equations (3.35)-(3.37), we obtain an expression for the radar cross-section

$$\sigma_{TM}(\phi, \phi_{inc}) = \frac{k}{4} \left| \int\int (\eta J_z + K_x \sin\phi - K_y \cos\phi) e^{jk(x'\cos\phi + y'\sin\phi)} dx'dy' \right|^2 \tag{3.42}$$

For a circular outer boundary, an FFT algorithm is usually used to calculate the radar cross-section. However, for an arbitrary outer boundary it is not possible to use the FFT method, and (3.42) needs to be used to approximate the radar cross-section. Since we are dealing with TM scattering, we are basically solving for the z-component of the scattered field. In order to find the electric current that appears in (3.42), it would seem reasonable to use the finite difference method to obtain the numerical derivative of the scattered electric field. However, we found that taking a numerical derivative is very unstable, especially in the region around the scatterer where the near field has many oscillations. To circumvent this problem, we have used the absorbing condition operator given by (3.25) to find the

normal derivative of the scattered field on the outer boundary from which the equivalent electric current is calculated. It should be understood that the use of the normal derivative expression given by (3.25) is also an approximation, but this method is found to be more stable than taking a numerical derivative via the finite difference method.

3.2.2.2 TE case

For TE incidence, the two-dimensional radar cross-section is

$$\sigma_{TE}(\phi,\phi_{inc}) = \lim_{\rho\to\infty} \frac{|H_z^s(\rho,\phi)|^2}{|H_z^i(0,0)|^2} \tag{3.43}$$

For a plane wave incident of the form

$$H_z^i(x,y) = e^{-jk(x\cos\phi_{inc} + y\sin\phi_{inc})} \tag{3.44}$$

the scattered magnetic field is given by

$$H_z^s(x,y) = \frac{\partial A_y}{\partial x} - \frac{\partial A_x}{\partial y} - j\frac{k}{\eta} F_z \tag{3.45}$$

Using the same far-field approximation as the one used earlier for the TM case, we obtain

$$\frac{\partial A_y}{\partial x} - \frac{\partial A_x}{\partial y} = -\frac{k}{4}\sqrt{\frac{2j}{\pi k\rho}} e^{-jk\rho} \int\int (J_y\cos\phi - J_x\sin\phi) e^{jk(x'\cos\phi + y'\sin\phi)} dx'dy' \tag{3.46}$$

$$F_z(\rho,\phi) = \frac{1}{4j}\sqrt{\frac{2j}{\pi k\rho}} e^{-jk\rho} \int\int K_z(x',y') e^{jk(x'\cos\phi + y'\sin\phi)} dx'dy' \tag{3.47}$$

Combining (3.43)-(3.47) gives the radar cross-section

$$\sigma_{TE}(\phi,\phi_{inc}) = \frac{k}{4}\left|\int\int\left(J_x\sin\phi - J_y\cos\phi + \frac{K_z}{\eta}\right)e^{jk(x'\cos\phi+y'\sin\phi)}dx'dy'\right|^2 \qquad (3.48)$$

In the case of a p.e.c. scatterer, the equivalent sources on the surface of the scatterer are purely electric and hence the radar cross-section simplifies to

$$\sigma_{TE}(\phi,\phi_{inc}) = \frac{k}{4}\left|\int\int(J_x\sin\phi - J_y\cos\phi)e^{jk(x'\cos\phi+y'\sin\phi}dx'dy'\right|^2 \qquad (3.49)$$

For TE scattering, one solves for the z-component of the scattered magnetic field which is directly proportional to the electric current on the scatterer. Therefore, the implementation of (3.49) to calculate the radar cross-section for a p.e.c. scatterer does not pose any numerical difficulty.

3.3 Numerical Results

As we indicated earlier, the form given in (3.31) is well-suited for numerical implementation for any arbitrary scatterer enclosed by any arbitrarily-shaped outer boundary Γ_2. Equation (3.31) was used to investigate the problem of scattering by several p. e. c. scatterers using some elongated and conformable outer boundaries. For mesh generation, Patran was used for all of the cases considered. Although (3.31) is valid for any order triangular elements, only first-order elements were used. For the TM case, a mesh density of 13 to 15 nodes per wavelength was used. Whereas for the TE case, to achieve a reasonable accuracy, a mesh density of 15 to 17 nodes per wavelength was

required. It was also noticed that denser meshes are required for larger scatterers.

3.3.1 TM incidence ($E^i = e^{-jkx}$)

The finite element solution gives the z-component of the scattered electric field. As indicated earlier, there is an added error in the radar cross-section computation due to the difficulties encountered in approximating the normal derivative at the outer boundary and, hence, in implementing (3.42). The first scatterer considered was a 4λ strip, shown in Figure 3.3, enclosed by an elongated boundary 1λ away from the end of the strip in the x-direction and 1λ away in the y-direction. The second scatterer was a 2λ by 1λ wedge, for which the outer boundary was chosen to be as conformable as possible to the surface of the scatterer, shown in Figure 3.4. The radar cross-section was calculated using the present method and the method of moments, and the results are shown in Figures 3.5 and 3.6. In both cases, the solutions obtained using the present method agree favorably with those derived via the method of moments. The third scatterer considered was a 9λ strip enclosed by an elongated boundary 1λ away from the end of the strip in the x-direction and 1λ away in the y-direction, shown in Figure 3.7. The near field was calculated on the outer boundary using the present method and the method of moments and plotted versus the angle ϕ where ϕ is as shown in Figures 3.2 and 3.7 (Figure 3.8). When the outer boundary was extended to 2λ away in the y- direction, as shown in Figure 3.7b, the solution obtained using the present method agreed favorably with that computed with the method of moments (Figure 3.9). The fourth scatterer considered was a 8λ by 4λ p.e.c. wedge, and the outer boundary was chosen to be conformable to the surface of the scatterer as shown in Figure 3.10. As Figure 3.11 indicates, the near field on the outer boundary given by the finite element method agrees reasonably well with the method of moments' solution.

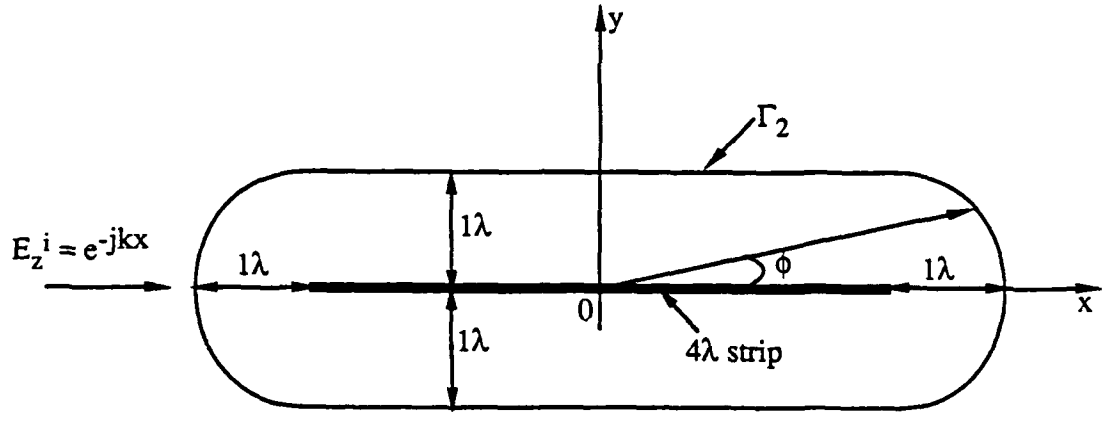

Figure 3.3. A 4λ strip enclosed with an elongated boundary Γ_2 1λ away in the x- and y-directions.

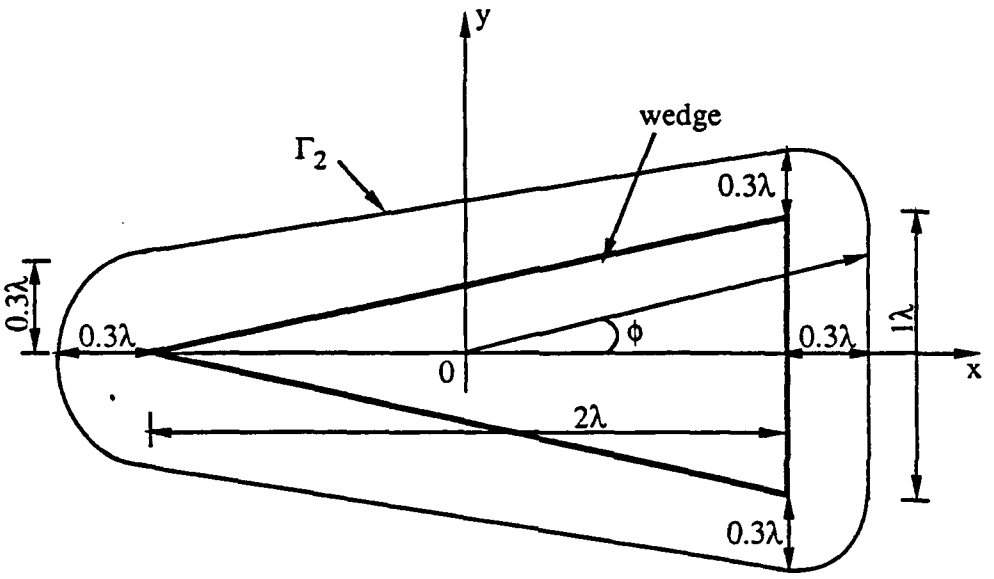

Figure 3.4. A 2λ by 1λ wedge enclosed by an outer boundary Γ_2 having a general shape similar to that of the scatterer.

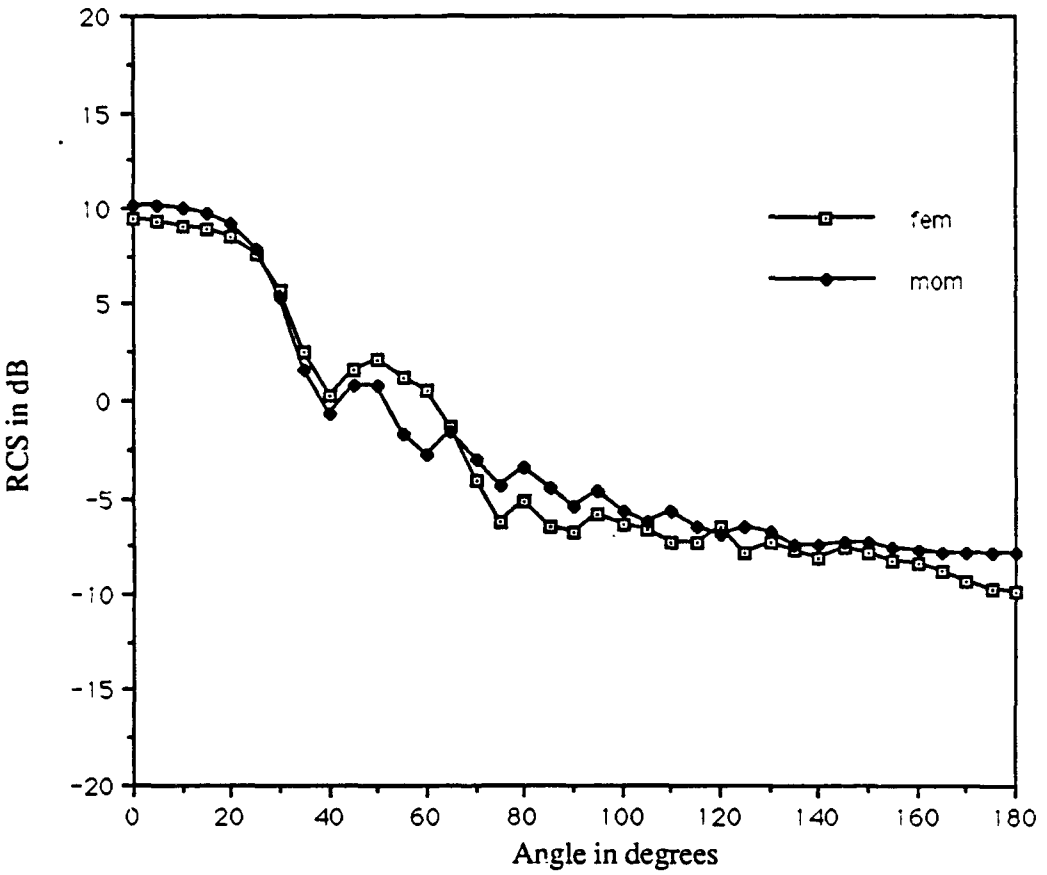

Figure 3.5. Radar cross section of a 4λ strip illuminated by a TM incident wave and enclosed by conformable outer boundary 1 λ away from the surface of the scatterer as shown in Figure 3.3.

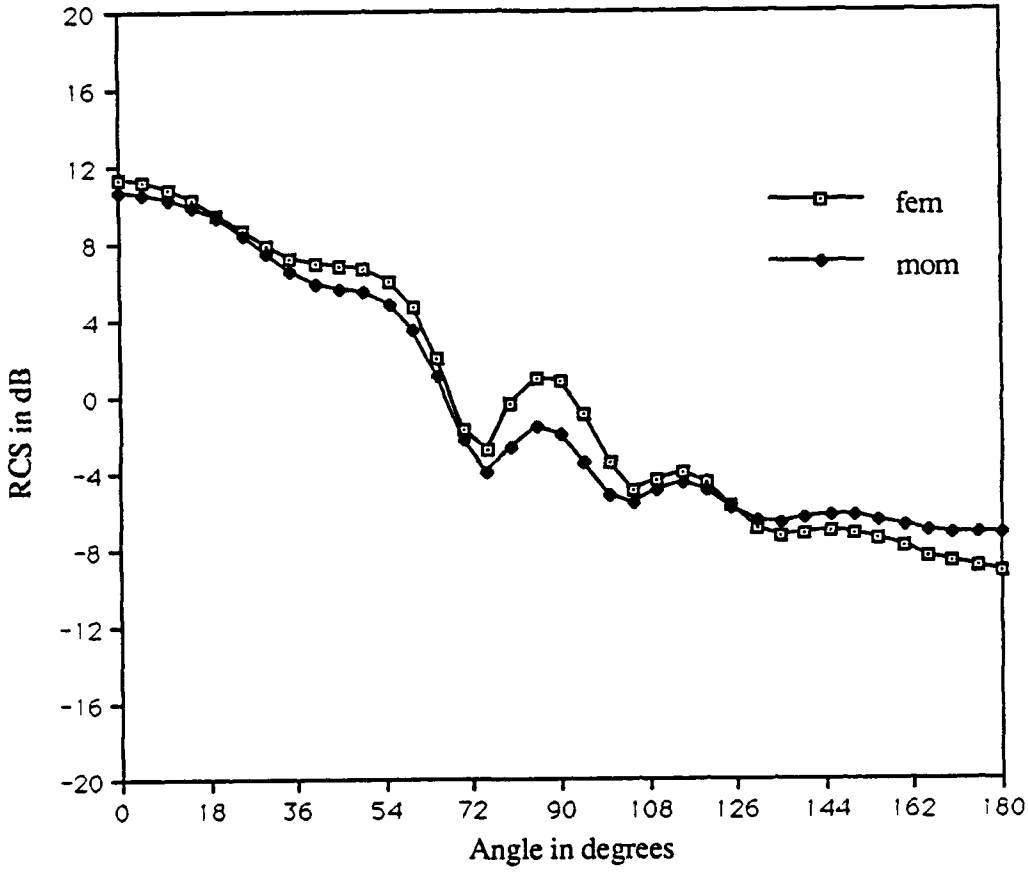

Figure 3.6. Radar cross section of 2λ by 1λ wedge illuminated by a TM incident wave and enclosed by a conformable outer boundary 0.3λ away from the surface of the scatterer as shown in Figure 3.4.

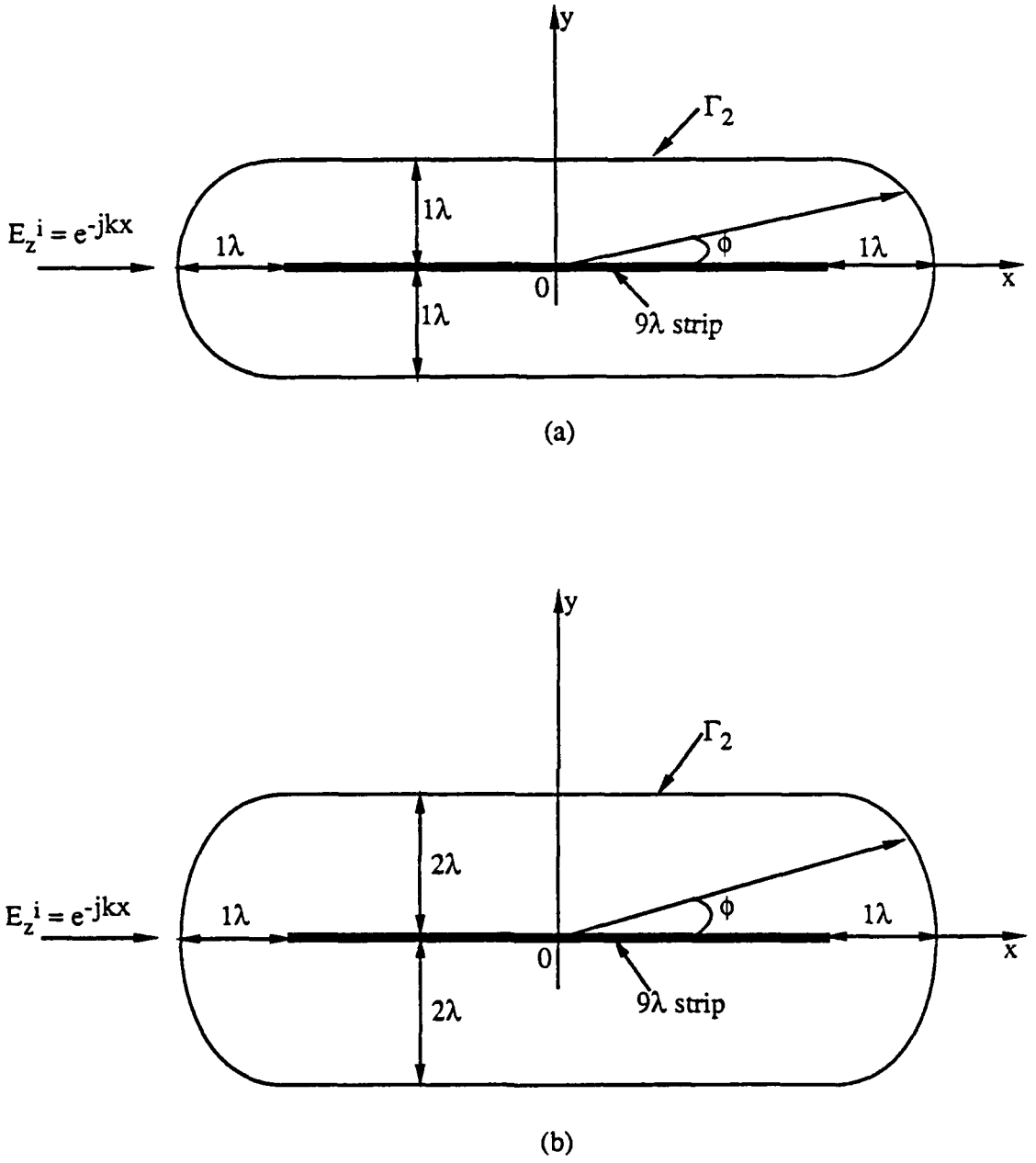

Figure 3.7. A 9λ strip enclosed with an elongated outer boundary Γ_2.

(a) Γ_2 is 1λ away from the surface of the scatterer in the x- and y-directions.

(b) Γ_2 is 1λ away from the surface of the scatterer in the x-direction and 2λ in the y-direction.

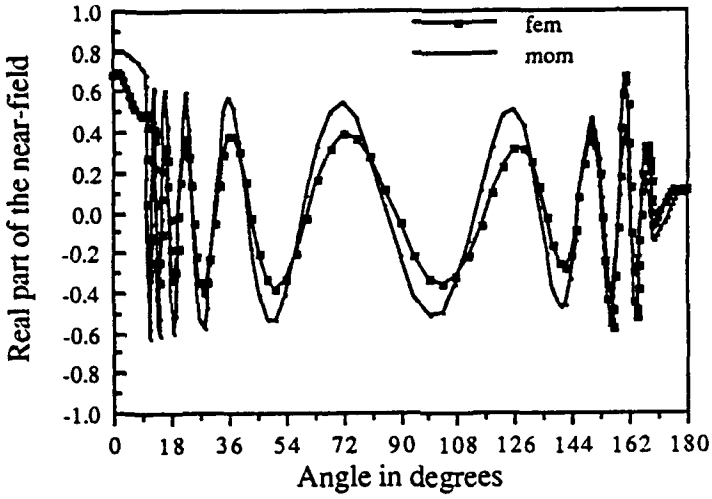

(a)

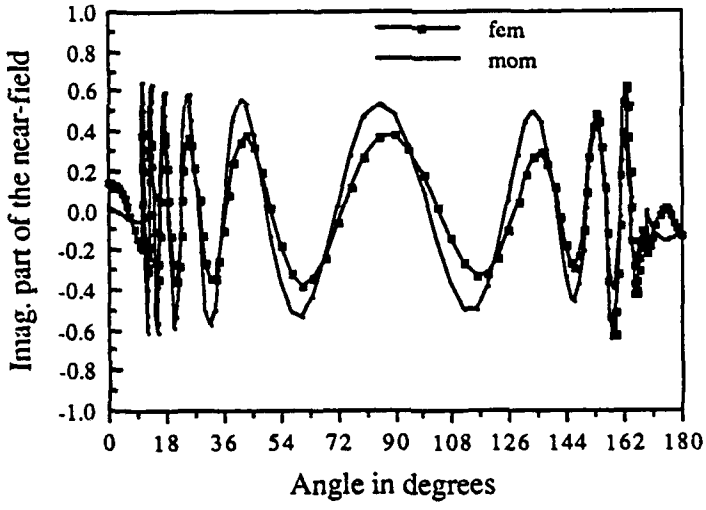

(b)

Figure 3.8. Near field on the outer boundary of a 9 λ strip illuminated by a TM incident wave and enclosed by an elongated boundary as shown in Figure 3.7(a).
a) Real part of near field.
b) Imaginary part of near field.

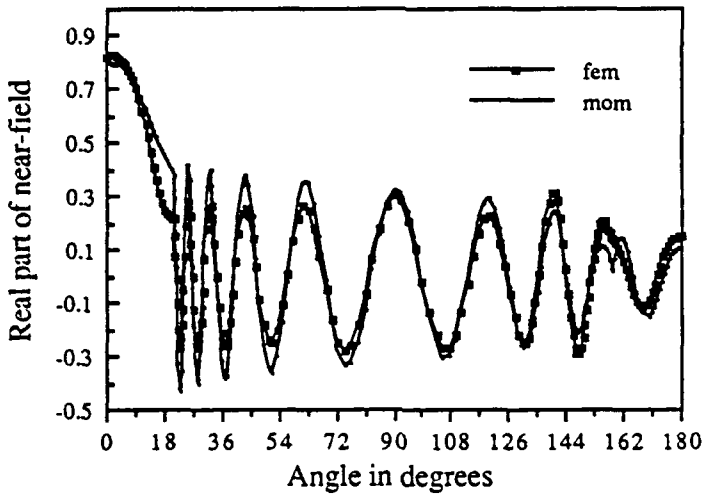

(a)

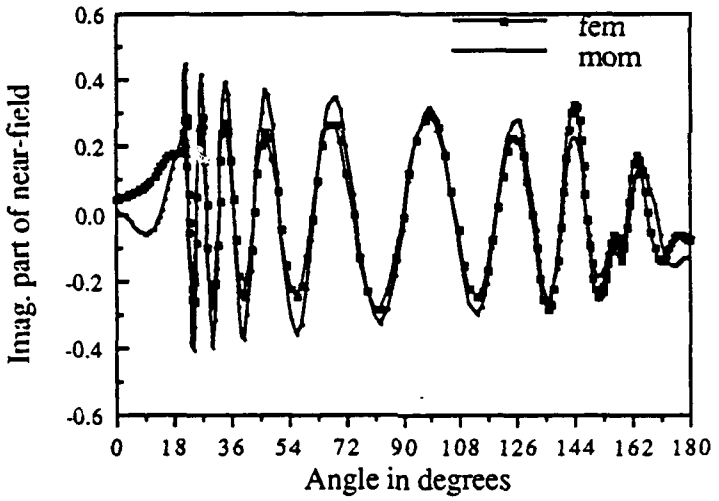

(b)

Figure 3.9. Near field on the outer boundary of a 9λ strip illuminated by a TM incident wave and enclosed by an elongated boundary as shown in Figure 3.7(b).
a) Real part of near field.
b) Imaginary part of near field.

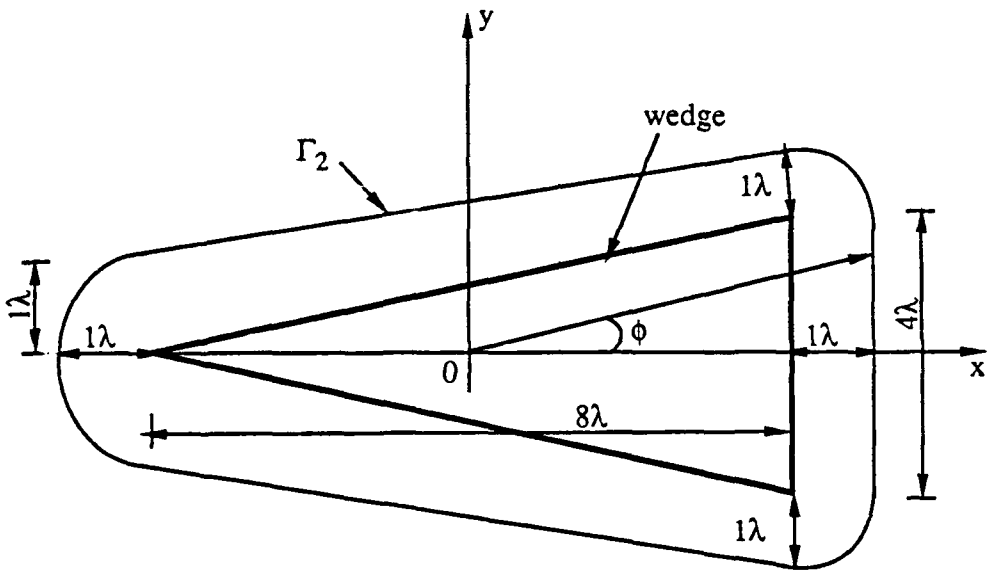

Figure 3.10. An 8λ by 4λ wedge enclosed by an outer boundary Γ_2 having a general shape similar to that of the scatterer.

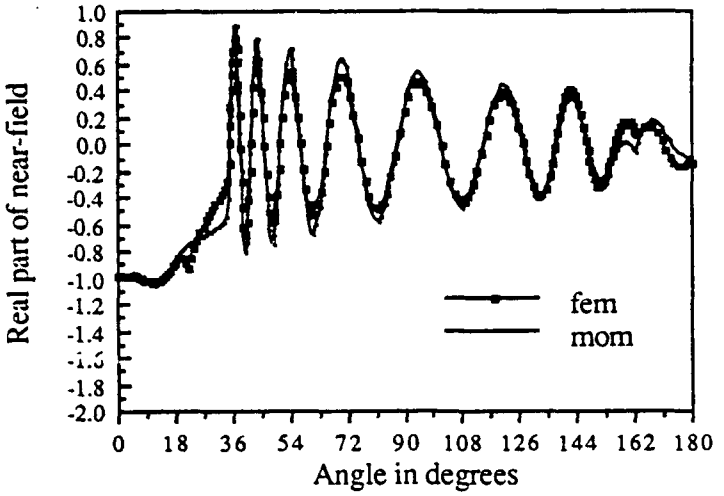

(a)

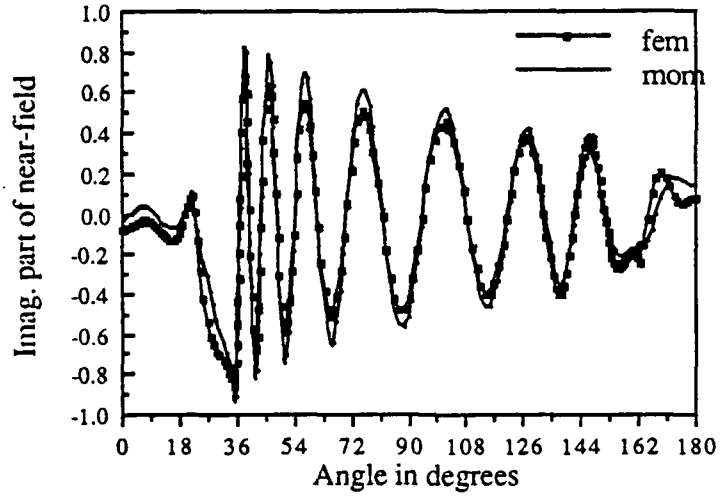

(b)

Figure 3.11. Near field on the outer boundary of an 8λ by 4λ wedge illuminated by a TM incident wave and enclosed by an elongated boundary as shown in Figure 3.10.
a) Real part of near field.
b) Imaginary part of near field.

3.3.2 TE incidence ($H^i = e^{-jky}$)

The finite element solution gives the z-component of the scattered magnetic field. Since the electric current on the p.e.c. scatterer is directly proportional to the magnetic field, the implementation of (3.49) does not represent any numerical difficulty. The wedge shown in Figure 3.4 was illuminated by a TE wave. For this case, the radar cross-section has been computed. As is evident from Figure 3.12, our results compare favorably with those obtained via the method of moments.

In order to achieve a reasonable accuracy for a slender scatterer like a strip, the outer boundary has to be placed a distance between L/10 and 2L/10 in the x-direction and between 2L/10 and 3L/10 in the y-direction away from the surface of the scatterer where L is the total length of the strip. For instance, to achieve a reasonable accuracy for the 9λ strip shown in Figure 3.7b, it was required to place the elongated outer boundary 1λ in the x-direction and 2λ in the y-direction away from the surface of the scatterer. Using a density of 225 nodes/λ^2 and optimizing the mesh, the 9λ strip shown in Figure 3.7b required a mesh size of 8200 nodes. If one were to enclose the 9λ strip with a circular outer boundary having a radius of 5.5λ and using the same mesh density as the one used for the elongated outer boundary, one would end up with a mesh size of 19100 nodes. For a sparse matrix solver the factorization time is proportional to N^2 while the matrix fill time is proportional to N, where N is the total number of nodes. Therefore, the use of an elongated instead of a circular outer boundary resulted in a reduction by a factor of 5.43 in the factorization time and a factor of 2.33 in the matrix fill time. Furthermore, the storage requirement is also reduced by at least a factor of 2.33. Clearly, there is a distinct advantage in using an elongated versus a circular outer boundary.

As the numerical results indicate, while the finite element yielded acceptable results for all the strips and wedges considered, the results for the wedges agreed more favorably

than those of the strips with the method of moments results. This can be explained by the fact that the scattered waves are purely outgoing only in the region outside the smallest circle that entirely encloses the scatterer. For a wedge, where the outer boundary resembles more closely a circular one, there are more points satisfying the above criterion (Figure 3.13) than there are for a strip where the outer boundary is elongated (Figure 3.14). In fact, the presence of incoming waves is more pronounced for the region of the elongated boundary enclosing the strip which is close to the origin.

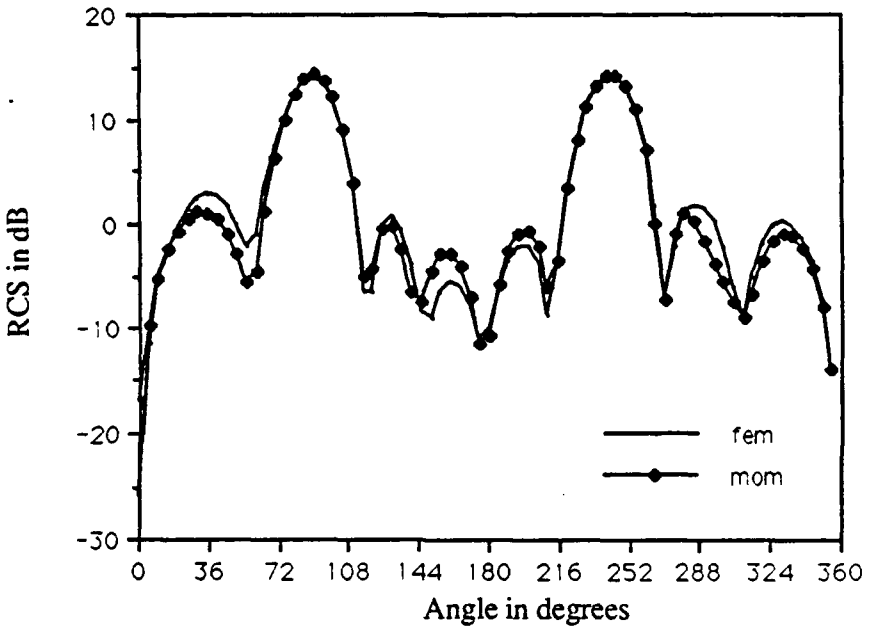

Figure 3.12. Radar cross section of a 2λ by 1λ wedge illuminated by a TE incident wave and enclosed by a conformable outer boundary 0.3λ away from the surface of the scatterer as shown in Figure 3.4.

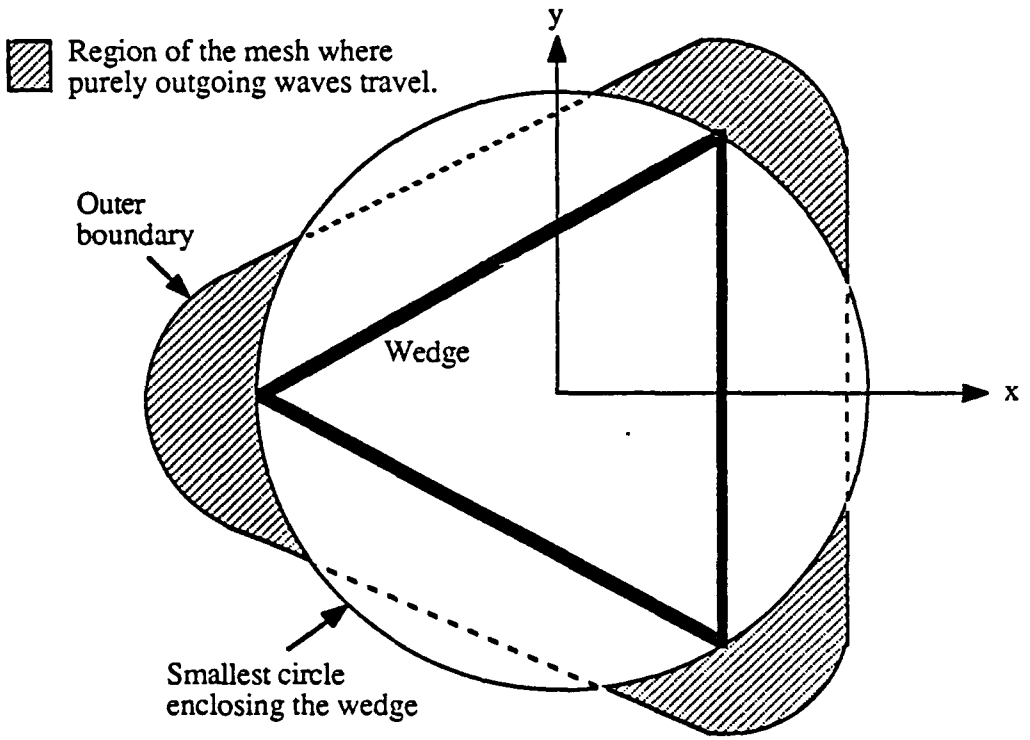

Figure 3.13. Region of purely outgoing waves for a wedge.

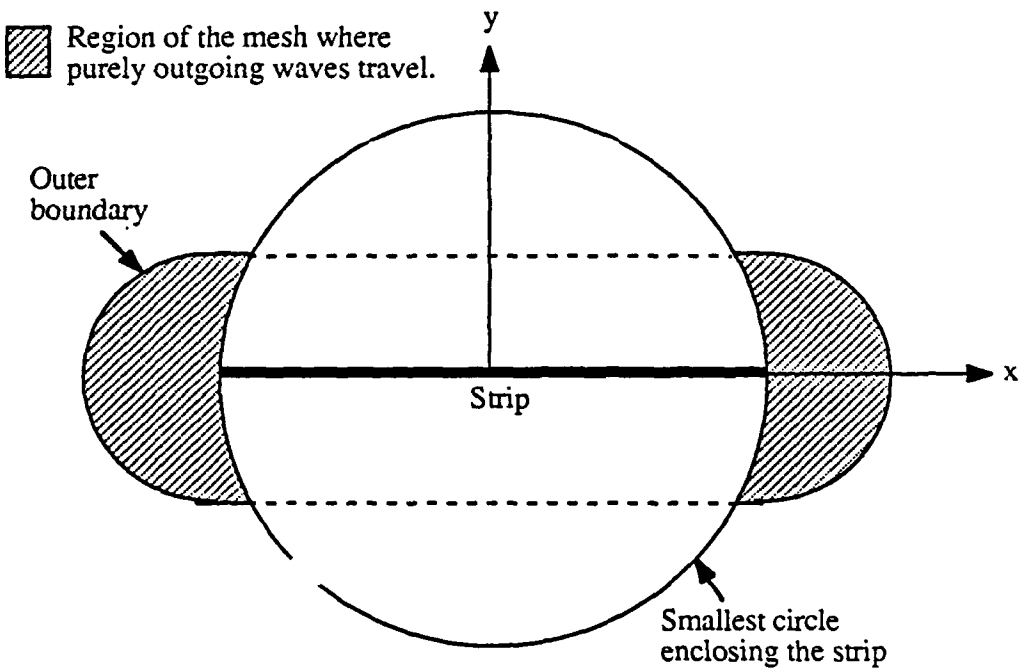

Figure 3.14. Region of purely outgoing waves for a strip.

3.4 Conclusions

In this chapter we have introduced a technique for mesh truncation using an arbitrary outer boundary and have derived the appropriate absorbing boundary condition (ABC) for such a boundary. An important feature of the new boundary condition is that it enables one to use a boundary that conforms to the geometry of the scatterer. The formulation has been verified by comparing the results with those obtained for the method of moments for scattering from a 4λ strip, a 2λ by 1λ wedge, a 9λ strip, and an 8λ by 4λ wedge. We believe that this boundary condition makes it practical to solve the arbitrarely-shaped large-body scattering problems using FEM by reducing the number of mesh points to a more manageable size than would be possible with a circular outer boundary. In Chapter 6, an absorbing boundary condition that takes into account both the lower- and higher-order harmonics, the higher-order absorbing boundary condition, will be addressed.

CHAPTER 4

AN ASYMPTOTIC BOUNDARY CONDITION FOR QUASI-TEM ANALYSIS OF TWO-DIMENSIONAL TRANSMISSION LINE STRUCTURES

4.1 Introduction

Microwave transmission lines have been investigated by many researchers who have employed a variety of methods to study the problem of computing the characteristic impedance and propagation constant along these lines. Some of these techniques include the Fourier transform method [34]-[35], variational method [36]-[37], spectral domain method [38]-[39], Green's function technique [40]-[46], [51], and [54] conformal mapping [47]-[48], boundary element method [49]-[50], and finite-element method [2], [3], and [7]. All but the last three approaches mentioned above are limited to thin strips and/or to structures containing dielectrics with planar interfaces. Although the finite element method method (FEM) is very general, and can handle any arbitrary configuration of conductors and dielectrics, it must deal with the practical problems of mesh truncation and the need for a large number of mesh nodes when applied to an open region problem. One approach to circumventing this difficulty is to truncate the mesh by introducing a fictitious conducting enclosure [2] and [7]. This approach yields satisfactory results only if the actual field decays sufficiently well as it reaches the outer boundary. Typically, this requires one to move the outer boundary far away from the structure in order to achieve acceptable accuracy and, this, in turn, results in a large mesh. An alternative approach is to use "infinite" elements [3], which extend to infinity, and cover the region outside of a fictitious boundary surrounding the structure. Although superior to the artificial p.e.c

boundary method, this approach nonetheless has its own drawbacks. First, the infinite elements require special care during the filling of the FEM matrix. Second, one needs to assume a certain asymptotic behavior of the field within the infinite elements, and this behavior may not be convenient to obtain.

In this chapter, we introduce, once again, the concept of an asymptotic boundary condition which provides us with an efficient means for dealing with the open region problems in the quasi-static regime. This asymptotic boundary condition does not suffer from the complications associated with the infinite elements, and yet enables us to bring the outer boundary much closer to the structure than would be possible with the p.e.c. artificial boundary. Furthermore, unlike many of the available ABCs that are restricted to separable outer boundaries, the one presented in this chapter is useful for an arbitrarily-shaped outer boundary. We will demonstrate the versatility of this new asymptotic boundary condition by considering the examples of one, two, and six conductor microstrip lines.

4.2 Derivation of the Asymptotic Boundary Condition

Figure 4.1 depicts the geometry of an open region problem consisting of N arbitrarily-shaped conductors embedded in a multilayered medium above a ground plane. Let Ω_T denote the region exterior to the conductors. For the finite mathematics techniques [17] and [29], the unbounded outer region Ω_T must be truncated and enclosed with an outer boundary Γ_2. In Chapter 2, we rederived the m^{th} order BGT operator for Laplace's equation. Due to the existence of a ground plane, the general solution to Laplace's equation is slightly different from (2.39). It reads as

$$u(\rho,\phi) = \sum_{n=1}^{\infty} \frac{a_n}{\rho^n} \cos n\phi \tag{4.1}$$

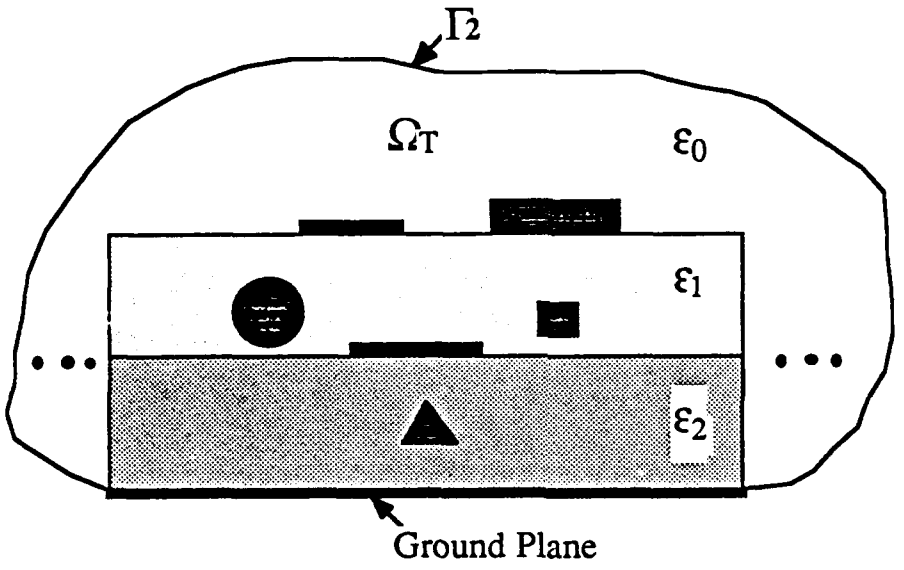

Figure 4.1. Multiconductor transmission line in a multilayered dielectric region above a ground plane.

where u is the potential function. Hence, B_2, the second-order BGT operator, is also slightly different from the one derived in Chapter 2. For the asymptotic form of the solution to Laplace's Equation (4.1), the B_2 operator takes the form

$$B_2 u \equiv \left(\frac{\partial}{\partial \rho} + \frac{3}{\rho}\right)\left(\frac{\partial u}{\partial \rho} + \frac{u}{\rho}\right) = O\left(\frac{1}{\rho^5}\right) \tag{4.2}$$

As will be seen later, the finite element formulation of the problem involves an integral over the outer boundary, Γ_2, and the normal derivative of u appears in this integrand. Hence, for our purposes, it is more desirable to find an asymptotic representation for the normal derivative of u rather than make direct use of the operator B_2. For a circular outer boundary, the normal derivative will simply be the radial one. Using (4.2) along with Laplace's equation to exchange the second-order derivative in ρ, $u_{\rho\rho}$, with the second-order angular derivative, $u_{\phi\phi}$, we obtain the desired asymptotic boundary condition:

$$u_\rho = \alpha(\rho)\, u + \beta(\rho)\, u_{\phi\phi} \tag{4.3}$$

where $\alpha(\rho)$ and $\beta(\rho)$ are given by

$$\alpha(\rho) = -\frac{2}{3\rho} \tag{4.4}$$

$$\beta(\rho) = \frac{1}{3\rho} \tag{4.5}$$

For a general, noncircular outer boundary it is necessary to generalize (4.3) and derive an expression for the normal derivative operator u_n in the local coordinate system (t,n) where t and n are tangent and normal to the boundary, respectively. An approximate expression for

this derivative can be obtained by following the procedure described in Chapter 3 and is given by

$$\frac{\partial u}{\partial n} = \overline{\alpha}\, u + \overline{\gamma}\, u_t + \overline{\beta}\, u_{tt} \tag{4.6}$$

where

$$\overline{\alpha} = (x_0 \sin\theta_0 - y_0 \cos\theta_0)\left(-\frac{2}{3\rho^2}\right) \tag{4.7}$$

$$\overline{\gamma} = \frac{-t\,(x_0 \sin\theta_0 - y_0 \cos\theta_0) + \frac{1}{2}\sin 2\theta_0\,(y_0^2 - x_0^2) + x_0 y_0 \cos 2\theta_0}{\rho^2} \tag{4.8}$$

$$\overline{\beta} = (x_0 \sin\theta_0 - y_0 \cos\theta_0)^3\left(\frac{1}{3\rho^2}\right) \tag{4.9}$$

and θ_0, x_0, y_0, and t are as shown in Figure 3.2.

4.3 Finite Element Implementation of the Asymptotic Boundary Condition

The problem at hand is to solve for the potential u satisfying the Laplace equation:

$$\nabla\cdot(\varepsilon\nabla u) = 0 \tag{4.10}$$

Multiplying (4.10) by a testing function v and integrating over the domain of the problem Ω_T, we obtain

$$\int_{\Omega_T} v\,\nabla\cdot(\varepsilon\nabla u)\,ds = 0 \tag{4.11}$$

From Green's identity we have

$$\int_{\Omega_T} v\,\nabla\cdot(\varepsilon\nabla u)\,ds = -\int_{\Omega_T} \varepsilon\nabla u\cdot\nabla v\,ds + \int_{\Gamma_2} v\,\varepsilon\frac{\partial u}{\partial n}\,dl \tag{4.12}$$

Inserting the above in (4.11), we obtain

$$\int_{\Omega_T} \varepsilon\nabla u\cdot\nabla v\,ds = \int_{\Gamma_2} v\,\varepsilon\frac{\partial u}{\partial n}\,dl \tag{4.13}$$

In the finite element formulation, one sets up a mesh in the region Ω_T, typically using triangular elements. The edges of the outermost elements prescribe Γ_2. Hence, considering one element at a time, the asymptotic boundary condition given in (4.6) may be incorporated into (4.13) to yield

$$\int_{\Omega_T} \varepsilon\nabla u\cdot\nabla v\,ds = \int_{\Gamma_2} v\,\varepsilon\,(\overline{\alpha}\,u + \overline{\gamma}\,u_t + \overline{\beta}\,u_{tt})\,dl \tag{4.14}$$

Since ε is constant over each element, we can integrate (4.14) by parts to obtain

$$\int_{\Omega_T} \varepsilon\nabla u\cdot\nabla v\;ds = \int_{\Gamma_2} \varepsilon\,(\overline{\alpha}\,vu + \overline{\gamma}\,vu_t - \overline{\beta}\,v_t u_t - \overline{\zeta}\,vu_t)\,dl \tag{4.15}$$

where

$$\overline{\zeta} = (x_0\sin\theta_0 - y_0\cos\theta_0)^3 (t + x_0\cos\theta_0 + y_0\sin\theta_0)\left(-\frac{2}{3\rho^4}\right) \tag{4.16}$$

The form given in (4.15) is well-suited for numerical implementation for any arbitrary conductor configuration enclosed by any arbitrarily-shaped outer boundary.

4.4 Numerical Results

4.4.1 One conductor

The microstrip line, shown in Figure 4.2, is enclosed by a rectangular outer boundary. We first solved the potential problem by applying the asymptotic boundary condition, given in Equation (4.6), on a rectangular outer boundary. Next, we introduced a p.e.c. shield at the outer boundary and solved the problem once again using the same mesh. As Table 4.1 indicates the relative error between the asymptotic boundary condition and the published results [45, 52, 53] is between 0.053 and 2.56 percent, whereas the error between the shield and the published results is between 14.55 and 30.04 percent. It is worth mentioning that the distance d from the microstrip line to the outer boundary in the x- and y-directions was chosen to be the same just for convenience, but in principle it needs not to be the same.

4.4.2 Two conductors

Two coupled microstrips, shown in Figure 4.3, are enclosed by a rectangular outer boundary. Table 4.2 presents some results for the same problem that have been published elsewhere [55], together with those obtained by using a p.e.c. shield and the asymptotic boundary condition in (4.6). The relative error in the self-terms is 0.27 percent for the

Table 4.1a. Characteristic impedance in Ohms for the microstrip line of Figure 4.2 ($\varepsilon_r = 6.0$).

w/h	ABC	Shield	Ref.[45]	Ref.[52]	Ref.[53]	Bound. location	Error ABC-[53]	Error Shield-[53]
0.4	90.797	62.892	92.278	91.172	89.909	0.65	0.987%	30.049%
0.7	73.000	53.543	73.962	73.613	71.995	0.75	1.396%	25.630%
1.0	62.531	45.650	62.811	62.713	60.970	0.75	2.560%	25.127%
2.0	41.922	34.778	42.998	43.149	41.510	1.20	0.992%	16.218%
4.0	26.047	22.018	26.971	27.301	26.027	1.50	0.077%	15.403%

Table 4.1b. Characteristic impedance in Ohms for the microstrip line of Figure 4.2 ($\varepsilon_r = 9.5$).

w/h	ABC	Shield	Ref.[45]	Ref.[52]	Ref.[53]	Bound. location	Error ABC-[53]	Error Shield-[53]
0.4	73.380	51.513	74.897	73.702	73.290	0.65	0.123%	29.713%
0.7	58.955	43.841	59.910	59.379	58.502	0.75	0.774%	25.061%
1.0	50.453	37.395	50.810	50.501	49.431	0.75	2.067%	24.350%
2.0	33.766	28.322	34.674	34.592	33.493	1.20	0.815%	15.439%
4.0	20.917	17.863	21.668	21.763	20.906	1.50	0.053%	14.556%

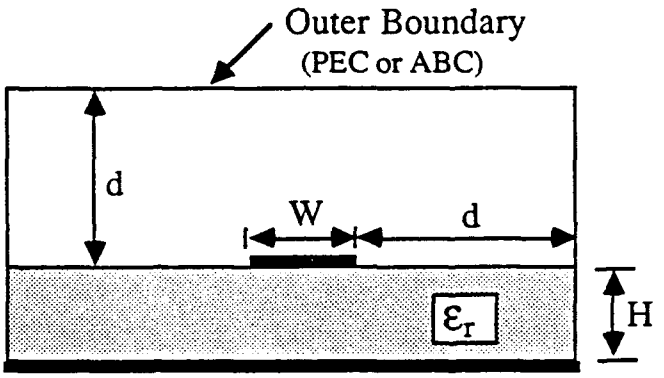

Figure 4.2. Microstrip line.

asymptotic boundary condition and 18.31 percent for the shield, and the error in the mutual terms is 5.2 percent for the asymptotic boundary condition and 44.59 percent for the shield.

Table 4.2. Capacitance matrix for the coupled microstrips of Figure 4.3.

C(i,j)	ABC	Shield	Reference [55]	Error ABC-[55]	Error Shield-[55]
C(1,1)	0.9249×10^{-10}	0.1091×10^{-9}	0.9224×10^{-10}	0.271%	18.310%
C(1,2)	-0.8061×10^{-11}	-0.4712×10^{-11}	-0.8504×10^{-11}	5.203%	44.591%
C(2,1)	-0.8061×10^{-11}	-0.4712×10^{-11}	-0.8504×10^{-11}	5.203%	44.591%
C(2,2)	0.9249×10^{-10}	0.1091×10^{-9}	0.9224×10^{-10}	0.271%	18.310%

4.4.3 Six conductors

The six conductor system, shown in Figure 4.4, is enclosed, once again, by a rectangular outer boundary. To the best of our knowledge, there are no published results for this configuration. However, we have compared our results with those derived by using the computer program developed by Harms et al. [56], which uses an integral equation formulation and an iterative method of solution. As Table 4.3 indicates, the relative error for the capacitance matrix is between 0.84 and 14.52 percent for the asymptotic boundary condition and between 3.95 and 74.10 percent for the p.e.c shield. That the distance D (Figure 4.4) from the microstrip line to the outer boundary in the x- and y-directions was chosen to be the same just for convenience, but in principle it needs not to be the same.

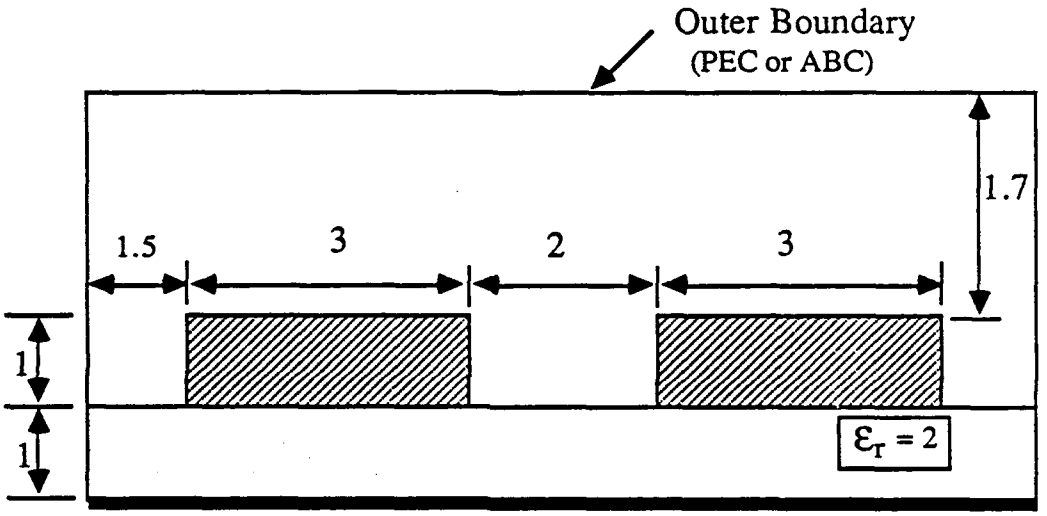

Figure 4.3. Coupled microstrips with rectangular outer boundary.

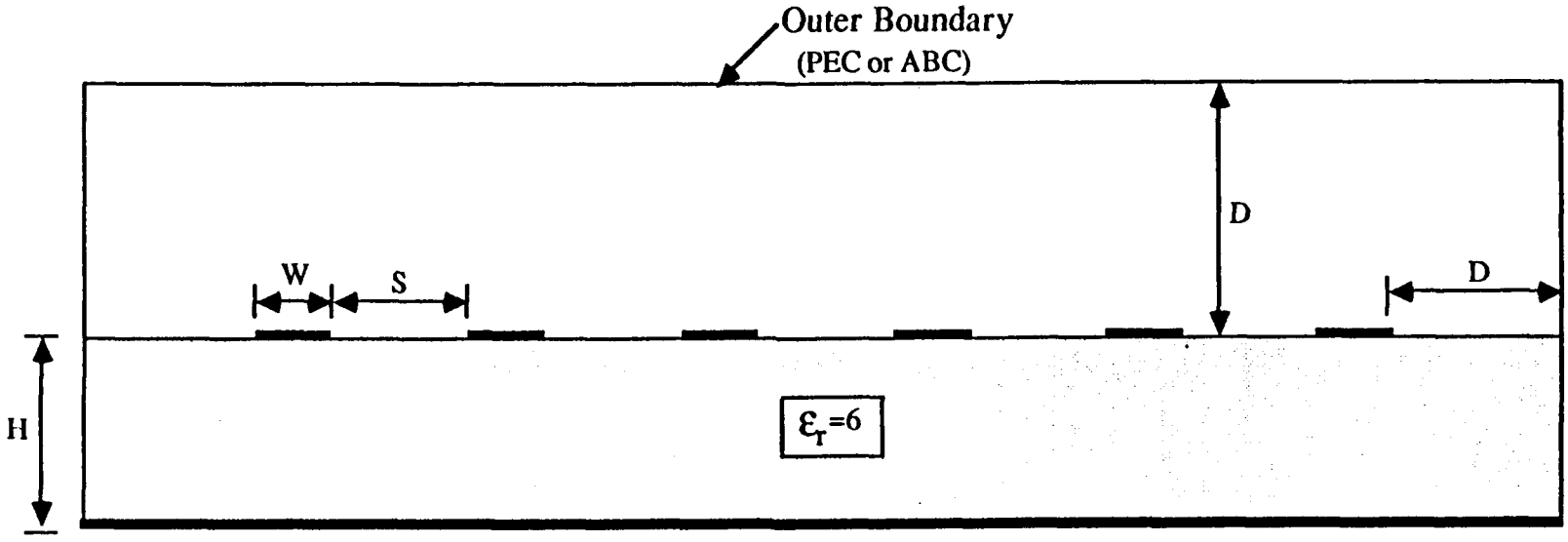

S=1 W=1
H=8 D=2

Figure 4.4. Six-conductor geometry.

Table 4.3. Capacitance matrix for the six-condutor structure of Figure 4.4.

C(i,j)	Iterative [56]	ABC	Shield	Error ABC-[56]	Error Shield-[56]
C(1,1)	0.668×10^{-10}	0.686×10^{-10}	0.848×10^{-10}	2.620%	26.83%
C(1,2)	-0.279×10^{-10}	-0.315×10^{-10}	-0.264×10^{-10}	13.05%	5.340%
C(1,3)	-0.549×10^{-11}	-0.600×10^{-11}	-0.371×10^{-11}	9.240%	32.56%
C(1,4)	-0.208×10^{-11}	-0.225×10^{-11}	-0.117×10^{-11}	8.320%	43.71%
C(1,5)	-0.999×10^{-12}	-0.101×10^{-11}	-0.456×10^{-12}	0.840%	54.30%
C(1,6)	-0.704×10^{-12}	-0.602×10^{-12}	-0.182×10^{-12}	14.52%	74.10%
C(2,1)	-0.279×10^{-10}	-0.315×10^{-10}	-0.264×10^{-10}	13.05%	5.34%
C(2,2)	0.789×10^{-10}	0.848×10^{-10}	0.876×10^{-10}	7.480%	11.03%
C(2,3)	-0.256×10^{-10}	-0.284×10^{-10}	-0.266×10^{-10}	11.10%	3.960%
C(2,4)	-0.465×10^{-11}	-0.487×10^{-11}	-0.385×10^{-11}	4.740%	17.23%
C(2,5)	-0.173×10^{-11}	-0.181×10^{-11}	-0.122×10^{-11}	4.610%	29.03%
C(2,6)	-0.999×10^{-12}	-0.101×10^{-11}	-0.456×10^{-12}	0.920%	54.30%
C(3,1)	-0.549×10^{-11}	-0.600×10^{-11}	-0.371×10^{-11}	9.240%	32.56%
C(3,2)	-0.256×10^{-10}	-0.284×10^{-10}	-0.266×10^{-10}	11.10%	3.960%
C(3,3)	0.794×10^{-10}	0.855×10^{-10}	0.874×10^{-10}	7.680%	10.14%
C(3,4)	-0.254×10^{-10}	-0.282×10^{-10}	-0.267×10^{-10}	10.91%	4.870%
C(3,5)	-0.465×10^{-11}	-0.487×10^{-11}	-0.385×10^{-11}	4.750%	17.23%
C(3,6)	-0.208×10^{-11}	-0.226×10^{-11}	-0.117×10^{-11}	8.410%	43.71%
C(4,1)	-0.208×10^{-11}	-0.225×10^{-11}	-0.117×10^{-11}	8.320%	43.71%
C(4,2)	-0.465×10^{-11}	-0.487×10^{-11}	-0.385×10^{-11}	4.740%	17.23%
C(4,3)	-0.254×10^{-10}	-0.282×10^{-10}	-0.267×10^{-10}	10.91%	4.870%
C(4,4)	0.794×10^{-10}	0.855×10^{-10}	0.874×10^{-10}	7.680%	10.14%
C(4,5)	-0.256×10^{-10}	-0.284×10^{-10}	-0.266×10^{-10}	11.10%	3.960%
C(4,6)	-0.549×10^{-11}	-0.601×10^{-11}	-0.371×10^{-11}	9.310%	32.56%
C(5,1)	-0.999×10^{-12}	-0.101×10^{-11}	-0.456×10^{-12}	0.840%	54.30%
C(5,2)	-0.173×10^{-11}	-0.181×10^{-11}	-0.122×10^{-11}	4.610%	29.03%
C(5,3)	-0.465×10^{-11}	-0.487×10^{-11}	-0.385×10^{-11}	4.750%	17.23%
C(5,4)	-0.256×10^{-10}	-0.284×10^{-10}	-0.266×10^{-10}	11.10%	3.960%
C(5,5)	0.789×10^{-10}	0.848×10^{-10}	0.876×10^{-10}	7.480%	11.03%
C(5,6)	-0.279×10^{-10}	-0.316×10^{-10}	-0.264×10^{-10}	13.08%	5.340%
C(6,1)	-0.704×10^{-12}	-0.602×10^{-12}	-0.182×10^{-12}	14.52%	74.10%
C(6,2)	-0.999×10^{-12}	-0.101×10^{-11}	-0.456×10^{-12}	0.920%	54.30%
C(6,3)	-0.208×10^{-11}	-0.226×10^{-11}	-0.117×10^{-11}	8.410%	43.71%
C(6,4)	-0.549×10^{-11}	-0.601×10^{-11}	-0.371×10^{-11}	9.310%	32.56%
C(6,5)	-0.279×10^{-10}	-0.316×10^{-10}	-0.264×10^{-10}	13.08%	5.340%
C(6,6)	0.668×10^{-10}	0.685×10^{-10}	0.848×10^{-10}	2.550%	26.83%

In all of the three numerical examples considered thus far, we have chosen a rectangular outer boundary because it facilitates the meshing procedure and because it is conformal to the structures considered. This meshing is done in a manner such that none of the triangular elements have more than one edge on the outer boundary. Since the finite element scheme considers one element at a time, the problem of the undefined normal at the rectangular corners is circumvented when the procedure described above is followed.

In order to illustrate the fact that the formulation described in this work is also applicable to an arbitrary outer boundary, we reconsider the two-conductor example described earlier. Figure 4.5 illustrates the coupled microstrips problem with an arbitrary outer boundary. Table 4.4 shows that the results obtained for this case are almost identical to those derived with the rectangular boundary.

Table 4.4. Capacitance matrix for the coupled microstrips of Figures 4.3 and 4.5.

C(i,j)	ABC with rectangular outer boundary	Reference [55]	ABC with arbitrary outer boundary
C(1,1)	0.9249×10^{-10}	0.9224×10^{-10}	0.9284×10^{-10}
C(1,2)	-0.8061×10^{-11}	-0.8504×10^{-11}	-0.8036×10^{-11}
C(2,1)	-0.8061×10^{-11}	-0.8504×10^{-11}	-0.8036×10^{-11}
C(2,2)	0.9249×10^{-10}	0.9224×10^{-10}	0.9284×10^{-10}

In order to illustrate the fact that the asymptotic boundary condition yields a significant saving in computer time and storage over the p.e.c shield, we reconsider the examples of one- and two-conductor described earlier. Table 4.5 shows the characteristic impedance for the microstrip line of Figure 4.2 using a p.e.c. shield as a boundary

condition for different values of the boundary location (d). As Table 4.5 indicates, the p.e.c. shield has to be placed at a distance d=4, instead of d=1 as for the asymptotic boundary condition, in order to achieve an acceptable accuracy. Using a density of 64 nodes/unit square, the configurations of Figure 4.2 required a mesh size of 384 and 2880 nodes if an asymptotic boundary condition and a p.e.c. shield were, respectively, used. For a sparse matrix solver the factorization time is proportional to N^2 while the matrix fill time is proportional to N, where N is the total number of nodes. Hence, the use of the asymptotic boundary condition instead of a p.e.c. shield for the one-conductor configuration of Figure 4.2 resulted in a reduction factor of 56.25 in the factorization time and 7.5 in the matrix fill time. In addition, the storage requirement is also reduced by at least a factor of 7.5.

Table 4.5. Characteristic impedance in Ohms for the microstrip line of Figure 4.2 using a p.e.c. shield as an outer boundary (ε_r = 6.0 and w/h = 1.0).

boundary location (d)	Shield	Reference [53]	Error Shield-[53]
0.75	45.650	60.970	25.12%
3.0	57.33		5.96%
4.0	58.869		3.44%

Figure 4.6 shows the coupled microstrips with the outer boundary placed at a distance equal to 7.5, instead of 1.5 as in Figure 4.3, in the x-direction and 8.0, instead of 1.7 as in Figure 4.3, in the y-direction. As Table 4.6 and Figure 4.6 indicate, the coupled microstrips configuration required, using a density of 64 nodes/unit square, a mesh size of

2120 and 12305 nodes if an asymptotic boundary condition and a p.e.c. shield were, respectively, used. For a sparse matrix solver the factorization time is proportional to N^2 while the matrix fill time is proportional to N, where N is the total number of nodes. Hence, the use of the asymptotic boundary condition instead of a p.e.c. shield for the coupled microstrips configuration of Figure 4.3 and 4.6 resulted in a reduction factor of 33.68 in the factorization time and 5.8 in the matrix fill time. In addition, the storage requirement is also reduced by at least a factor of 5.8. Obviously, there is great advantage in using an asymptotic boundary condition.

Table 4.6. Capacitance matrix for the coupled microstrips of Figure 4.6.

C(i,j)	Shield	Reference [55]	Error Shield-[55]
C(1,1)	0.8845×10^{-10}	0.9224×10^{-10}	4.1%
C(1,2)	-0.7982×10^{-11}	-0.8504×10^{-11}	6.14%
C(2,1)	-0.7982×10^{-11}	-0.8504×10^{-11}	6.14%
C(2,2)	0.8845×10^{-10}	0.9224×10^{-10}	4.1%

Finally, we point out that no special treatment is needed at the dielectric interfaces because in the finite element formulation the medium is modeled as being homogeneous within each element and, consequently, the line integral in Equation (4.15) is always confined to within a homogeneous region inside the element.

The term "Error" that appeared several times in the Tables should not be interpreted as an absolute error but rather as a difference between our results and the published ones.

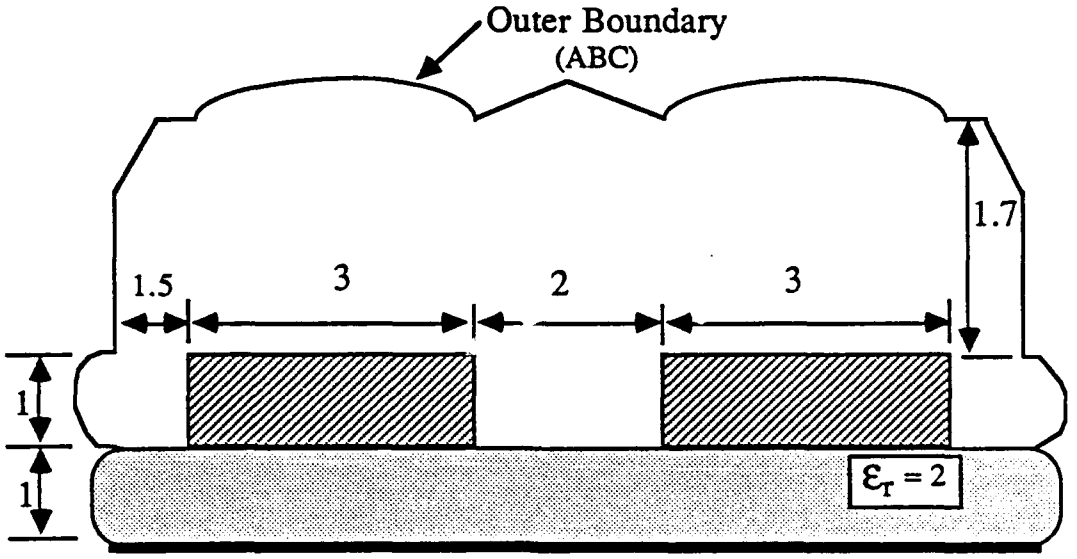

Figure 4.5. Coupled microstrips with arbitrary outer boundary.

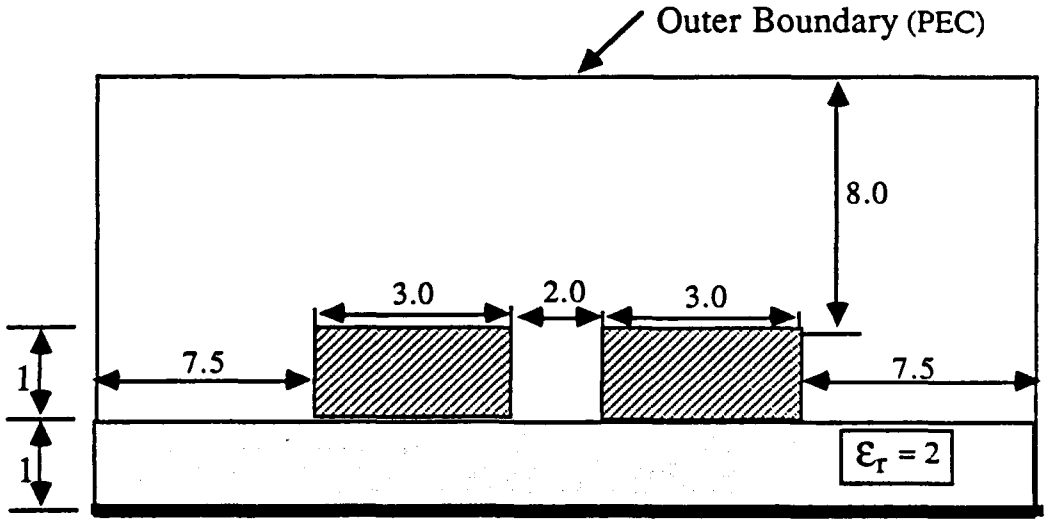

Figure 4.6. Coupled microstrips with rectangular outer boundary.

4.5 Conclusions

In this chapter, we have shown how an asymptotic boundary condition for quasi-static fields can be applied to a potential field at distances quite close to a transmission line configuration to derive an FEM-based solution in a numerically efficient manner. It is evident from the numerical results that the asymptotic boundary condition consistently yields more accurate results than those obtainable with a perfectly conducting shield placed at the same location. However, in some situations, the accuracy obtained with the approximate ABC presented in this chapter may still not be adequate, as for instance in the off-diagonal terms of the capacitance matrix in the six-conductor configuration. This aspect of the problem will be investigated further in Chapter 6 where an improved version of the asymptotic boundary condition will be derived. In the next chapter, the three-dimensional version of the asymptotic boundary condition will be addressed.

CHAPTER 5

ASYMPTOTIC BOUNDARY CONDITIONS FOR QUASI-TEM ANALYSIS OF THREE-DIMENSIONAL TRANSMISSION LINE DISCONTINUITIES

5.1 Introduction

In Chapter 4, an asymptotic boundary condition was introduced and applied to two-dimensional transmission line structures. Typically, a printed circuit board contains not only uniform transmission line etches that are essentially invariant in the longitudinal direction, but also chip sockets and connectors for interboard communication that can not be modeled as uniform lines. Furthermore, the transmission lines themselves may have various discontinuities such as bends, changes in width, open circuits, gaps and steps. In recent years, there has been an increasing interest in modeling such discontinuities, and a number of papers [4] and [57]-[72] have been written on this subject. In most of these papers, the integral equation technique has been used to study planar conductors and structures containing a homogeneous dielectric with planar interfaces. Castillo [4] has used the finite element method (FEM), which can handle any arbitrary configuration of conductors and dielectrics. When using the FEM, one needs to deal with the practical problem of mesh truncation and the large number of mesh nodes. Similar to the two-dimensional problems, the most widely-used approach for dealing with the mesh truncation problem for the three-dimensional geometry is to place a fictitious, box-type conducting enclosure sufficiently far from the structure [4]. This approach, which assumes that the field decays significantly before reaching the outer boundary, typically results in an undesirably large mesh, especially for three-dimensional geometries. In Chapter 4, we

have introduced an asymptotic boundary condition (ABC), which provided us with an efficient means for dealing with open region two-dimensional microwave transmission line problems in the quasi-static regime. The usefulness of the ABC for obtaining an accurate solution to a problem with a reasonable number of node points was demonstrated in that chapter. For three-dimensional problems, where the total number of mesh points is usually large, it is expected that the availability of an accurate ABC will play an even more crucial role in the solution of practical problems.

In this chapter, we use a similar, but more elaborate approach than in Chapter 4 to derive an asymptotic boundary condition for three-dimensional open region problems in the quasi-static regime. Once again, this asymptotic boundary condition enables us to bring the outer boundary much closer to the structure than would be possible with the p.e.c. artificial boundary. In order to reduce the number of unknowns as much as possible, we have chosen an outer boundary in the shape of a parallelepiped (we will refer to it in this chapter as a box for the sake of brevity) because it is the most conformable to the structures considered.

5.2 Derivation of the Three-Dimensional Asymptotic Boundary Conditions

The asymptotic or the absorbing boundary condition has seen an increasing use in connection with the partial differential equation (PDE) techniques for solving open region electromagnetic problems because it preserves the sparsity of the discretized PDE matrix [16]-[29] and [32]. In this section, we use a similar approach to the one in Chapter 4 to derive an asymptotic boundary condition for three-dimensional quasi-static problems.

Consider the three-dimensional open region problem consisting of an arbitrarily-shaped discontinuity embedded in a multilayered medium above a ground plane shown in Figure 5.1. Let Ω_T be the region exterior to the conductors and Γ_2 be the outer boundary.

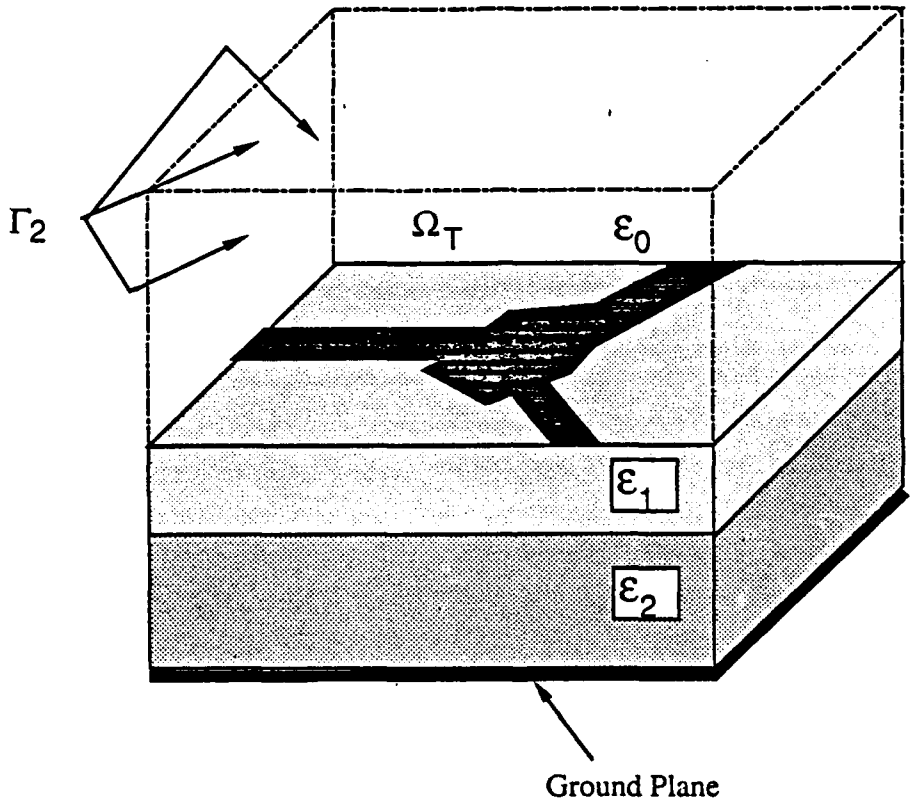

Figure 5.1. Geometry for the finite element approach to the problem of a general transmission line discontinuity in a multilayered dielectric region above a ground plane.

Our objective is to derive an operator which, when applied on the outer boundary, makes the field emulate the asymptotic behavior at infinity, and thus yields an accurate result for the interior region with only a moderate number of nodes. Equivalently, we accomplish this task by imposing an asymptotic boundary condition (ABC) on the field on the outer boundary.

The boundary value problem to be solved can be expressed by the set of equations:

$$\nabla\cdot(\varepsilon\nabla u) = 0 \quad \text{in } \Omega_T \tag{5.1}$$

$$u = g_i \text{ on the } i^{th} \text{ conductor} \tag{5.2}$$

$$B_m u = 0 \text{ on } \Gamma_2 \tag{5.3}$$

where u *is the electrostatic potential,* g_i *is the potential on the* conductors, and B_m is the m^{th} order asymptotic boundary operator.

For large r, the general solution of the Laplace equation in spherical coordinates can be written in terms of spherical harmonics and powers of r as [62]

$$u(r,\theta,\phi) = \sum_{l=0}^{\infty}\sum_{m=-l}^{l} \frac{B_{lm}}{r^{l+1}} Y_{lm}(\theta,\phi) \tag{5.4}$$

where $Y_{lm}(\theta,\phi)$ are spherical harmonics. Equation (5.4) can be rewritten in the following form

$$u(r,\theta,\phi) = \sum_{l=0}^{\infty} \frac{1}{r^{l+1}} F_{lm}(\theta,\phi) \tag{5.5}$$

where

$$F_{lm}(\theta,\phi) = \sum_{m=-l}^{l} B_{lm}\, Y_{lm}(\theta,\phi) \tag{5.6}$$

or more explicitly as

$$u(r,\theta,\phi) = \frac{1}{r} F_{1m}(\theta,\phi) + \frac{1}{r^2} F_{2m}(\theta,\phi) + \frac{1}{r^3} F_{3m}(\theta,\phi) + \ldots \tag{5.7}$$

We will now derive a set of boundary condition operators that can be applied on the artificial boundary. From (5.7), we note

$$\frac{\partial u}{\partial r} + \frac{u}{r} = O\left(\frac{1}{r^3}\right) \tag{5.8}$$

We then define the first-order operator B_1 as

$$B_1 u \equiv \frac{\partial u}{\partial r} + \frac{u}{r} = O\left(\frac{1}{r^3}\right) \tag{5.9}$$

The second-order operator can be obtained by letting $v = B_1 u$ and by observing that

$$\frac{\partial v}{\partial r} + \frac{3v}{r} = O\left(\frac{1}{r^5}\right) \tag{5.10}$$

The second-order operator B_2 can thus be defined as

$$B_2 u \equiv \left(\frac{\partial}{\partial r} + \frac{3}{r}\right)\left(\frac{\partial u}{\partial r} + \frac{u}{r}\right) = O\left(\frac{1}{r^5}\right) \tag{5.11}$$

In general, it can be shown that the m^{th} order asymptotic boundary condition operator can be written as

$$B_m u = \prod_{j=1}^{m}\left(\frac{\partial}{\partial r} + \frac{2j-1}{r}\right)u \tag{5.12}$$

The boundary contribution in the finite element formulation enters into a surface integral representation over the outer boundary, Γ_2, where the integrand is the product of a testing function and the normal derivative of u. As a consequence, the asymptotic boundary condition needs to be imposed on the normal derivative of u. For a spherical outer boundary, the normal derivative is simply the radial one. Using (5.11) in conjunction with Laplace's equation in the spherical coordinates, we obtain the following asymptotic boundary condition operator

$$u_r = \alpha(r)u + \beta(r)u_\theta + \gamma(r)u_{\theta\theta} + \xi(r)u_{\phi\phi} \tag{5.13}$$

where

$$\alpha(r) = -\frac{1}{r} \tag{5.14}$$

$$\beta(r) = \frac{\cot\theta}{2r} \tag{5.15}$$

$$\gamma(r) = \frac{1}{2r} \tag{5.16}$$

$$\xi(r) = \frac{1}{2r \sin^2\theta} \tag{5.17}$$

As indicated earlier, we need to use a conformable outer boundary in order to minimize the number of node points as much as possible. For three-dimensional transmission line structures, this conformable outer boundary should be a box. It is, therefore, necessary to derive the appropriate normal derivative expressions for the different faces of the box representing the outer boundary.

For the x=constant face of the box, the normal derivative is plus or minus u_x. Using the Chain rule, we can write u_x as

$$u_x = \frac{\partial u}{\partial r}\frac{\partial r}{\partial x} + \frac{\partial u}{\partial \theta}\frac{\partial \theta}{\partial x} + \frac{\partial u}{\partial \phi}\frac{\partial \phi}{\partial x} \tag{5.18}$$

Using the relations between the Cartesian and spherical coordinates, Equation (5.18) can be rewritten as

$$u_x = \frac{\partial u}{\partial r}\left(\frac{x}{r}\right) + \frac{\partial u}{\partial \theta}\left(\frac{zx}{r^2\rho}\right) + \frac{\partial u}{\partial \phi}\left(-\frac{y}{\rho^2}\right) \tag{5.19}$$

where $\rho = (x^2 + y^2)^{1/2}$ and $r = (x^2 + y^2 + z^2)^{1/2}$.

Using (5.12) - (5.19), the Chain rule, and the relations between the angular and the tangential derivatives, we obtain a final expression for the normal derivative on the face where x=constant and u_x is

$$\begin{aligned} u_x = {} & \alpha_1(x,y,z)u + \beta_1(x,y,z)u_z + \gamma_1(x,y,z)u_{zz} \\ & + \zeta_1(x,y,z)u_y + \eta_1(x,y,z)u_{yy} + \xi_1(x,y,z)u_{yz} \end{aligned} \tag{5.20}$$

where

$$\alpha_1(x,y,z) = -\frac{x}{r^2} \tag{5.21}$$

$$\beta_1(x,y,z) = -z\frac{3x^3+4xy^2}{2r^2\rho^2} \tag{5.22}$$

$$\gamma_1(x,y,z) = \frac{x^3 + xy^2}{2r^2} \tag{5.23}$$

$$\zeta_1(x,y,z) = \frac{4x^3yz^2+ 3xy^3z^2-xy(\rho^4 + 2r^2\rho^2)}{2r^2\rho^4} \tag{5.24}$$

$$\eta_1(x,y,z) = \frac{z^2y^2x + x^3r^2}{2r^2\rho^2} \tag{5.25}$$

$$\xi_1(x,y,z) = -\frac{zxy}{r^2} \tag{5.26}$$

On the y=constant face, the normal derivative is plus or minus u_y. Invoking the Chain rule, once again, we can express u_y as

$$u_y = \frac{\partial u}{\partial r}\frac{\partial r}{\partial y} + \frac{\partial u}{\partial \theta}\frac{\partial \theta}{\partial y} + \frac{\partial u}{\partial \phi}\frac{\partial \phi}{\partial y} \tag{5.27}$$

Following the same procedure as before, we obtain the following expression for u_y

$$u_y = \alpha_2(x,y,z)u + \beta_2(x,y,z)u_z + \gamma_2(x,y,z)u_{zz} + \zeta_2(x,y,z)u_x + \eta_2(x,y,z)u_{xx} + \xi_2(x,y,z)u_{xz} \tag{5.28}$$

where

$$\alpha_2(x,y,z) = -\frac{y}{r^2} \tag{5.29}$$

$$\beta_2(x,y,z) = -z\frac{3y^3+4yx^2}{2r^2\rho^2} \tag{5.30}$$

$$\gamma_2(x,y,z) = \frac{y^3+yx^2}{2r^2} \tag{5.31}$$

$$\zeta_2(x,y,z) = \frac{4y^3xz^2+3yx^3z^2-xy(\rho^4+2r^2\rho^2)}{2r^2\rho^4} \tag{5.32}$$

$$\eta_2(x,y,z) = \frac{z^2x^2y+y^3r^2}{2r^2\rho^2} \tag{5.33}$$

$$\xi_2(x,y,z) = -\frac{zxy}{r^2} \tag{5.34}$$

Similarly, for the z=constant face, we can obtain an expression for u_z, which reads:

$$u_z = \alpha_3(x,y,z)u + \beta_3(x,y,z)u_x + \gamma_3(x,y,z)u_{xx} + \zeta_3(x,y,z)u_y + \eta_3(x,y,z)u_{yy} + \xi_3(x,y,z)u_{xy} \tag{5.35}$$

where

$$\alpha_3(x,y,z) = -\frac{z}{r^2} \tag{5.36}$$

$$\beta_3(x,y,z) = -\frac{3xz}{2r^2} \tag{5.37}$$

$$\gamma_3(x,y,z) = \frac{x^2z^3 + y^2zr^2}{2r^2\rho^2} \tag{5.38}$$

$$\zeta_3(x,y,z) = -\frac{3yz}{2r^2} \tag{5.39}$$

$$\eta_3(x,y,z) = \frac{y^2z^3 + x^2zr^2}{2r^2\rho^2} \tag{5.40}$$

$$\xi_3(x,y,z) = -\frac{zxy}{r^2} \tag{5.41}$$

It is evident that one needs to use the appropriate normal derivative expression on different faces of the box-shaped outer boundary. As can be seen from Equations (5.12)-(5.41), it is much easier to choose a spherical outer boundary where the normal derivative is simply u_r. However, for the purpose of truncating the unbounded region surrounding the transmission lines in an efficient manner, one needs to use a conformable outer boundary which, as mentioned earlier, is typically a box-shaped surface for three-dimensional transmission line structures. The asymptotic boundary condition expressions that we have just derived will be implemented in the finite element scheme in the next section.

5.3 Finite Element Implementation of the Asymptotic Boundary Condition

The finite element method and its implementation are well-documented in the literature [1], [3]-[6], and [30]-[31]. In this section, we will be concerned with the implementation of the asymptotic boundary condition in the finite element method. As indicated earlier, the region of interest, Ω_T, is bounded by an artificial boundary, Γ_2, to limit the number of unknowns. Over the bounded region, the Laplace equation is solved at a finite number of grid points. This equation is discretized through the use of a weak form of variational representation.

Multiplying the Laplace Equation (5.1) by a testing function f and integrating over the volume Ω_T, result in

$$\int_{\Omega_T} f\nabla\cdot(\varepsilon\nabla u)\, dv = 0 \tag{5.42}$$

Using the Green's second identity, we obtain

$$\int_{\Omega_T} f\nabla\cdot(\varepsilon\nabla u)\, dv = -\int_{\Omega_T} \varepsilon\nabla u\cdot\nabla f\, dv + \int_{\Gamma_2} f\varepsilon \frac{\partial u}{\partial n}\, ds \tag{5.43}$$

Clearly, the second term of the right-hand side of (5.43) is the boundary integral contribution which is usually neglected when a p.e.c. outer boundary is used [4].

Inserting (5.43) into (5.42), we get

$$\int_{\Omega_T} \varepsilon\nabla u\cdot\nabla f\, dv = \int_{\Gamma_2} f\varepsilon \frac{\partial u}{\partial n}\, ds \tag{5.44}$$

The region Ω_T is discretized into tetrahedral elements. The triangular faces of the

outermost elements make up the outer boundary Γ_2. In finite element formulation, the implementation of (5.44) is carried out on an element-by-element basis. For all but the outermost tetrahedral elements, the right-hand side of Equation (5.44) is zero. The asymptotic boundary condition is needed to treat those outermost elements.

For those elements having a face on the surface prescribed by x=constant, where the outward normal is in the plus or minus x-direction, the asymptotic boundary condition given in (5.20) may be incorporated into (5.44) to yield

$$\int_{\Omega_T} \varepsilon \nabla u \cdot \nabla f \, dv = \pm \int_{\Gamma_2} f\varepsilon(\alpha_1(x,y,z)u + \beta_1(x,y,z)u_z + \gamma_1(x,y,z)u_{zz} + \zeta_1(x,y,z)u_y + \eta_1(x,y,z)u_{yy} + \xi_1(x,y,z)u_{yz}) \, dydz \qquad (5.45)$$

Similarly, for the elements having a face on the surface prescribed by y=constant, the asymptotic boundary condition given in (5.28) is used in (5.44) to give

$$\int_{\Omega_T} \varepsilon \nabla u \cdot \nabla f \, dv = \pm \int_{\Gamma_2} f\varepsilon(\alpha_2(x,y,z)u + \beta_2(x,y,z)u_z + \gamma_2(x,y,z)u_{zz} + \zeta_2(x,y,z)u_x + \eta_2(x,y,z)u_{xx} + \xi_2(x,y,z)u_{xz}) \, dxdz \qquad (5.46)$$

For the elements having a face on the surface prescribed by z=constant, where the outward normal is in the plus z-direction, (5.35) is incorporated into (5.44) to yield

$$\int_{\Omega_T} \varepsilon \nabla u \cdot \nabla f \, dv = \int_{\Gamma_2} f\varepsilon \, (\alpha_3(x,y,z)u + \beta_3(x,y,z)u_x + \gamma_3(x,y,z)u_{xx} + \zeta_3(x,y,z)u_y + \eta_3(x,y,z)u_{yy} + \xi_3(x,y,z)u_{xy}) \, dxdy \qquad (5.47)$$

Therefore, for those elements which do not share a face with Γ_2, the boundary contribution is zero. However, for the outermost elements, depending on the outward normal, the

appropriate asymptotic boundary condition has to be used (i.e., either the right-hand side of (5.45), (5.46), or (5.47) has to be added to the corresponding element matrix).

5.4 Numerical Results

A rectangular section of a microstrip transmission line of length L, width W, and height H above the ground plane is shown in Figure 5.2. The outer boundary Γ_2 was chosen to have the shape of a box. Using the same mesh, we have solved the potential problem twice, first by applying the asymptotic boundary condition on the outer boundary, and second by placing a perfect electric conducting shield at the same location. After solving for the electrostatic potential, we computed the normalized capacitance CH/ε(area) for both cases. Tables 5.1 and 5.2 show the results of computation for the normalized capacitance for different values of L/W and for three dielectric constants (ε_r = 1.0, 6.0, 9.6). As Tables 5.1 and 5.2 indicate, the asymptotic boundary condition yields more accurate results than those obtainable with a perfectly conducting shield [60]. Clearly, for this problem there is a distinct advantage in using an asymptotic boundary condition in place of a p.e.c. shield.

Table 5.1. Normalized capacitance $\left(\frac{CH}{\varepsilon \text{ Area}}\right)$ for $\frac{L}{W}$ = 0.2, $\frac{H}{W}$=0.2, $D_x=D_y=D_z$ =0.5.

ε_r	P.E.C. Shield	ABC (Present Method)	Reference [60]
1.0	1.34	3.73	3.5
6.0	1.04	2.25	2.2
9.6	1.02	2.12	2.1

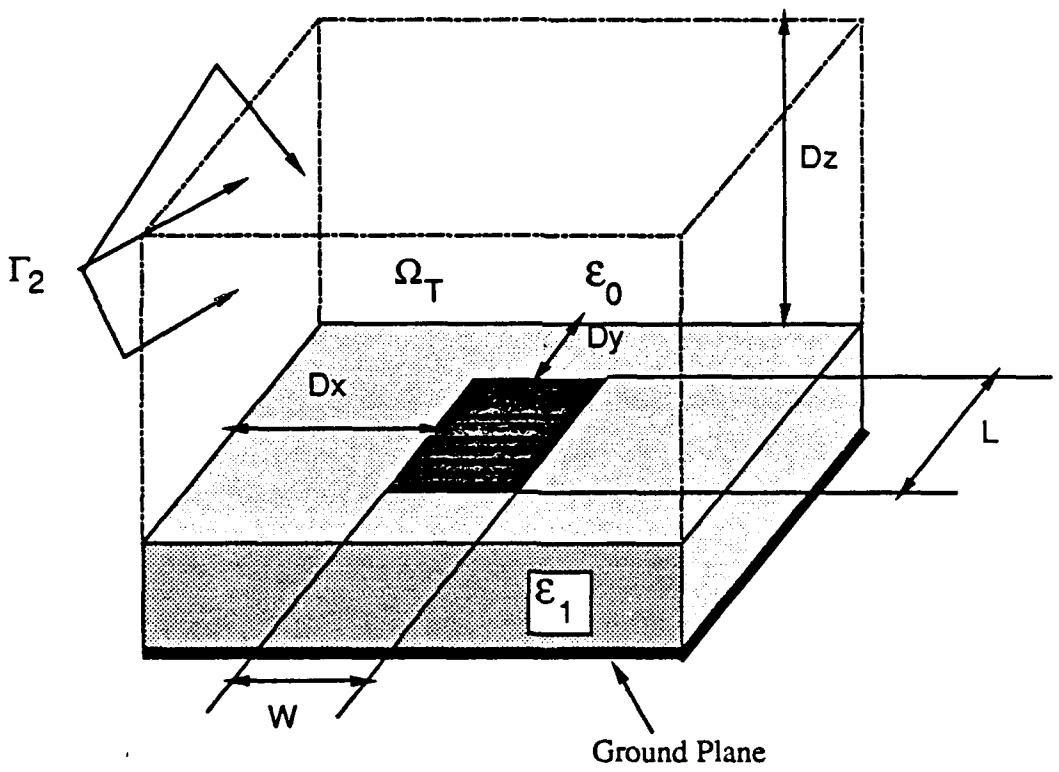

Figur 5.2. A microstrip rectangular patch enclosed by an outer boundary having the shape of a box in order to minimize the number of mesh points.

Table 5.2. Normalized capacitance $\left(\frac{CH}{\varepsilon \text{ Area}}\right)$ for $\frac{L}{W} = 1.0$, $\frac{H}{W}=1.0$, $D_x=D_y=D_z=2.0$.

ε_r	P.E.C. Shield	ABC (Present Method)	Reference [60]
1.0	2.19	4.90	5.0
6.0	1.36	3.11	3.4
9.6	1.31	2.84	2.9

Finally, we would like to mention that the boundary surface integral is always confined within a homogeneous region inside the element because the finite element method models the medium to be homogeneous within each element; consequently, no special treatment is needed at the dielectric interfaces.

5.5 Conclusions

Starting from the general solution of the Laplace equation in spherical coordinates, we derived a set of asymptotic boundary conditions for three-dimensional quasi-static problems for a spherical outer boundary. The second-order boundary condition was then generalized to a box-shaped outer boundary and implemented in the finite element method to solve the potential problem of a rectangular microstrip patch. The numerical results show that the asymptotic boundary conditions yield more accurate results than those obtainable with a perfectly conducting shield placed at the same location.

CHAPTER 6

IMPROVEMENT ON THE BOUNDARY CONDITIONS: THE HIGHER-ORDER BOUNDARY CONDITIONS

6.1 Introduction

The finite element method (FEM) is very appealing for solving open region problems due to its simplicity in modeling complex-shaped structures and inhomogeneous dielectric scatterers. The local, or the absorbing boundary condition (ABC), makes the FEM even more powerful because it preserves the sparsity of the discretized matrix. Furthermore, the absorbing boundary condition operator mimics, to a certain degree, the asymptotic behavior of the wave function at infinity and yields reasonably accurate results in the interior region without the need of an exorbitantly large number of mesh points. Among the available absorbing boundary conditions [8]-[32], the Bayliss, Gunzburger, and Turkel (BGT) boundary conditions are the most commonly used. In Chapter 3, we have presented a generalization of the original BGT absorbing boundary condition so as to make it applicable to an arbitrary, rather than circular, outer boundary. The use of the generalized version of the BGT enables one to reduce the number of node points significantly and to solve larger sized problems than had been possible in the past. In Chapter 4, we derived the static version of the BGT boundary condition. As the numerical results in Chapter 4 show, the asymptotic boundary condition consistently yielded more accurate results than those obtainable with a perfectly conducting shield placed at the same location. Nevertheless, most forms of the absorbing boundary condition operators have been based on the use of only the first few terms of the asymptotic representation of the solution to the differential equation. Typically, the first two terms of the series are used to

obtain the desired absorbing boundary condition operator. In [24], [27], and [28], it was demonstrated that while the absorbing boundary condition, which is based on the first terms of the series, works quite well for the lower-order harmonics, it exhibits a significant error for the higher-order harmonics, which, in turn, may cause a noticeable error in the finite element solution.

In this chapter, we derive a higher-order absorbing condition which unlike many of the available ABCs that take into account only the lower-order harmonics, considers both lower- and higher-order harmonics. In common with the other available ABCs, the derivation of this new absorbing condition is based on the same principle of the asymptotic representation of the solution to the differential equation. However, unlike the available ABCs which assume that in the far region the solution can adequately be represented by the first few terms of the series, the higher-order absorbing condition requires that the asymptotic representation be a combination of lower- and higher-order harmonics. As will be demonstrated later, the use of the higher-order ABC results in a significant improvement in the finite element solution for a variety of scatterers and transmission line structures.

6.2 Derivation of the Higher-Order Absorbing Boundary Condition

Consider the geometry of the scattering problem described in Figure 2.3. The region Ω is bounded with the contour Γ_1 and its exterior region is denoted by Ω_T. Let Γ_2 be the outer contour, which truncates the open region Ω_T, where the absorbing boundary condition will be applied. Obviously, one can now use a partial differential equation (PDE) technique to solve the approximate problem provided that the region bounded by Γ_2 is not so large as to require an unmanageable number of unknowns. The approximate problem, shown in Figure 2.3, is equivalent to

$$\nabla^2 u + k^2 u = 0 \text{ in } \Omega_T \tag{6.1}$$

$$\frac{\partial u}{\partial n} = g \text{ on } \Gamma_1 \tag{6.2}$$

$$B_m u = 0 \text{ on } \Gamma_2 \tag{6.3}$$

where u is the scattered field, g is the contribution from the incident field, and B_m is the m^{th} order absorbing boundary condition operator. Unlike the asymptotic representation of the scattered field given in Chapter 2, where only the first terms of the series are kept, we suggest the following asymptotic form

$$u = \frac{e^{-jk\rho}}{\sqrt{\rho}}\left(\frac{a_{n1}(\phi)}{\rho^{n1}} + \frac{a_{n2}(\phi)}{\rho^{n2}} + \frac{a_{n3}(\phi)}{\rho^{n3}} + \ldots\right), \; n_1 < n_2 < n_3 \tag{6.4}$$

Note that the asymptotic representation of the scattered field given by (2.22) can be obtained from (6.4) by choosing the set $\{n_1, n_2, n_3\}$ to be equal to $\{0, 1, 2\}$.

From (6.4), we can see that

$$\frac{\partial u}{\partial \rho} = -jku - \frac{e^{-jk\rho}}{\rho^{3/2}}\left(\frac{a_{n1}}{\rho^{n1}}\left(\frac{1}{2}+n_1\right) + \frac{a_{n2}}{\rho^{n2}}\left(\frac{1}{2}+n_2\right) + \frac{a_{n3}}{\rho^{n3}}\left(\frac{1}{2}+n_3\right) + \ldots\right) \tag{6.5}$$

Taking a closer look at the right-hand side of (6.5), we note that

$$\frac{\partial u}{\partial \rho} + jku + \frac{\left(\frac{1}{2} + n_1\right)}{\rho} u = O\left(\frac{1}{\rho^{n2+3/2}}\right) \tag{6.6}$$

Thus we define the boundary operator on the left side of (6.6) to be

$$B_1 \equiv \frac{\partial}{\partial \rho} + jk + \frac{\left(\frac{1}{2} + n_1\right)}{\rho} \tag{6.7}$$

Note that if n_1 is chosen to be equal to 1, the operator B_1 is equivalent to the first-order BGT operator [29]. If (6.7) is explicitly written, it would have the form

$$B_1 u = -\frac{e^{-jk\rho}}{\rho^{3/2}}\left(\frac{a_{n2}}{\rho^{n2}}(n_2 - n_1) + \frac{a_{n3}}{\rho^{n3}}(n_3 - n_1) + \ldots\right) \tag{6.8}$$

The second-order boundary operator can readily be obtained by letting $v = B_1 u$ and observing that

$$\frac{\partial v}{\partial \rho} + jkv + \frac{\left(\frac{3}{2} + n_2\right)}{\rho} v = O\left(\frac{1}{\rho^{n3+5/2}}\right) \tag{6.9}$$

or

$$B_2 u = \left(\frac{\partial}{\partial \rho} + jk + \frac{\left(\frac{3}{2} + n_2\right)}{\rho}\right)\left(\frac{\partial}{\partial \rho} + jk + \frac{\left(\frac{1}{2} + n_1\right)}{\rho}\right) u = O\left(\frac{1}{\rho^{n3+5/2}}\right) \tag{6.10}$$

Note that if the set $\{n_1, n_2\}$ is chosen to be equal to $\{1, 2\}$, the operator B_2 is equivalent to the second-order BGT operator [29].

Similarly, a third-order boundary operator can be obtained

$$B_3 \equiv \left(\frac{\partial}{\partial \rho} + jk + \frac{\left(\frac{5}{2} + n_3\right)}{\rho}\right)\left(\frac{\partial}{\partial \rho} + jk + \frac{\left(\frac{3}{2} + n_2\right)}{\rho}\right)\left(\frac{\partial}{\partial \rho} + jk + \frac{\left(\frac{1}{2} + n_1\right)}{\rho}\right) \tag{6.11}$$

Note that if the set $\{n_1, n_2, n_3\}$ is chosen to be equal to $\{1, 2, 3\}$, the operator B_3 is equivalent to the third-order BGT operator [29].

As was indicated in Chapter 3, the boundary integral contribution is a line integral over Γ_2 where its integrand is a product of the testing function and the normal derivative of the unknown field. Hence, for our purposes, it is more useful to find an asymptotic representation for the normal derivative of u rather than make direct use of the boundary condition operators obtained above. For a circular outer boundary, the normal derivative is simply the radial one. Using the B_3 operator as given by (6.11) and the Helmholtz equation given by (6.1), we obtain an asymptotic representation for the radial derivative that reads

$$\frac{\partial u}{\partial \rho} = \alpha(n_1, n_2, n_3, \rho)u + \beta(n_1, n_2, n_3, \rho)u_{\phi\phi} \tag{6.12}$$

where

$$\alpha(n_1,n_2,n_3,\rho) = -\Bigg[\frac{1}{\rho}\Big(n_1n_2n_3+\frac{1}{4}(n_1+n_2+n_3)+\frac{1}{2}(n_1n_2+n_1n_3+n_2n_3)+\frac{1}{8}\Big)$$

$$+ jk\Big(n_1n_2+n_1n_3+n_2n_3+2(n_1+n_2+n_3)+\frac{13}{4}\Big)-2\rho k^2(n_1+n_2+n_3+4)-4\rho^2jk^3)\Bigg]\Big/$$

$$\Bigg[\Big(n_1n_2+n_1n_3+n_2n_3+n_1+n_2+n_3+\frac{3}{4}\Big) + 2\rho jk(n_1+n_2+n_3+3) - 4\rho^2k^2\Bigg] \tag{6.13}$$

and

$$\beta(n_1,n_2,n_3,\rho) = \frac{\frac{1}{\rho}\Big(n_1+n_2+n_3+\frac{3}{2}\Big)+3jk}{\Big(n_1n_2+n_1n_3+n_2n_3+n_1+n_2+n_3+\frac{3}{4}\Big)+ 2\rho jk(n_1+n_2+n_3+3) - 4\rho^2k^2} \tag{6.14}$$

Note that the absorbing boundary condition operator shown in (6.12) depends on the harmonics $\{n_1, n_2, n_3\}$.

In deriving (6.12), we have used the first-order boundary condition operator B_1 to approximate the term $u_{\phi\phi\rho}$ as follows

$$u_{\phi\phi\rho} \approx -\left(\frac{\left(\frac{1}{2}+n_1\right)}{\rho}+jk\right)u_{\phi\phi} \tag{6.15}$$

The absorbing boundary condition that we have derived in (6.12) applies to a circular outer boundary where the normal derivative of u is simply its radial derivative u_ρ. Our next task is to transform the above absorbing boundary operator into a form suitable for arbitrary boundaries. Using the same transformation and the same approach as the one used in Chapter 3, we obtain the following absorbing boundary condition operator that can be applied on an arbitrary outer boundary

$$\frac{\partial u}{\partial n} = \bar{\alpha}u + \bar{\gamma}u_t + \bar{\beta}u_{tt} \tag{6.16}$$

where

$$\ddot{\alpha} = -(x_0\sin\theta_0 - y_0\cos\theta_0)\Big[\ \frac{1}{\rho}\Big(n_1n_2n_3+\frac{1}{4}(n_1+n_2+n_3)+\frac{1}{2}(n_1n_2+n_1n_3+n_2n_3)+\frac{1}{8}\Big)$$

$$+jk\Big(n_1n_2+n_1n_3+n_2n_3+2(n_1+n_2+n_3)+\frac{13}{4}\Big)-2\rho k^2(n_1+n_2+n_3+4)-4\rho^2jk^3)\Big]\Big/$$

$$\Big[\rho\Big(n_1n_2+n_1n_3+n_2n_3+n_1+n_2+n_3+\frac{3}{4}\Big)+2\rho^2jk(n_1+n_2+n_3+3)-4\rho^3k^2\Big] \qquad (6.17)$$

$$\bar{\gamma} = \frac{-t\,(x_0\sin\theta_0 - y_0\cos\theta_0)+\frac{1}{2}\sin2\theta_0\,(y_0^2-x_0^2)+x_0y_0\cos2\theta_0}{\rho^2} \qquad (6.18)$$

$$\bar{\beta} = \Big[(x_0\sin\theta_0-y_0\cos\theta_0)\Big(n_1+n_2+n_3+\frac{3}{2}\Big)+3jk\rho\Big]\Big/\Big[(\,n_1n_2$$

$$+n_1n_3+n_2n_3+n_1+n_2+n_3+\frac{3}{4})+2jk\rho(n_1+n_2+n_3+3)-4\rho^2k^2\Big] \qquad (6.19)$$

and θ_0, x_0, y_0, and t are as shown in Figure 3.2.

The higher-order boundary condition given by (6.16) is implemented in the finite element scheme in the same way as the modified BGT boundary condition discussed in Chapter 3.

6.3 Derivation of the Higher-Order Asymptotic Boundary Condition

Consider the problem of N arbitrarily-shaped conductors embedded in a multilayered medium above a ground plane, shown in Figure 4.1. Let Ω_T denote the region exterior to the conductors and Γ_2 the outer boundary enclosing the truncated region. The asymptotic boundary condition should mimic the asymptotic behavior of the field at infinity and yield reasonably accurate results in the interior region. The potential u must satisfy Laplace's equation everywhere in Ω_T, the constant potential condition on the conductors, and the asymptotic boundary condition on the outer boundary Γ_2.

Equivalently, the problem can be described in terms of the following equations:

$$\nabla\cdot(\varepsilon\nabla u) = 0 \text{ in } \Omega_T \tag{6.20}$$

$$u = g_i \text{ on the } i^{th} \text{ conductor} \tag{6.21}$$

$$B_m u = 0 \text{ on } \Gamma_2 \tag{6.22}$$

where u is the electrostatic potential and B_m is the m^{th} order asymptotic boundary condition.

In Chapter 4, the asymptotic boundary condition was based on the first two terms of the asymptotic representation of the general solution to Laplace's equation. In this chapter, we suggest the following asymptotic form for the potential u

$$u = \frac{a_{n1}}{\rho^{n1}}\cos n_1\phi + \frac{a_{n2}}{\rho^{n2}}\cos n_2\phi + \frac{a_{n3}}{\rho^{n3}}\cos n_3\phi + \ldots \tag{6.23}$$

Note that the asymptotic representation of the potential u given in Chapter 2 can be obtained from (6.23) by choosing the set $\{n_1, n_2, n_3\}$ to be equal to $\{1, 2, 3\}$.

From (6.23), we can see that

$$\frac{\partial u}{\partial \rho} + \frac{n_1 u}{\rho} = \frac{a_{n2}}{\rho^{n2+1}}\cos n_2\phi(n_1-n_2) + \frac{a_{n3}}{\rho^{n3+1}}\cos n_3\phi(n_1-n_3) + \ldots \tag{6.24}$$

We, therefore, define the first-order operator B_1 to be

$$B_1 u \equiv \frac{\partial u}{\partial \rho} + \frac{n_1 u}{\rho} = O\left(\frac{1}{\rho^{n2+1}}\right) \tag{6.25}$$

Note that if n_1 is chosen to be equal to 1, the B_1 operator given in Chapter 4 can be recovered from (6.25).

The second-order boundary operator can readily be obtained by letting $v = B_1 u$ and observing that

$$\frac{\partial v}{\partial \rho} + (n_2+1)\frac{v}{\rho} = O\left(\frac{1}{\rho^{n3+2}}\right) \tag{6.26}$$

Thus, the second-order operator is defined by

$$B_2 u \equiv \left(\frac{\partial}{\partial \rho} + \frac{n_2+1}{\rho}\right)\left(\frac{\partial}{\partial \rho} + \frac{n_1}{\rho}\right)u \tag{6.27}$$

Note that the B_2 operator of Chapter 4 can be recovered from (6.27) by choosing the set $\{n_1, n_2\}$ to be equal to $\{1, 2\}$.

The third-order operator can be obtained by letting $z = B_2 v$, and defining B_3 to be equal to

$$B_3 u \equiv \left(\frac{\partial}{\partial \rho} + (n_3+2)\frac{1}{\rho}\right)\left(\frac{\partial}{\partial \rho} + (n_2+1)\frac{1}{\rho}\right)\left(\frac{\partial u}{\partial \rho} + n_1 \frac{u}{\rho}\right) \tag{6.28}$$

As explained earlier, we need to find an asymptotic representation for the normal derivative of u rather than make direct use of the boundary condition operators obtained above. For a circular outer boundary, the normal derivative is simply the radial one. Using the B_3 operator as given in (6.28) and making use of the Laplace equation to trade the second-order derivative in ρ, $u_{\rho\rho}$, for the second-order angular derivative, $u_{\phi\phi}$, we obtain an

asymptotic representation for the radial derivative that reads

$$\frac{\partial u}{\partial \rho} = \lambda(n_1, n_2, n_3, \rho)u + \xi(n_1, n_2, n_3, \rho)u_{\phi\phi} \tag{6.29}$$

where

$$\lambda(n_1, n_2, n_3, \rho) = -\frac{n_1 n_2 n_3}{\rho(n_1 n_2 + n_1 n_3 + n_2 n_3)} \tag{6.30}$$

$$\xi(n_1, n_2, n_3, \rho) = \frac{n_1 + n_2 + n_3}{\rho(n_1 n_2 + n_1 n_3 + n_2 n_3)} \tag{6.31}$$

In deriving (6.29), we used the first-order boundary condition operator B_1 to approximate the term $u_{\phi\phi\rho}$, that is,

$$u_{\rho\phi\phi} \approx -n_1 \frac{u_{\phi\phi}}{\rho} \tag{6.32}$$

The asymptotic boundary condition operator given by (6.29) is valid only for a circular outer boundary. However, for the purpose of reducing the number of mesh points as much as possible, one needs to use a conformable outer boundary. Thus, we need to generalize (6.29) and obtain an operator valid for an arbitrary outer boundary. Following the procedure described in Chapter 3, we obtain an expression for the normal derivative u_n in the local coordinate system (t,n) where t and n are tangent and normal to the triangular edge lying on the outer boundary Γ_2, respectively,

$$\frac{\partial u}{\partial n} = \bar{\lambda}(n_1, n_2, n_3, \rho)u + \bar{\gamma}u_t + \bar{\xi}(n_1, n_2, n_3, \rho)u_{tt} \tag{6.33}$$

where u_t and u_{tt} are the first- and second-order tangential derivatives, respectively, and

$$\bar{\lambda}(n_1, n_2, n_3, \rho) = -(x_0\sin\theta_0 - y_0\cos\theta_0)\frac{n_1 n_2 n_3}{\rho^2(n_1n_2 + n_1n_3 + n_2n_3)} \tag{6.34}$$

$$\bar{\xi}(n_1, n_2, n_3, \rho) = (x_0\sin\theta_0 - y_0\cos\theta_0)^3\frac{n_1 + n_2 + n_3}{\rho^2(n_1n_2 + n_1n_3 + n_2n_3)} \tag{6.35}$$

where θ_0, x_0, y_0, and t are as shown in Figure 3.2.

6.4 Numerical Results

The higher-order boundary condition is implemented in the finite element scheme in the same way as the simple absorbing boundary condition because they both yield the same form of absorbing boundary condition operator. To demonstrate the significant improvement in the finite element solution achieved by using the higher-order boundary conditions, we considered both circuits and scattering problems. For all the cases considered, a conformable outer boundary is used to truncate the open region.

6.4.1 Digital circuit applications

6.4.1.1 Two conductors

Consider the two coupled microstrips shown in Figure 4.3. The higher-order asymptotic boundary condition operator given by (6.33) was applied on a rectangular outer boundary. Choosing the set $\{n_1, n_2, n_3\}$ to be equal to $\{1, 2, 4\}$, the finite element problem was solved for the electrostatic potential. Table 6.1 shows the capacitance matrix

for the same problem that has been published elsewhere [55], together with those obtained by using a p.e.c. shield, the asymptotic boundary condition (the method of Chapter 4), and the higher-order asymptotic boundary condition (present method). As Table 6.1 indicates, while both the present method and the simple asymptotic boundary condition yield more accurate results than those obtainable with a perfectly conducting shield placed at the same location, the higher-order asymptotic boundary condition results compare more favorably with the published work.

Table 6.1. Capacitance matrix for the coupled microstrips of Figure 4.3.

C(i,j)	Reference [55]	ABC	Higher Order ABC	Error ABC-[55]	Error HOABC-[55]
C(1,1)	0.9224×10^{-10}	0.9249×10^{-10}	0.9230×10^{-10}	0.271%	0.069%
C(1,2)	-0.8504×10^{-11}	-0.8061×10^{-11}	-0.8377×10^{-11}	5.203%	1.489%
C(2,1)	-0.8504×10^{-11}	-0.8061×10^{-11}	-0.8377×10^{-11}	5.203%	1.489%
C(2,2)	0.9224×10^{-10}	0.9249×10^{-10}	0.9230×10^{-10}	0.271%	0.069%

6.4.1.2 Six conductors

Consider the six-conductor system shown in Figure 4.4. As we indicated in Chapter 4, there are no published results for this configuration. However, we have compared our results with those derived by using the computer program developed by Harms et al. [56], which uses an integral equation formulation and an iterative method of solution. For this configuration, although the simple ABC of Chapter 4 yields more accurate results than those obtainable with a perfectly conducting shield placed at the same location, the error in the capacitance matrix is noticeable, especially for the off-diagonal terms. The higher-order asymptotic boundary condition operator given by (6.33) was

applied on a conformable rectangular outer boundary with a choice of the set $\{n_1, n_2, n_3\}$ to be equal to $\{1, 5, 10\}$. As Table 6.2 indicates, the higher-order asymptotic boundary condition yields a significant improvement over the simple asymptotic boundary condition, especially for the off-diagonal terms of the capacitance matrix.

Clearly, the improvements brought about by the higher-order asymptotic boundary condition are a direct consequence of its ability to incorporate lower- and higher-order terms through the choice of the set $\{n_1, n_2, n_3\}$. Based on numerical investigations, it was determined that the optimal choice of the set $\{n_1, n_2, n_3\}$ is $\{1, \rho/2, \rho\}$ where ρ is the distance from the origin to the middle of the edge of the triangular element residing on the outer boundary (see Figure 3.2).

6.4.2 Scattering applications

6.4.2.1 *Perfect electric conductor circular cylinder*

Consider a perfect electric conductor cylinder with a radius of 5λ enclosed with a circular outer boundary of radius 5.15λ shown in Figure 6.1. For a TE incident wave, the finite element method was used to obtain an approximate solution which was then compared to the exact series solution. Using the same mesh, the finite element problem was solved twice using two different boundary conditions: once by using the BGT absorbing boundary condition and the other by using the higher-order absorbing boundary condition. Figure 6.2 shows the radar cross-section (RCS) for the exact series solution, together with the one obtained by using the BGT absorbing boundary condition and the higher-order absorbing boundary condition (present method). Figure 6.3 shows the error in the finite element RCS computation. As Figures 6.2 and 6.3 indicate, the higher-order absorbing boundary condition yields a significant improvement in accuracy over the BGT

Table 6.2. Capacitance matrix for the six-conductor structure of Figure 4.4.

C(i,j)	Iterative [56]	ABC	Higher-Order ABC	Error ABC-[56]	Error HOABC-[56]
C(1,1)	0.668×10^{-10}	0.686×10^{-10}	0.667×10^{-10}	2.620%	0.213%
C(1,2)	-0.279×10^{-10}	-0.315×10^{-10}	-0.293×10^{-10}	13.05%	4.983%
C(1,3)	-0.549×10^{-11}	-0.600×10^{-11}	-0.565×10^{-11}	9.240%	2.826%
C(1,4)	-0.208×10^{-11}	-0.225×10^{-11}	-0.192×10^{-11}	8.320%	7.631%
C(1,5)	-0.999×10^{-12}	-0.101×10^{-11}	-0.792×10^{-12}	0.840%	20.73%
C(1,6)	-0.704×10^{-12}	-0.602×10^{-12}	-0.445×10^{-12}	14.52%	36.74%
C(2,1)	-0.279×10^{-10}	-0.315×10^{-10}	-0.293×10^{-10}	13.05%	4.983%
C(2,2)	0.789×10^{-10}	0.848×10^{-10}	0.803×10^{-10}	7.480%	1.713%
C(2,3)	-0.256×10^{-10}	-0.284×10^{-10}	-0.269×10^{-10}	11.10%	5.220%
C(2,4)	-0.465×10^{-11}	-0.487×10^{-11}	-0.464×10^{-11}	4.740%	0.193%
C(2,5)	-0.173×10^{-11}	-0.181×10^{-11}	-0.155×10^{-11}	4.610%	9.869%
C(2,6)	-0.999×10^{-12}	-0.101×10^{-11}	-0.792×10^{-12}	0.920%	20.67%
C(3,1)	-0.549×10^{-11}	-0.600×10^{-11}	-0.565×10^{-11}	9.240%	2.826%
C(3,2)	-0.256×10^{-10}	-0.284×10^{-10}	-0.269×10^{-10}	11.10%	5.220%
C(3,3)	0.794×10^{-10}	0.855×10^{-10}	0.812×10^{-10}	7.680%	2.307%
C(3,4)	-0.254×10^{-10}	-0.282×10^{-10}	-0.265×10^{-10}	10.91%	4.043%
C(3,5)	-0.465×10^{-11}	-0.487×10^{-11}	-0.464×10^{-11}	4.750%	0.127%
C(3,6)	-0.208×10^{-11}	-0.226×10^{-11}	-0.192×10^{-11}	8.410%	7.416%
C(4,1)	-0.208×10^{-11}	-0.225×10^{-11}	-0.192×10^{-11}	8.320%	7.631%
C(4,2)	-0.465×10^{-11}	-0.487×10^{-11}	-0.464×10^{-11}	4.740%	0.193%
C(4,3)	-0.254×10^{-10}	-0.282×10^{-10}	-0.265×10^{-10}	10.91%	4.043%
C(4,4)	0.794×10^{-10}	0.855×10^{-10}	0.812×10^{-10}	7.680%	2.307%
C(4,5)	-0.256×10^{-10}	-0.284×10^{-10}	-0.269×10^{-10}	11.10%	5.220%
C(4,6)	-0.549×10^{-11}	-0.601×10^{-11}	-0.566×10^{-11}	9.310%	3.053%
C(5,1)	-0.999×10^{-12}	-0.101×10^{-11}	-0.792×10^{-12}	0.840%	20.74%
C(5,2)	-0.173×10^{-11}	-0.181×10^{-11}	-0.155×10^{-11}	4.610%	9.869%
C(5,3)	-0.465×10^{-11}	-0.487×10^{-11}	-0.464×10^{-11}	4.750%	0.127%
C(5,4)	-0.256×10^{-10}	-0.284×10^{-10}	-0.269×10^{-10}	11.10%	5.220%
C(5,5)	0.789×10^{-10}	0.848×10^{-10}	0.803×10^{-10}	7.480%	1.713%
C(5,6)	-0.279×10^{-10}	-0.316×10^{-10}	-0.293×10^{-10}	13.08%	4.983%
C(6,1)	-0.704×10^{-12}	-0.602×10^{-12}	-0.445×10^{-12}	14.52%	36.74%
C(6,2)	-0.999×10^{-12}	-0.101×10^{-11}	-0.792×10^{-12}	0.920%	20.67%
C(6,3)	-0.208×10^{-11}	-0.226×10^{-11}	-0.192×10^{-11}	8.410%	7.417%
C(6,4)	-0.549×10^{-11}	-0.601×10^{-11}	-0.566×10^{-11}	9.310%	3.053%
C(6,5)	-0.279×10^{-10}	-0.316×10^{-10}	-0.293×10^{-10}	13.08%	4.983%
C(6,6)	0.668×10^{-10}	0.685×10^{-10}	0.666×10^{-10}	2.550%	0.328%

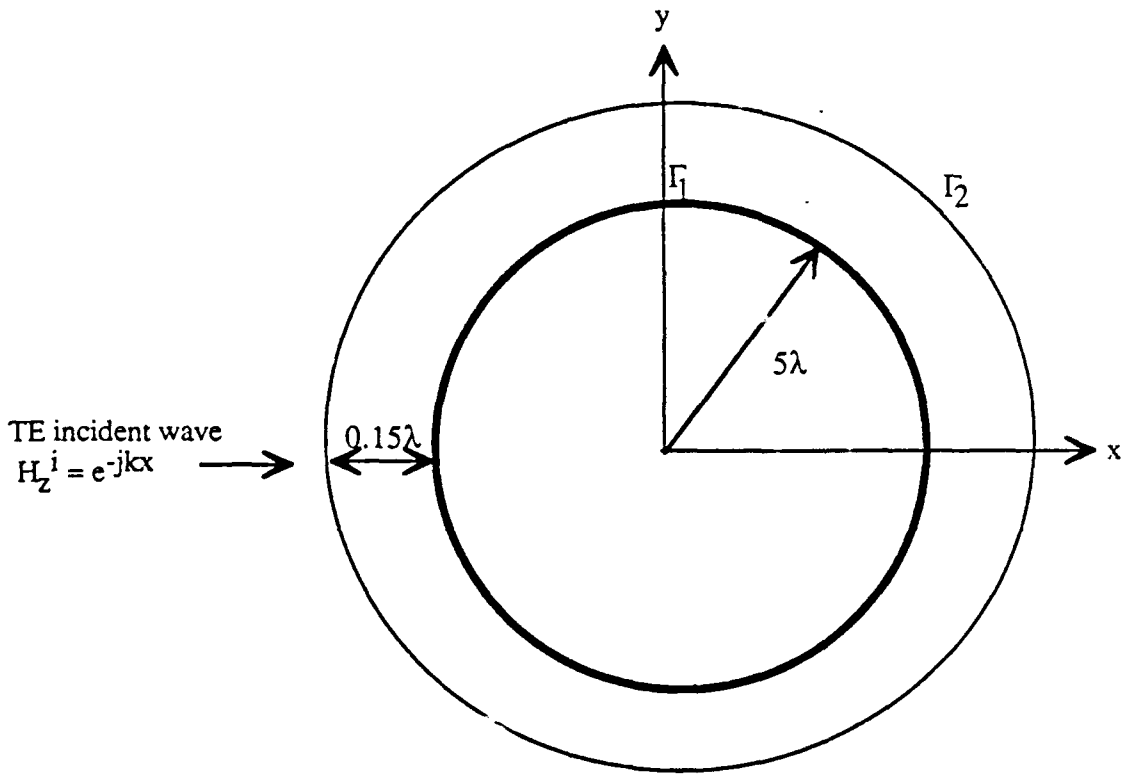

Figure 6.1. A TE incident wave on a 5λ p.e.c cylinder enclosed by a circular outer boundary 0.15λ away from the surface of the scatterer.

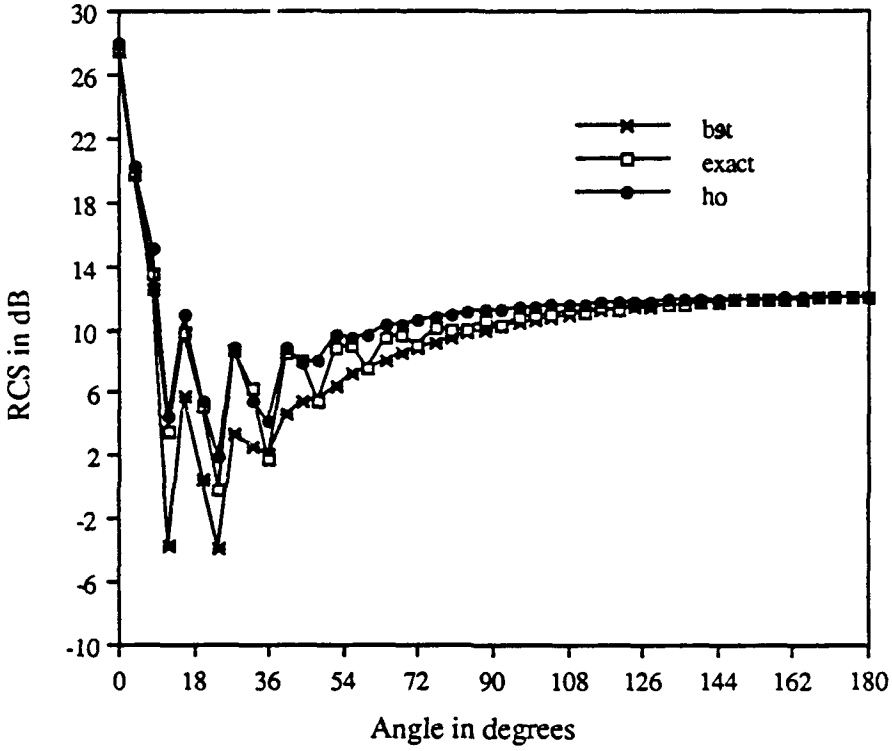

Figure 6.2. The radar cross-section of a 5λ cylinder illuminated by a TE incident wave and enclosed by a circular outer boundary 0.15 λ away from the surface of the scatterer as shown in Figure 6.1.

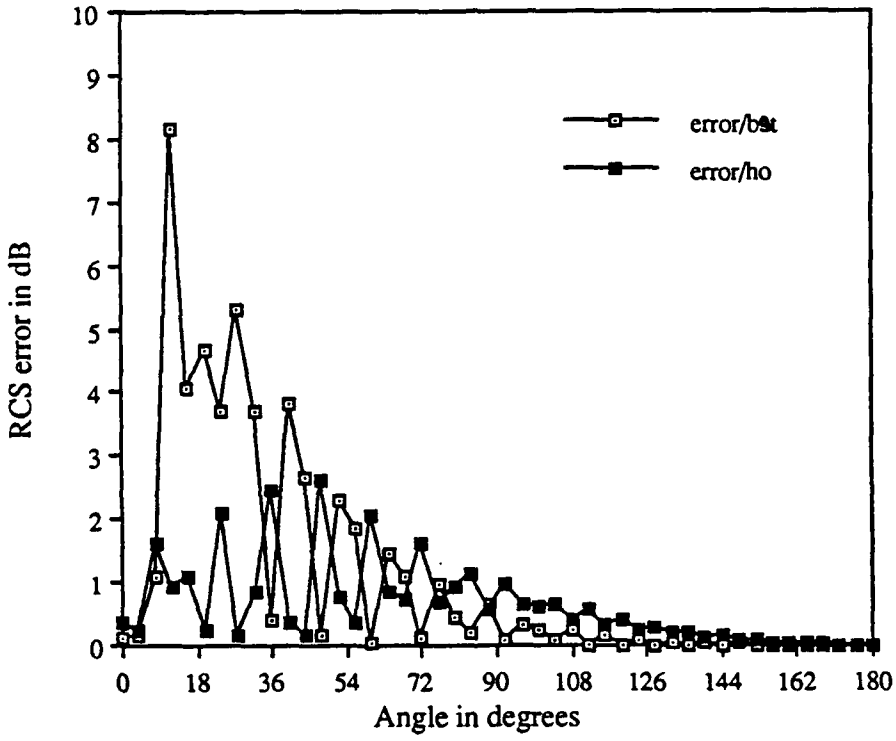

Figure 6.3. The error in the radar cross-section between the finite element and the exact series solutions for a 5 λ cylinder illuminated by a TE incident wave and enclosed by a circular outer boundary 0.15 λ away from the surface of the scatterer as shown in Figure 6.1.

boundary condition. It is worth mentioning that for a TM wave incident on the same cylinder the higher-order and the BGT boundary conditions give almost the same result which compares very well with that for the exact series solution.

6.4.2.2 Perfect electric conductor wedge

Consider a 6λ by 3λ perfect electric conductor wedge illuminated by a TM incident wave ($E^i = e^{-jkx}$). In order to minimize the number of mesh points, the wedge was enclosed by a conformable outer boundary 1λ away from the surface of the scatterer (Figure 6.4). The near field was calculated on the outer boundary using the higher-order boundary condition (present method), the BGT boundary condition, and the method of moments. From Figure 6.5, we can deduce that the use of the higher-order boundary condition results in considerable improvement over the BGT boundary condition. In order to see more clearly the difference between higher-order and the BGT boundary conditions, we have plotted the results obtained by the two methods on separate graphs in Figure 6.6.

6.4.2.3 Perfect electric conductor strip

Figure 6.7 shows a 6λ strip illuminated by a TM incident wave ($E^i = e^{-jkx}$). Again, for the purpose of reducing the number of mesh points, the outer boundary was chosen to be as conformable as possible to the surface of the scatterer. The near field was calculated on the outer boundary using the higher-order boundary condition , the BGT boundary condition, and the method of moments. The results obtained via the use of the higher-order and the BGT boundary conditions are again compared to the method of moments results. As Figures 6.8 and 6.9 show, the higher-order boundary condition compares more favorably than the BGT boundary condition with the method of moments.

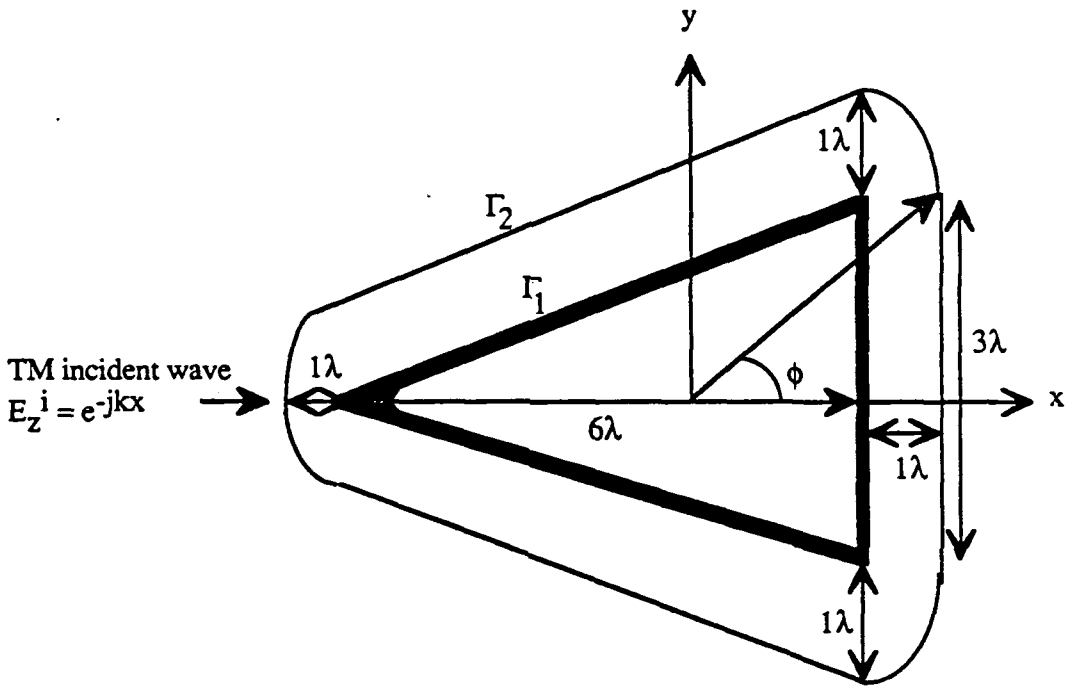

Figure 6.4. A TM incident wave on a 6 λ by 3λ p.e.c wedge enclosed by a conformable outer boundary 1 λ away from the surface of the scatterer.

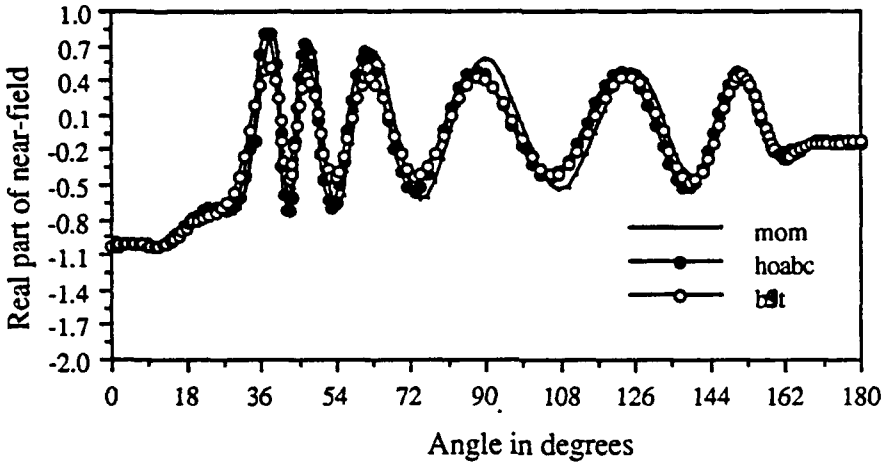

(a)

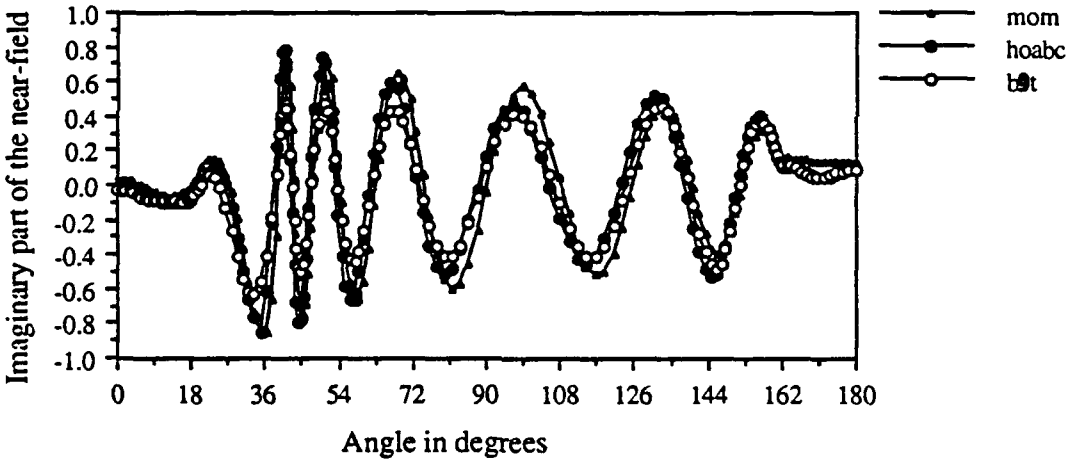

(b)

Figure 6.5. Near field on the outer boundary for a 6λ by 3λ p.e.c. wedge illuminated by a TM incident wave ($E^i = e^{-jkx}$) and enclosed by a conformable outer boundary as shown in Figure 6.4. Shown are the method of moments, the higher-order boundary condition, and the BGT boundary condition results.
a) Real part of the near field.
b) Imaginary part of the near field.

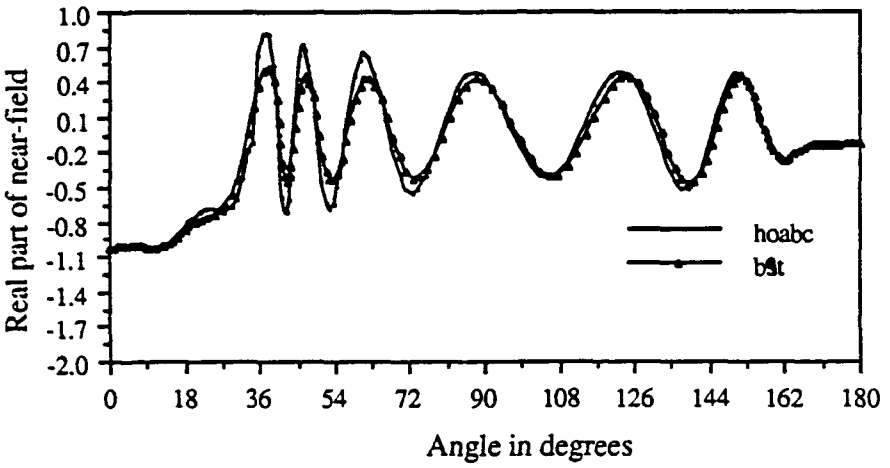

(a)

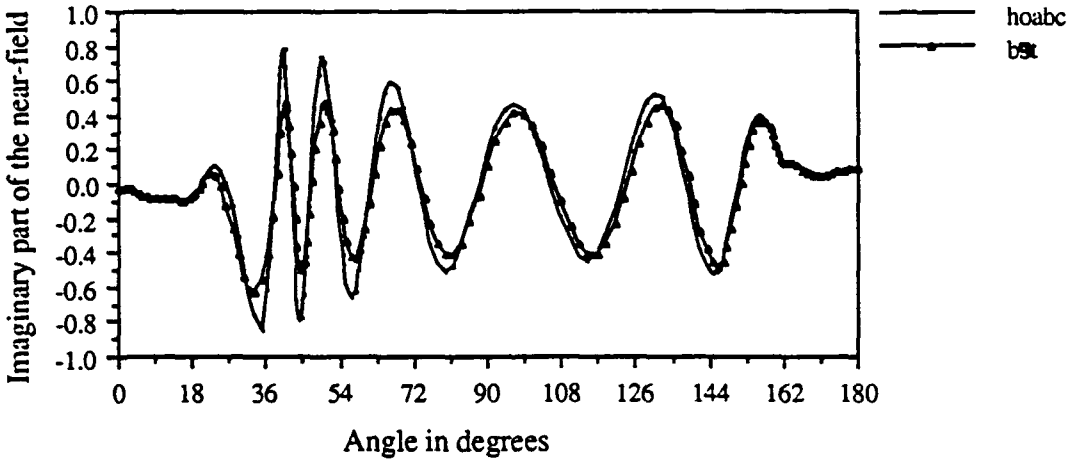

(b)

Figure 6.6. Same as Figure 6.5 but in this graph only the higher-order and the BGT absorbing boundary conditions results are shown.

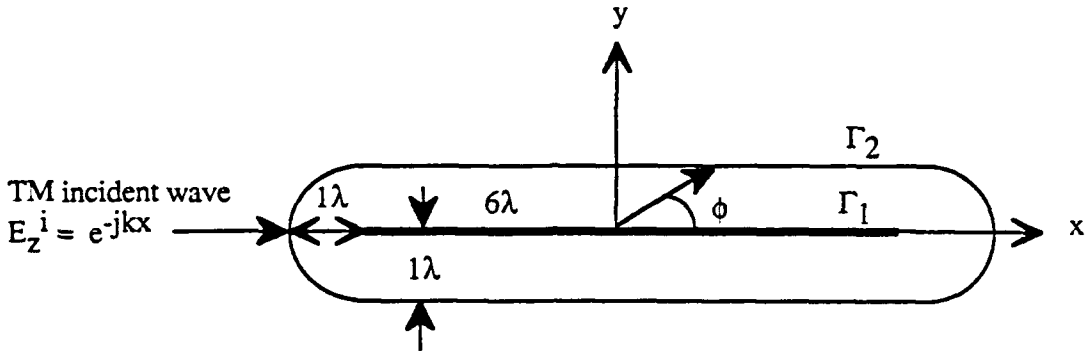

Figure 6.6. A TM incident wave on a 6 λ p.e.c. strip enclosed by a conformable outer boundary 1λ away to minimize the number of mesh points.

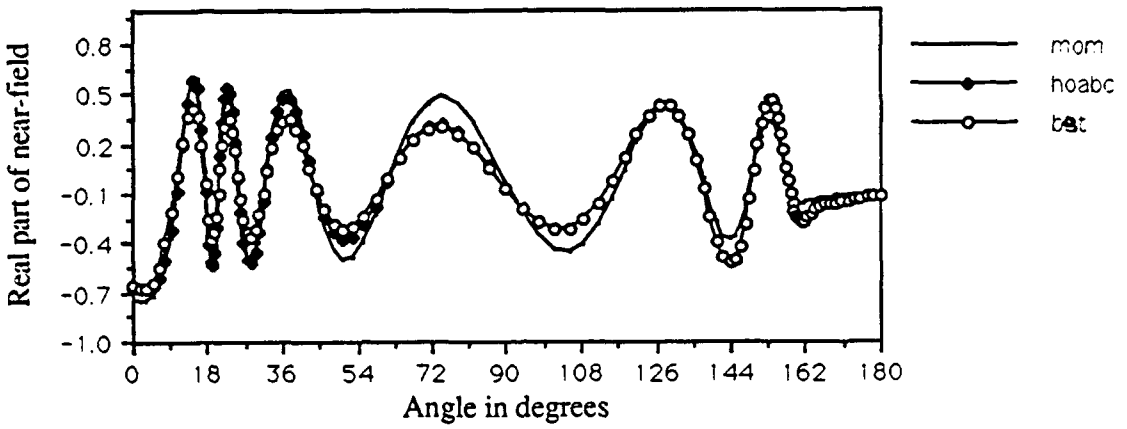

(a)

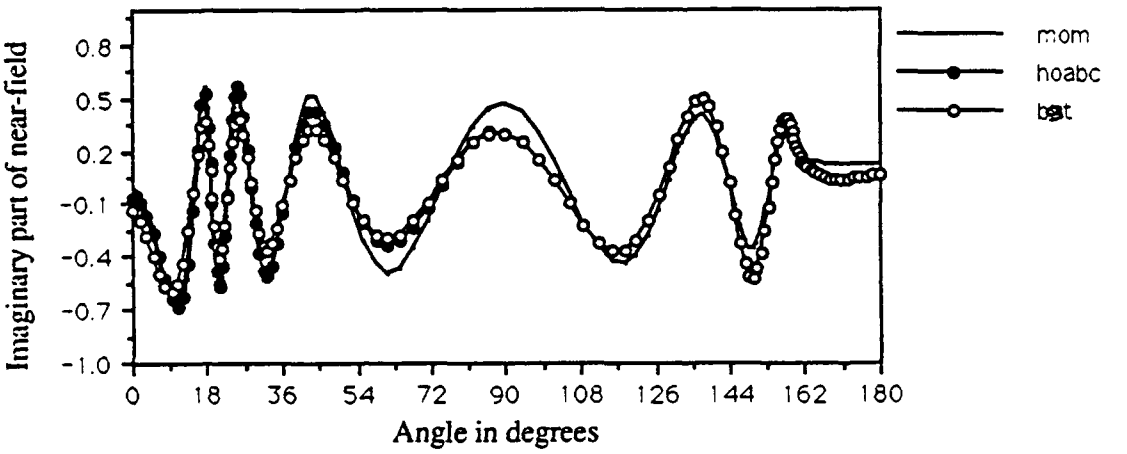

(b)

Figure 6.8. Near field on the outer boundary for a 6λ p.e.c. strip illuminated by a TM incident wave ($E^i = e^{-jkx}$) and enclosed by a conformable outer boundary as shown in Figure 6.7. Shown are the method of moments, the higher-order boundary condition, and the BGT boundary condition results.
a) Real part of the near field.
b) Imaginary part of the near field.

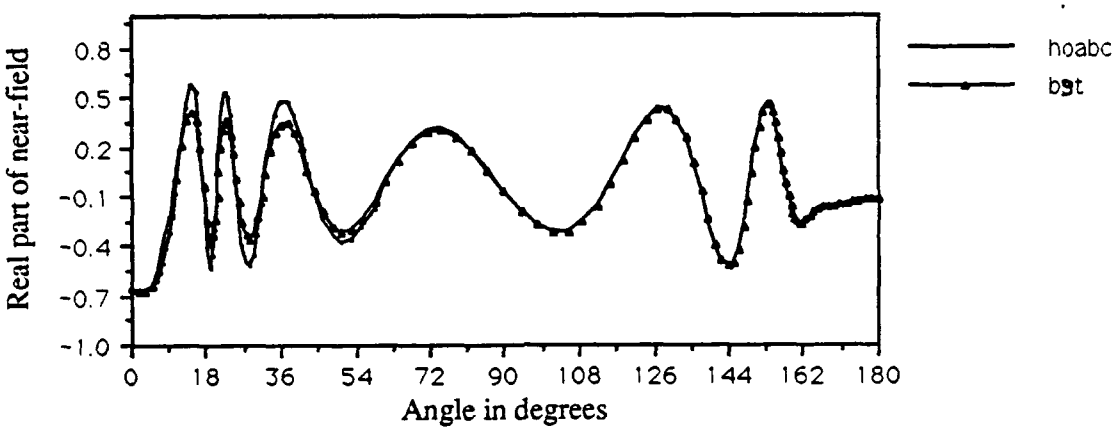

(a)

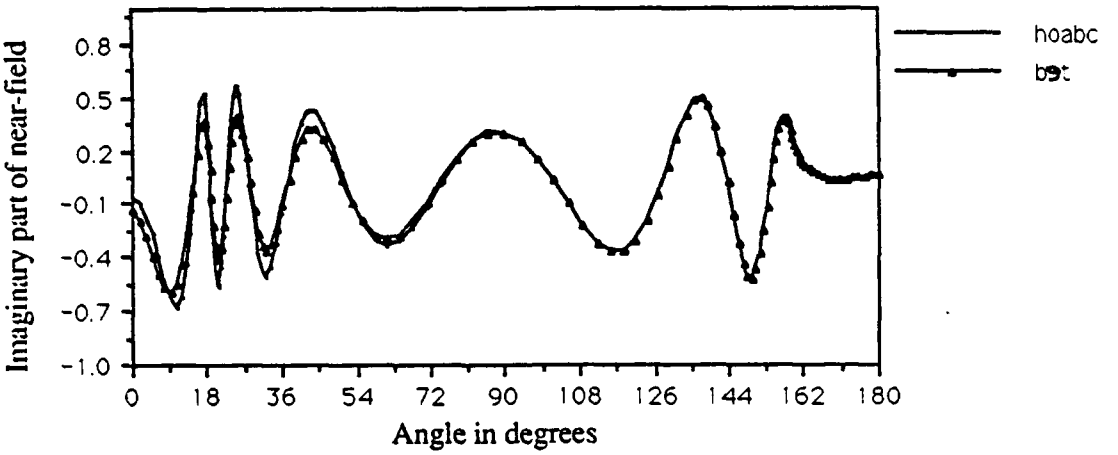

(b)

Figure 6.9. Same as Figure 6.8 except in this graph only the higher-order and the BGT absorbing boundary condition results are shown.

The higher-order boundary condition operator depends on the set $\{n_1, n_2, n_3\}$. This set is chosen in a way that includes both the lower- and the higher-order harmonics. Let γ denotes the ratio u_ρ/u ($\gamma = u_\rho/u$) where u the scattered field and u_ρ is its normal derivative. The imaginary and real parts of γ are related to the propagating and decaying waves, respectively. The exact of value of γ is given by $H_n'(k\rho)/H_n(k\rho)$. The approximate value of γ can readily by computed by using Equation (3.5) for the BGT boundary condition and Equation (6.12) for the higher-order boundary condition. Thus, a proper choice of the harmonics is a one that approximates γ (γ_{approx}) as close as possible to γ_{exact}. As Figure 6.10 indicates ($k\rho = 32$), the BGT boundary condition is quite satisfactory for the lower-order harmonics up to n=20, and then begins to deviate from the exact one for n>20. However, by letting the set $\{n_1, n_2, n_3\}$ to take roughly the value of $\{0, k\rho/2, k\rho\}$, where k is the free-space wavenumber and ρ is the distance from the origin to the middle of the triangular edge residing on the outer boundary, the higher-order absorbing boundary condition yields a value of γ_{approx} which, on the average, matches γ_{exact} on a wider range of harmonics than does the one given by the BGT boundary condition.

As the numerical results indicate, the improvement brought about by the higher-order absorbing boundary condition is more significant for the wedge than for the strip. This difference can be explained by the fact that the strip scatters more of the higher-order harmonics than does the wedge, which, in turn, may require more than three sampling of the harmonics in order to achieve a significant improvement.

The term "Error" that appeared several times in the Tables should not be interpreted as an absolute error but rather as a difference between our results and the published ones.

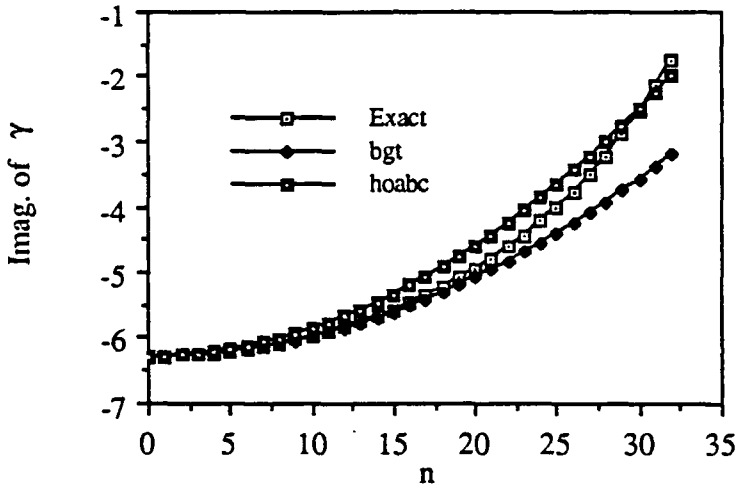

Figure 6.10. Imaginary part of γ versus the harmonic number n.

6.5 Conclusions

Based on the asymptotic representation of the general solution of the Helmholtz and Laplace equations, we derived higher-order absorbing and asymptotic boundary conditions that combine both the lower- and higher-order terms. The higher-order boundary conditions were then generalized and made valid for an arbitrary outer boundary. These boundary conditions were implemented in the finite element scheme and used to obtain the solution for both digital circuit and scattering applications. The numerical results showed that the higher-order boundary conditions constantly yielded a significant improvement over those for the BGT boundary condition.

CHAPTER 7

CONCLUSIONS AND FUTURE WORK

In this thesis, the subjects of the absorbing and asymptotic boundary conditions for the finite element (FEM) mesh truncation applied to scattering and digital circuit problems were investigated. Three new boundary condition concepts were introduced, viz., the boundary condition for arbitrary outer boundaries, the asymptotic boundary condition for digital circuit applications, and the higher-order asymptotic and absorbing boundary conditions.

Using a rotation and a translation transformation and neglecting the mixed derivative term (u_{nt}), the most commonly used absorbing boundary condition operator for electromagnetic scattering problems, e.g., the Bayliss, Gunzburger, and Turkel (BGT), was generalized and made applicable to an arbitrary, rather than circular, outer boundary for the purpose of minimizing the number of mesh points. The generalized boundary condition operator was implemented in the finite element method and used to study the scattering from a 4λ strip, a 2λ by 1λ wedge, a 9λ strip, and an 8λ by 4λ wedge. The numerical investigation indicated that while the finite element yielded acceptable results for all the strips and wedges considered, the results for the wedges agreed more favorably than those of the strips with the results obtainable via the Method of Moments. This can be explained by the fact that the scattered waves are purely outgoing only in the region outside the smallest circle that entirely encloses the scatterer. For a wedge, where the outer boundary resembles more closely a circular one, there are more points satisfying the above criterion than there are for a strip where the outer boundary is elongated. In fact, the presence of incoming waves is more pronounced for the region of the elongated boundary enclosing the strip which is close to the origin.. The issue of absorbing boundary

condition for scattering problems was examined again in Chapter 6 where a higher-order boundary condition was used in conjunction with the finite element method The higher-order absorbing boundary condition was derived from the asymptotic solution of the Helmholtz equation. Unlike most available absorbing boundary conditions, e.g., the Bayliss, Gunzburger, and Turkel (BGT), the higher-order absorbing boundary condition took into account both the lower- and higher-order harmonics. Using the transformations of Chapter 3, this boundary condition was also generalized and made valid for an arbitrary outer boundary. The numerical results showed that the higher-order absorbing boundary condition constantly yielded a significant improvement over those for the BGT boundary condition for a variety of scatterers. In the course of this study, it was realized that whether one uses the BGT or the higher-order boundary conditions, the outer boundary needed to be placed at a reasonable distance from the surface of the scatterer considered.

The corresponding concept to the absorbing boundary condition for digital circuit applications is the asymptotic boundary condition. The term "asymptotic" is used instead of "absorbing" because the digital circuits were analyzed in the quasi-TEM regime and, hence, there was no propagation or reflection of waves. Using a similar approach to the one used to obtain an absorbing boundary condition for scattering problems, an asymptotic boundary condition was derived for open region digital circuit problems. The asymptotic boundary condition was then implemented in the two-dimensional FEM scheme to model one-, two-, and six-conductor configurations. The numerical results indicated that the asymptotic boundary condition consistently yielded more accurate results than those obtainable with a perfectly conducting shield placed at the same location. Furthermore, this asymptotic boundary condition did not suffer from the complications associated with the infinite elements. However, in some situations, the accuracy obtained with the asymptotic boundary condition was not adequate, as for instance in the off-diagonal terms of the capacitance matrix in the six-conductor configuration. Those inadequate results were

improved in Chapter 6 where the higher-order asymptotic boundary condition was used. The later boundary condition, unlike the one used in Chapter 3, took into account both the lower- and higher-order terms.

Since digital circuits do not consist of only two-dimensional structures but also contain various three-dimensional transmission line discontinuities, it was necessary to derive the three-dimensional version of the asymptotic boundary condition. The general form of the solution to Laplace's equation was again used to derive the asymptotic boundary condition. In order to reduce the number of mesh points as much as possible, a box-shaped outer boundary was chosen because it was the most conformable to the structures considered. The method was used to compute the capacitance of a rectangular microstrip patch, and the results were found to be in good agreement with data published elsewhere. Once again, the asymptotic boundary condition enabled us to bring the outer boundary much closer to the structure than would have been possible with the p.e.c. artificial boundary. Actually, the role played by the three-dimensional asymptotic boundary condition was more crucial than the one played by the two-dimensional asymptotic boundary condition because the total number of mesh points for three-dimensional problems is usually large. Although the cost of FEM calculation for the three-dimensional problem was quite high, the method is worth using because it handles very general structures and, hence, helps in solving practical problems.

The absorbing and asymptotic boundary conditions are fairly new concepts in both scattering and digital circuit analyses. The work presented in this thesis just scratched the surface of those concepts and a considerable effort still needs to be done before they become standard techniques for FEM mesh truncation. A possible area of research is suggested by the fact that the outer boundary had to be placed at a reasonable distance from the object in order to achieve an acceptable accuracy. For a relatively large scatterer such as the 9λ strip considered earlier, even though a conformable outer boundary was used, a

couple of thousand mesh points were required in order to obtain satisfactory results. A considerable savings in computer time and storage can be achieved if a boundary condition that helps to bring the outer boundary closer than the one used in this work is found. But how close to the object could the outer boundary be placed? The answer to this question is still an unknown issue that requires a great deal of future research.

In this work, only two-dimensional scattering problems were considered. However, most of the practical scattering problems are three-dimensional in nature. Although three-dimensional vector absorbing boundary condition are reported in the literature, very little has been done in terms of implementing them in the FEM. Thus, there is a need to develop computer codes that incorporate those absorbing boundary condition operators into the FEM which will help to solve the most general scattering problems, i.e., the vector three-dimensional problems.

For digital circuit problems, the asymptotic boundary conditions derived in this work were valid only in the quasi-TEM regime. However, with the increasing speed of digital circuits, it is often inadequate and insufficient to rely on the quasi-TEM approximations. Thus, there is an urgent need to derive absorbing boundary conditions and incorporate them into the FEM for the full-wave vector analysis of two- and three-dimensional high-speed digital circuit problems.

REFERENCES

[1] P.P. Silvester and R.L. Ferrari, *Finite Elements for Electrical Engineers*. Cambridge, U.K.: Cambridge University Press, 1983.

[2] P. Daly, "Hybrid-mode analysis of microstrip by finite-element method," *IEEE Trans. Microwave Theory Tech.*, vol. MTT-19, pp. 19-25, January 1971.

[3] Z. Pantic and R. Mittra, "Quasi-TEM analysis of microwave transmission lines in multilayered dielectric media," *IEEE Trans. Microwave Theory Tech.*, vol. MTT-32, pp. 705-710, July 1984.

[4] S. P. Castillo, "Electromagnetic modeling of high-speed digital circuits," Ph.D. dissertation, University of Illinois, Urbana, IL, 1987.

[5] Z. Pantic and R. Mittra, "Quasi-TEM analysis of microwave transmission lines by the finite-element method," *IEEE Trans. Microwave Theory Tech.*, vol. MTT-34, pp. 1096-1103, November 1986.

[6] Z. Pantic and R. Mittra, "Finite element matrices for loss calculation in quasi-TEM analysis of transmission lines," *Microwave and Opt. Tech. Letters*, vol. 1, pp. 142-146, June 1988.

[7] M. Ikeuchi, H. Sawami, and H. Niki, "Analysis of open-type dielectric waveguides by the finite-element iterative method," *IEEE Trans. Microwave Theory Tech.*, vol. MTT-29, pp. 243-239, March 1981.

[8] B. H. McDonald and A. Wexler, "Finite element solution of unbounded field problems," *IEEE Trans. Microwave Theory Tech.*, vol. MTT-20, no. 12, pp. 841-847, December 1972.

[9] R. MacCamy and S. Marin, "A finite element method for exterior interface problems," *Int. J. Math. Sci.*, vol. 3, no. 2, pp. 311-350, June 1980.

[10] G. Kriegsmann and C. Morawetz, " Solving the Helmholtz equation for exterior problems with variable index of refraction: I," *SIAM J. Sci. Stat.*, vol. 1, no. 3., pp. 371-385, September 1980.

[11] G. Meltz, B. McCartin and L. Bahrmasel, "Application of the control region approximation to electromagnetic scattering," URSI Radio Science Meeting Program and Abstracts, p. 185, Blacksburg, Virginia, June 1987. Also submitted for publication in *JEWA*.

[12] K. Mei, "Unimoment method of solving antenna and scattering problems," *IEEE Trans. Antennas Propag.*, vol. AP-22, no. 6, pp. 760-766, November 1974.

[13] S. Chang and K. Mei, "Application of the unimoment method to electromagnetic scattering of dielectric cylinders, " *IEEE Trans. Antennas Propag.*, vol. AP-24, no.1, pp. 34-42, January 1976.

[14] M. Morgan and K Mei, "Finite-element computation of scattering by inhomogeneous penetrable bodies of revolution," *IEEE Trans. Antennas Propagat.*, vol. AP-27, no. 2, pp. 202-214, March 1979.

[15] M. Morgan, S. K. Chang, and K. Mei, "Coupled azimuthal potentials for electromagnetic field problems in inhomogeneous axially symmetric media," *IEEE Trans. Antennas Propag.*, vol. AP-25, no. 3, pp. 413-417, May 1977.

[16] B. Engquist and A. Majda, "Radiation boundary conditions for the numerical simulation of waves," *Math. Comp.*, vol. 31, no. 139, pp. 629-651, July 1977.

[17] A. Bayliss, M. Gunzburger and E. Turkel, " Boundary conditions for the numerical solution of elliptic equations in exterior regions," *SIAM J. Appl. Math.*, vol. 42, no. 2, pp. 430-451, April 1982.

[18] C. H. Wilcox, "An expansion theorem for electromagnetic fields, " *Commun. Pure Appl. Math.*, vol. 9, no. 2, pp. 115-134, May 1956.

[19] A. Khebir, A. B. Kouki, and R. Mittra, " Absorbing boundary condition for quasi-TEM analysis of microwave transmission lines via the finite element method", *JEWA*, vol. 4, no. 2, 1990.

[20] T. G. Moore, J. G. Blaschak, A. Taflove, and G. A. Kriegsmann, "Theory and application of radiation boundary operators," *IEEE Trans. Antennas Propag.*, vol. AP-36, no. 12, pp. 1797-1812, December 1988.

[21] A. Bayliss and E. Turkel, "Radiation boundary conditions for wave-like equations," *Commun. Pure & Appl. Math.*, vol. 23, pp. 707-725, 1980.

[22] G. Mur, "Absorbing boundary conditions for the finite-difference approximation of time-domain electromagnetic field equations," *IEEE Trans. Elect. Comp.*, vol. EMC-23, pp. 377-382, November 1981.

[23] R. L. Higdon, "Absorbing boundary conditions for the difference approximation to the multidimensional wave equation," *Math. Comp.*, vol. 47, pp. 437-459, 1986.

[24] R. Mittra and O. Ramahi, "Absorbing boundary conditions for the direct solution of partial differential equations arising in electromagnetic scattering problems," in *Differential Methods in Electromagnetic Scattering*, vol. II, M. Morgan, Ed. New York, NY: Elsevier Science, Inc., 1989.

[25] L. N. Trefethen and L. Halpern, "Well-posedness of one-way wave equations and absorbing boundary conditions," *Math. Comp.*, vol. 47, pp. 421-435, October 1986.

[26] O. Ramahi and R. Mittra, "A systematic approach to improving the absorbing boundary condition," *URSI Radio Meeting Program and Abstracts*, p. 182, Syracuse, June 1988.

[27] R. Mittra, O. Ramahi, A. Khebir, R. Gordon, and A. Kouki, "A review of absorbing boundary conditions for two- and three-dimensional electromagnetic scattering problems," *IEEE Trans. Magn.*, vol. 25, pp. 3034-3039, July 1989.

[28] O. Ramahi, A. Khebir, and R. Mittra, "Numerically-derived absorbing boundary conditions for the solution of open region scattering problems," (to appear).

[29] S. Hariharan, "Absorbing boundary conditions for exterior problems," CR 177944, VA: NASA Langley Research Center, July 1985.

[30] G. Strang and G. Fix, *An Analysis of the Finite Element Method*. Englewood Cliffs,

N.J. : Prentice-Hall, Inc, 1973.

[31] J. N. Reddy, *An Introduction to Finite-Element Method.* New York, N.Y. : McGraw-Hill, 1984.

[32] A. Khebir, O. Ramahi, and R. Mittra, "An efficient partial differential equation technique for solving the problem of scattering by objects of arbitrary shape," *Microwave and Opt. Techn. Letters*, vol. 2, pp. 229-233, July 1989.

[33] R. F. Harrington, *Time Harmonic Electromagnetic Fields*. New York, NY : McGraw-Hill, 1961.

[34] R. Mittra and T. Itoh, "Charge and potential distributions in shielded striplines," *IEEE Trans. Microwave Theory Tech.*, vol. MTT-18, pp. 149-156, March 1970.

[35] A. El-Sherbiny, "Exact analysis of shielded microstrip lines and bilateral fin lines," *IEEE Trans. Microwave Theory Tech.*, vol. MTT-29, pp. 669-675, July 1981.

[36] E. Yamashita and R. Mittra, "Variational method for the analysis of microstrip lines," *IEEE Trans. Microwave Theory Tech.*, vol. MTT-16, pp. 251-256, April 1968.

[37] S. K. Koul and B. Bhat, "Generalized analysis of microstrip-like transmission lines and coplanar strips with anisotropic substrates for MIC, electrooptic modulator, and SAW applications," *IEEE Trans. Microwave Theory Tech.*, vol. MTT-31, pp. 1051-1058, December 1983.

[38] T. Itoh and A. S. Herbert, "A generalized spectral domain analysis for coupled suspended microstriplines with tunning septums," *IEEE Trans. Microwave Theory Tech.*, vol. MTT-26, pp. 820-826, October 1978.

[39] T. Itoh, "Generalized spectral domain method for multiconductor printed lines and its application to tunable suspended microstrips," *IEEE Trans. Microwave Theory Tech.*, vol. MTT-26, pp. 983-987, December 1978.

[40] D. M. Syahkal and J. B. Davies, "Accurate solution of microstrip and coplanar structures for dispersion and for dielectric conductor losses," *IEEE Trans. Microwave Theory Tech.*, vol. MTT-27, pp. 694-699, July 1979.

[41] P. Silvester, "TEM wave properties of microstrip transmission lines," *Proc. IEE*, vol. 115, pp. 43-48, January 1968.

[42] T. G. Bryant and T. A. Weiss, "Parameters of microstrip transmission lines and of coupled pairs of microstrip lines," *IEEE Trans. Microwave Theory Tech.*, vol. MTT-16, pp. 1021-1027, December 1968.

[43] E. Yamashita and K. Atsuki, "Analysis of thick-strip transmission lines," *IEEE Trans. Microwave Theory Tech.*, vol. MTT-19, pp. 120-122, January 1971.

[44] R. Crampagne, M. Ahmadpanah, and T. Guirand, "A simple method for determining the Green's function for a large class of MIC lines having multilayered dielectric structures," *IEEE Trans. Microwave Theory Tech.*, vol. MTT-26, pp. 82-87, February 1978.

[45] C. Wei, R. Harrington, L. Mautz, and T. Sarkar, "Multiconductor lines in multilayered dielectric media," *IEEE Trans. Microwave Theory Tech.*, vol. MTT-32,

pp. 439-449, April 1984.

[46] R. Mittra and C. Chan, "Iterative approaches to the solution of electromagnetic boundary value problems," *Electromagnetics*, 1985.

[47] S. Cohn, "Characteristic impedances of broadside-coupled strip transmission lines," *IRE Trans. Microwave Theory Tech.*, vol. MTT-8, pp. 633-637, November 1960.

[48] T. Chen, "Determination of the capacitance inductance and characteristic impedance of rectangular lines," *IRE Trans. Microwave Theory Tech.*, vol. MTT-8, pp. 510-519, September 1960.

[49] H. A. Wheeler, "Transmission-line properties of parallel strips separated by a dielectric sheet," *IEEE Trans. Microwave Theory Tech.*, vol. MTT-13, pp. 172-185, March 1965.

[50] R. F. Harrington, *Field Computation by Moment Methods*. New York: Krieger, 1983.

[51] B. E. Spielman, "Dissipation loss effects in isolated and coupled transmission lines," *IEEE Trans. Microwave Theory Tech.*, vol. MTT-25, pp. 648-655, August 1977.

[52] A. Farrar and A. T. Adams, "Characteristic impedance of microstrip by the method of moments," *IEEE Trans. Microwave Theory Tech.*, vol. MTT-18, pp. 65-66, January 1970.

[53] H. Sobol, "Extending IC technology to microwave equipment," *Electron.*, vol. 40, pp. 112-124, March, 1967.

[54] C. Wei and R. F. Harrington, "Computation of the parameters of multiconductor transmission lines in two dielectric layers above a ground plane," *Department of Electrical and Computer Engineering*, Syracuse University, Rep. TR-82-12, November 1982.

[55] W. T. Weeks, "Calculation of coefficients of capacitance of multiconductor transmission lines in the presence of a dielectric interface," *IEEE Trans. Microwave Theory Tech.*, vol. MTT-18, pp. 35-43, January 1970.

[56] P. H. Harms, C. H. Chan, and R. Mittra, "Modeling of planar transmission line structures for digital circuit applications," *AEU 43*, pp. 245-250, 1989.

[57] P. Silvester and P. Benedek, "Equivalent capacitances of microstrip open circuits," *IEEE Trans. Microwave Theory Tech.*, vol. MTT-20, pp. 511-516, August 1972.

[58] P. Silvester and P. Benedek, "Microstrip discontinuity capacitances for right-angle bends, T-junctions and crossings," *IEEE Trans. Microwave Theory Tech.*, vol. MTT-21, pp. 341-346, May 1973.

[59] A. Farrar and A. T. Adams, "Computation of lumped microstrip capacitance by matrix methods - Rectangular sections and end effect, " *IEEE Trans. Microwave Theory Tech.*, vol. MTT-19, pp. 495-497, May 1971.

[60] A. Farrar and A. T. Adams, "Matrix methods for microstrip three-dimensional problems," *IEEE Trans. Microwave Theory Tech.*, vol. MTT-20, pp. 497-504, August 1972.

[61] T. Itoh, R. Mittra, and R. Ward, "A method for computing edge capacitance of finite and semi-infinite microstrip lines," *IEEE Trans. Microwave Theory Tech.*, vol. MTT-21, pp. 380-386, June 1973.

[62] J. D. Jackson, *Classical Electro Dynamics*. New York: Wiley & Sons, 1975.

[63] D. S. James and S. H. Tsc, "Microstrip end effects," *Electron. Lett.*, pp. 46-47, January 1972.

[64] P. Troughton, "Design of complex microstrip circuits by measurements and computer modeling," *Proc. IEE,* vol. 118, nos. 3/4, pp. 469-474, March/April 1971.

[65] I. Wolff, G. Kompa, and R. Mehran, "Calculation method for microstrip discontinuities and T-junctions," *Electron. Lett.*, vol. 8, no. 7, pp. 177-179, April , 1972.

[66] A. Gopinath and P. Silvester, "Calculation of inductance of finite-length strips and its variation with frequency," *IEEE Trans. Microwave Theory Tech.*, vol. 22, pp. 880-883, 1974.

[67] A. Gopinath and B. Easter, "Moment method of calculating discontinuity inductance of microstrip right-angle bends," *IEEE Trans. Microwave Theory Tech.*, vol. 23, pp. 648-655, 1975.

[68] K. C. Gupta, R. Garge, and R. Chadha, *Computer-Aided Design of Microwave Circuits*. Norwood Ma.: Artech House, 1981.

[69] A. Gopinath and C. Gupta, "Capacitance parameters of discontinuities in microstriplines," *IEEE Trans. Microwave Theory Tech.*, vol. 26, pp. 831-835, October 1978.

[70] P. Anders and F. Arndt, "Microstrip discontinuity capacitance and inductance for double steps, mitered bends with arbitrary angle and asymmetric right-angle bends," *IEEE Trans. Microwave Theory Tech.*, vol. 28, pp. 1213-1217, 1980.

[71] P. D. Patel, "Calculation of capacitance coefficients for a system of irregular finite conductors on a dielectric sheet," *IEEE Trans. Microwave Theory Tech.*, vol. 19, pp. 862-869, 1971.

[72] R. K. Hoffman, *Handbook of Microwave Integrated Circuits,* (H. H. Howe, Jr., English Translator). Norwood, MA.: Artech House, Inc., 1987.